國 立 交 通 大 學
材 料 科 學 與 工 程 研 究 所
博 士 論 文

奈米碳管於直接甲醇燃料電池電極上之應用與特性分析

Applications and Characterizations of carbon nanotubes as electrodes for direct methanol fuel cells

研 究 生：陳 建 仲
指 導 教 授：陳 家 富 博 士

中 華 民 國 九 十 五 年 八 月

奈米碳管於直接甲醇燃料電池電極上之應用與特性分析

Applications and Characterizations of carbon nanotubes as electrodes for direct methanol fuel cells

研 究 生： 陳 建 仲　　Student：Chien-Chung Chen
指導教授： 陳 家 富 博 士　　Advisor：Dr. Chia-Fu Chen

國 立 交 通 大 學

材 料 科 學 與 工 程 研 究 所

博 士 論 文

A Thesis

Submitted to Department of material Science and Engineering

College of Engineering

National Chiao Tung University

In partial Fulfillment of the Requirements

For the Degree of Doctor of Philosophy

In Material Science and Engineering

August 2006

Hsinchu, Taiwan, Republic of China

中 華 民 國 九 十 五 年 八 月

誌　　謝

細數讀博士班的這四年來，要感謝的人實在太多了，多虧有你們我才能完成我的研究；寫這篇致謝的順序並不代表大家對我的重要性，因為對我來說，你們都很重要，沒有你們大家的幫助，也沒有這份論文的誕生。首先要感謝的是我的指導教授－陳家富老師，謝謝陳老師在論文研究上的指導與鼓勵，使得這篇論文能順利完成。更重要的是陳老師對學生的照顧與愛護。再來特別感謝我的博士論文審查委員汪大永校長、施漢章老師、薛富盛老師、陳密老師及張立老師的指導及寶貴意見，在此亦由衷的表示感謝。

接著感謝學弟劉家駿、莊方慈，學妹李依璇幫忙實驗的分析及討論。也感謝蔡佳倫學長、林琨程學長、施士塵學長、羅宏鈞學長/弟、顏志坤同學、伍泰霖學弟、詹適宇學弟、陳瑤真學妹、陳宜輝學弟、劉厥揚學弟、施騰凱學弟、王瑞豪學弟、洪淙琦學弟、陳建銘學弟、徐振航學弟等在實驗上提供意見及生活上的幫助。另外也感謝國科會貴儀中心的操作員吳美玲同學的幫忙。誠如我一開始所說的，這篇致謝的順序並不代表大家對我的重要性，你們都很重要，非常感謝你們。

當然我也要感謝我的家人及女友，這些年來對我全力的支持，讓我能無後顧之憂的完成我的博士學業。

最後，我也要感謝那些曾經批評過我及傷害過我的人，由於你們，讓我更充滿了鬥智，也讓我能不斷的檢視我自己。

僅以此論文獻給所有幫助過我的人。

奈米碳管於直接甲醇燃料電池電極上之應用與特性分析

研究生：陳建仲　　指導教授：陳家富　博士

國立交通大學材料工程研究所

摘　　要

燃料電池由於具有無污染、高效率、低噪音等優點，被視為下一個世紀最具淺力的替代能源，其中以可微小化的直接甲醇燃料電池最受青睞。本研究主要乃是將具有高表面積、高導電性之奈米碳管作為直接甲醇燃料電池之電極材料，藉以改善直接甲醇燃料電池中觸媒用量過大、利用率不佳及反應速率過低等缺點。

本研究分兩個階段實驗，第一是將奈米碳管直接成長於碳布上作為直接甲醇燃料電池電極之觸媒載體，嘗試分別以濺鍍法及濕式沉浸法(wet impregnation)來披覆鉑(Pt)金屬觸媒，針對所製作之膜電極組(membrane electrode assembly)進行電化學分析及單電池效能測試。實驗結果發現，以濺鍍法雖可合成較小粒徑之鉑觸媒，但礙於載體的遮蔽效應(shield effect)，鉑觸媒的質量效能(mass efficiency)，濺鍍時間超過 15 分鐘以上時有漸減的趨勢，造成燃料電池的效能提升幅度有限。然而利用濕式沉浸法雖無遮蔽效應的影響，但由於碳管表面為化學惰性，導致觸媒的群聚現象，造成直接甲醇燃料電池的能量密度(power density)，在鉑的披覆量為 0.4 mg/cm^{2}時，70^{o}C的操作溫度之下，甲醇燃料電池的能量密度只有 4.6 mW/cm^2。而在 2.0 mg/cm^{2}的高鉑披覆量之下，亦只達到 27.4mW/cm^2。

因此，為了解決觸媒群聚的現象及有效提升電池效能，第二階段我們嘗試對奈米碳管表面進行改質處理，首先我們利用硝酸溶液來進行奈米碳管的表面改質，結果顯示改質後的奈米碳管有效解決了觸媒的群聚效應，且電池效能在 0.4 mg/cm^{2}鉑批覆量，70^{o}C的操作溫度下的能量密度可達到 15.8 mW/cm^2；於 30^{o}C的室溫下，亦可有 8.6 mW/cm^{2}的效能表現。接著我們利用微波消化 (microwave digestion) 法對奈米碳管做快速及有效率的表面改質；我們從FTIR, Raman光譜和XPS的結果發現，藉由微波消化

法進行奈米碳管的表面改質，可以在較短時間內(1 小時) 比硝酸處理 18 小時後的碳管，能接上較多的官能基及有較高的觸媒質量效能，有效率且大幅度地縮短了奈米碳管表面改質的時間。

除此之外，我們更嘗試比較使用硫酸、氫氧化鉀與 2-硫醇乙醇作為蝕刻溶劑，針對不同溶液的改質後所形成的官能基與觸媒間的影響進行分析及探討，實驗結果發現以 2-硫醇乙醇硫化後的奈米碳管，有較小的觸媒粒徑及其質量效能(mass efficiency)可達到 304.2 mA/mg，電池效能在 0.5 mg/cm^{2}鉑批覆量，70^{o}C的操作溫度下的能量密度可達到 20.6 mW/cm^2,高於一般以硝酸溶液酸化後的奈米碳管。

Applications and Characterizations of carbon nanotubes as electrodes for direct methanol fuel cells

Student：Chien-Chung Chen Advisor : Dr. Chia-Fu Chen

Institute of Material Science and Engineering

National Chiao Tung University

Abstract

Fuel cells are regarded as the most potential power source to replace fossil oil due to their low pollution, high efficiency and low noise. Among all, direct methanol fuel cell (DMFC) which can be minified catches everyone eyes. However, high catalysts loading, low utility of catalysts and low reaction rates are advantages of DMFC. In this thesis, high surface area and high conductivity carbon nanotubes (CNTs) were used as the electrodes to improve the utility of catalysts of the direct methanol fuel cell. This research was divided into two parts. The first part includes directly synthesizes CNTs on carbon cloth as the catalyst supports and disperses metallic catalysts on CNTs by sputtering and wet impregnation. After that, we fabricate and characterize the membrane electrode assembly of a DMFC. We found that although dispersing catalysts by sputtering method can form Pt catalysts with small size (about 3nm), the mass efficiency will decrease with long sputtering time due to the shield effect of CNTs. This will result in the degradation of cell performance. On the other hand, the shield effect can be solved by wet impregnation method, but the agglomeration of catalysts occurred and strongly decreases the performance of DMFC.

The second part of this thesis focuses on the surface modification/ functionalization of CNTs for solving the agglomeration of catalysts and improving the cell performance. The surface modifications of CNTs were carried out by refluxing pristine CNTs in HNO_3 for

attaching the functional groups. From the results of cyclic voltammograms (CVs) and single cell test of Pt/MWCNTs electrodes, we can found the significant improvement of cell performance of DMFC after modifying MWCNTs. The power density of Pt dispersed on HNO_3 treated MWCNTs is 15.8, 12.6 and 8.6 mW/cm^2 at 70^{o}C, 50^{o}C and 30^{o}C with 0.4 mg/cm^2 Pt loading ,respectively. This is much higher than the DMFCs with Pt/pristine-MWCNTs and sputter deposited Pt/MWCNTs based cells. Furthermore, we introduce a fast and effective method for modifying CNTs by microwave digestion method. The functionalization of CNTs for increasing more anchoring sites can be achieved in a short time by this approach. The CVs results show that the microwave digestion modified Pt/MWCNTs electrode exhibits the larger electrochemical Pt surface area and higher current density of methanol oxidation than pristine and HNO_3 treated Pt/MWCNTs electrodes. This technique can be widely used for effective modifying CNTs and shorting the process time. Finally, the effects of functionalization of CNTs with different functional groups, such H_2SO_4, KOH and 2-mercaptoethanol were discussed in this part. The Pt/sulfonated-MWCNTs has the maximum methanol oxidation current density about 152.1 mA/cm^2 and mass efficiency about 304mA/g. The power density of Pt dispersed on thiolated MWCNTs is 20.6 mW/cm^2 at 70^{o}C, with 0.5 mg/cm^2 Pt loading, which is much higher than the Pt/HNO_3 treated-MWCNTs.

Contents

List of Tables

List of Figures

Chapter 1

Introduction

1.1 Preface

Nowadays, to discovery a new power source with less pollution and lower price in replace of fossil oil is a noteworthy topic among resource industry. With its high efficiency and less pollution, fuel cells have become the most possible and popular power source to the next generation. Actually, Fuel cells are an aged technology. Retrospect to 1839, W. R. Grove discovered that the fuel cells and used hydrogen and oxygen as fuels. Fuel cells generate electricity from a simple electrochemical reaction in which oxygen and hydrogen combine to form water and generate electrons. The reactions are shown below:

Anode: $2H_2 \rightarrow 4H^+ + 4e^-$

Cathode: $O_2 + 4H^+ + 4e^- \rightarrow 2H_2O$

Overall: $2H_2 + O_2 \rightarrow 2H_2O$

In 1960s, fuel cell was initially applied as an auxiliary power source in the Gemini space flights. Subsequently, advances in this technology were stagnant until the late 1980s when the fundamental design underwent significant reconfiguration. Even though, there are challenges and obstacles with developing fuel cells, scientists never cease devoting their energy and effort on fuel cell territory.

1.2 Types of fuel cells

Fuel cells are classified primarily by the kind of electrolyte they employ. This determines the kind of chemical reactions that take place in the cell, the kind of catalysts required, the temperature range in which the cell operates, the fuel required, and other factors. These characteristics, in turn, affect the applications for which these cells are most suitable. There are several types of fuel cells currently under development, each with its own advantages, limitations, and potential applications. A few of the most promising types include proton exchange membrane fuel cell (PEMFC), alkaline fuel cell (AFC), phosphoric acid fuel cell (PAFC), molten carbonate fuel cell (MCFC), and solid oxide fuel cell (SOFC), which are on the basis of the type of electrolyte. Details of these fuel cells are describes as follow.

1.2.1 Polymer Electrolyte Membrane Fuel Cell

Polymer electrolyte membrane (PEM) fuel cells, also called proton exchange membrane

fuel cells, deliver high power density and offer the advantages of low weight and volume, compared to other fuel cells. PEM fuel cells use a solid polymer as an electrolyte and porous carbon electrodes containing a platinum catalyst. They need only hydrogen, oxygen from the air, and water to operate and do not require corrosive fluids like some fuel cells. They are typically fueled with pure hydrogen supplied from storage tanks or onboard reformers. Polymer electrolyte membrane fuel cells operate at relatively low temperatures, around 80°C. Low temperature operation allows them to start quickly and results in less wear on system components, resulting in better durability. However, it requires that a noble-metal catalyst be used to separate the electrons and protons of hydrogen, resulting high cost of system. The platinum catalyst is also extremely sensitive to CO poisoning, making it necessary to employ an additional reactor to reduce CO in the fuel gas if the hydrogen is derived from an alcohol or hydrocarbon fuel. This also increases the cost. Developers are currently exploring Pt-Ru catalysts that are more resistant to CO. PEM fuel cells are used primarily for transportation applications and some stationary applications. Due to their fast startup time, low sensitivity to orientation, and favorable power-to-weight ratio, PEM fuel cells are particularly suitable for use in passenger vehicles, such as cars and buses. A significant barrier to using these fuel cells in vehicles is hydrogen storage. Most fuel cell vehicles powered by pure hydrogen must store the hydrogen onboard as a compressed gas in pressurized tanks. Due to the low energy density of hydrogen, it is difficult to store enough hydrogen onboard to allow vehicles to travel the same distance as gasoline-powered vehicles before refueling, typically 300-400 miles. Higher-density liquid fuels such as methanol, ethanol, natural gas, liquefied petroleum gas, and gasoline can be used for fuel, but the vehicles must have an onboard fuel processor to reform the methanol to hydrogen. This increases costs and maintenance requirements. The reformer also releases carbon dioxide, though less than that emitted from current gasoline-powered engines.

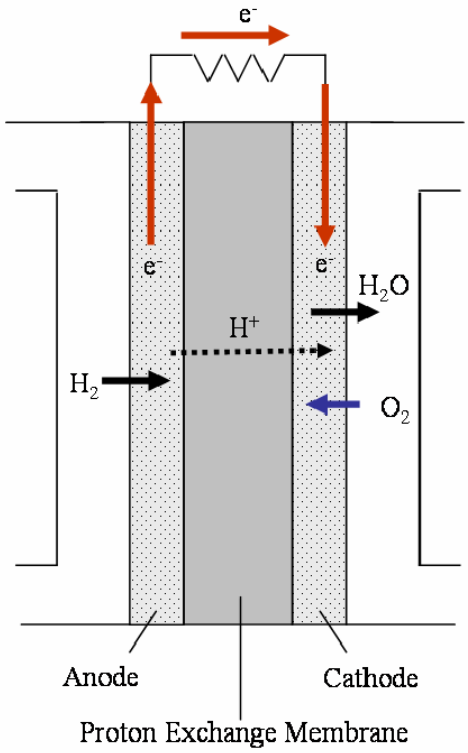

Fig.1-1 Schematic diagram of a PEMFC.

1.2.2 Phosphoric Acid Fuel Cell

Phosphoric acid fuel cells use liquid phosphoric acid as an electrolyte—the acid is contained in a Teflon-bonded silicon carbide matrix—and porous carbon electrodes containing a platinum catalyst. The chemical reactions that take place in the cell are shown in the diagram to the right. The phosphoric acid fuel cell (PAFC) is considered the "first generation" of modern fuel cells. It is one of the most mature cell types and the first to be used commercially, with over 200 units currently in use. This type of fuel cell is typically used for stationary power generation, but some PAFCs have been used to power large vehicles such as city buses. PAFCs are more tolerant of impurities in the reformate than PEM cells, which are easily poisoned by CO2—CO2 binds to the platinum catalyst at the anode, decreasing the fuel cell's efficiency. They are 85 percent efficient when used for the co-generation of electricity and heat, but less efficient at generating electricity alone. This is only slightly more efficient than combustion-based power plants, which typically operate at 33 to 35 percent efficiency. PAFCs are also less powerful than other fuel cells, given the

same weight and volume. As a result, these fuel cells are typically large and heavy. PAFCs are also expensive. Like PEM fuel cells, PAFCs require an expensive platinum catalyst, which raises the cost of the fuel cell.

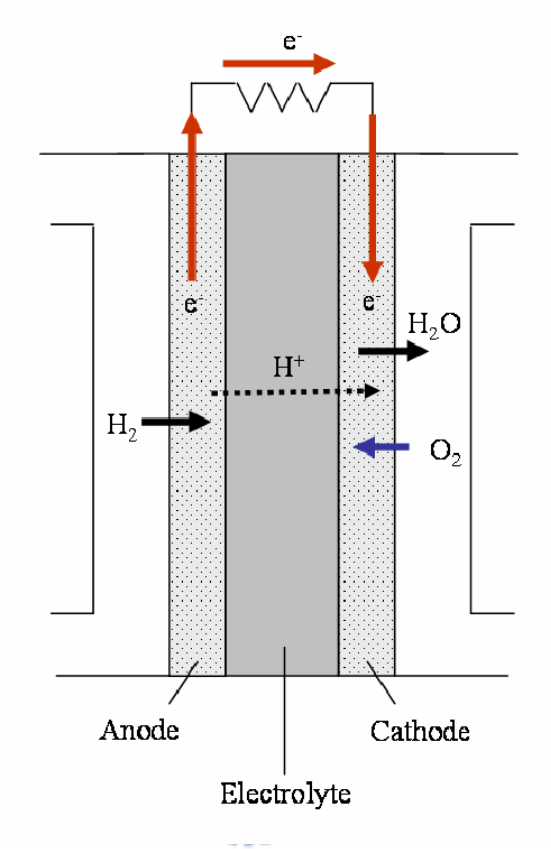

Fig.1-2 Schematic diagram of a PAFC.

1.2.3 Alkaline Fuel Cell

Alkaline fuel cells (AFCs) were one of the first fuel cell technologies developed, and they were the first type widely used in the U.S. space program to produce electrical energy and water onboard spacecraft. These fuel cells use a solution of potassium hydroxide in water as the electrolyte and can use a variety of non-precious metals as a catalyst at the anode and cathode. High-temperature AFCs operate at temperatures between 100ºC and 250ºC. However, more-recent AFC designs operate at lower temperatures of roughly 23ºC to 70ºC. AFCs are high-performance fuel cells due to the rate at which chemical reactions take place in the cell. They are also very efficient, reaching efficiencies of 60 percent in space applications. The disadvantage of this fuel cell type is that it is easily poisoned by carbon

CO_2. In fact, even the small amount of CO_2 in the air can affect the cell's operation, making it necessary to purify both the hydrogen and oxygen used in the cell. This purification process is costly. Susceptibility to poisoning also affects the cell's lifetime, further adding to cost. Cost is less of a factor for remote locations such as space or under the sea. However, to effectively compete in most mainstream commercial markets, these fuel cells will have to become more cost effective. AFC stacks have been shown to maintain sufficiently stable operation for more than 8,000 operating hours. To be economically viable in large-scale utility applications, these fuel cells need to reach operating times exceeding 40,000 hours. This is possibly the most significant obstacle in commercializing this fuel cell technology.

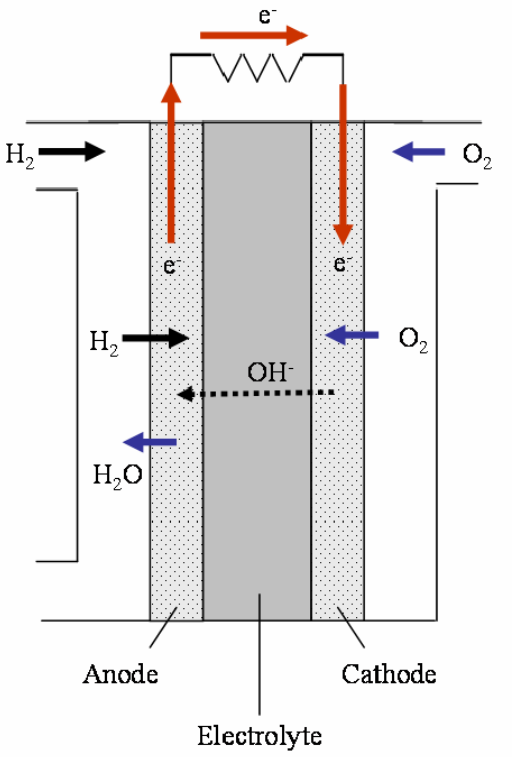

Fig.1-3 Schematic diagram of an AFC.

1.2.4 Molten Carbonate Fuel Cell

Molten carbonate fuel cells (MCFCs) are currently being developed for natural gas and coal-based power plants for electrical utility, industrial, and military applications. MCFCs are high-temperature fuel cells that use an electrolyte composed of a molten carbonate salt mixture suspended in a porous, chemically inert ceramic lithium aluminum oxide ($LiAlO_2$)

matrix. Since they operate at extremely high temperatures of 650ºC and above, non-precious metals can be used as catalysts at the anode and cathode, reducing costs. Improved efficiency is another reason MCFCs offer significant cost reductions over phosphoric acid fuel cells (PAFCs). Molten carbonate fuel cells can reach efficiencies approaching 60 percent, considerably higher than the 37-42 percent efficiencies of a phosphoric acid fuel cell plant. When the waste heat is captured and used, overall fuel efficiencies can be as high as 85 percent. Unlike alkaline, phosphoric acid, and polymer electrolyte membrane fuel cells, MCFCs don't require an external reformer to convert more energy-dense fuels to hydrogen. Due to the high temperatures at which they operate, these fuels are converted to hydrogen within the fuel cell itself by a process called internal reforming, which also reduces cost. Molten carbonate fuel cells are not prone to CO or CO_2 poisoning, making them more attractive for fueling with gases made from coal. Although they are more resistant to impurities than other fuel cell types, scientists are looking for ways to make MCFCs resistant enough to impurities from coal, such as sulfur and particulates. The primary disadvantage of current MCFC technology is durability. The high temperatures at which these cells operate and the corrosive electrolyte used accelerate component breakdown and corrosion, decreasing cell life. Scientists are currently exploring corrosion-resistant materials for components as well as fuel cell designs that increase cell life without decreasing performance.

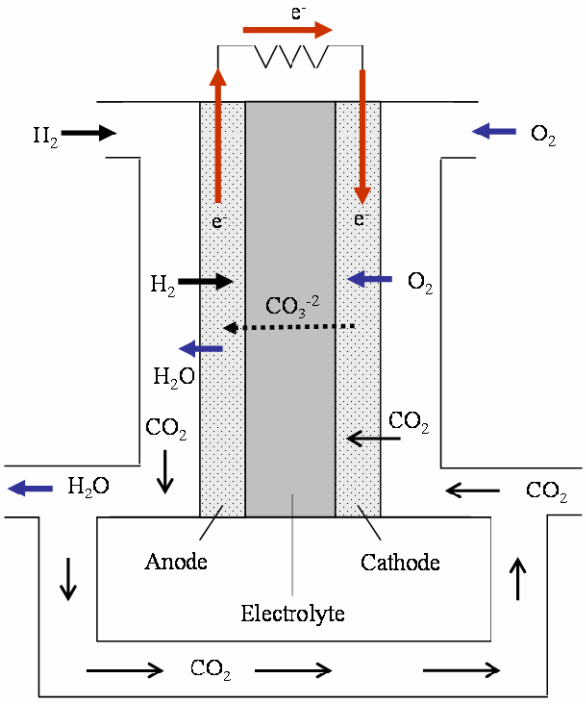

Fig.1-4 Schematic diagram of an MCFC.

1.2.5 Solid Oxide Fuel Cell

Solid oxide fuel cells (SOFCs) use a hard, non-porous ceramic compound as the electrolyte. Since the electrolyte is a solid, the cells do not have to be constructed in the plate-like configuration typical of other fuel cell types. SOFCs are expected to be around 50-60 percent efficient at converting fuel to electricity. In applications designed to capture and utilize the system's waste heat, overall fuel use efficiencies could top 80-85 percent. Solid oxide fuel cells operate at very high temperatures. High temperature operation removes the need for precious-metal catalyst, thereby reducing cost. It also allows SOFCs to reform fuels internally, which enables the use of a variety of fuels and reduces the cost associated with adding a reformer to the system. SOFCs are also the most sulfur-resistant fuel cell type; they can tolerate several orders of magnitude more sulfur than other cell types. In addition, they are not poisoned by CO, which can even be used as fuel. This allows SOFCs to use gases made from coal. High-temperature operation has disadvantages. It results in a slow startup and requires significant thermal shielding to retain heat and protect personnel, which may be acceptable for utility applications but not for transportation and small portable

applications. The high operating temperatures also place stringent durability requirements on materials. The development of low-cost materials with high durability at cell operating temperatures is the key technical challenge facing this technology. Scientists are currently exploring the potential for developing lower-temperature SOFCs operating at or below 800ºC that have fewer durability problems and cost less. Lower-temperature SOFCs produce less electrical power, however, and stack materials that will function in this lower temperature range have not been identified.

The differences and features of these fuel cells are summarized in Tab.1-1.

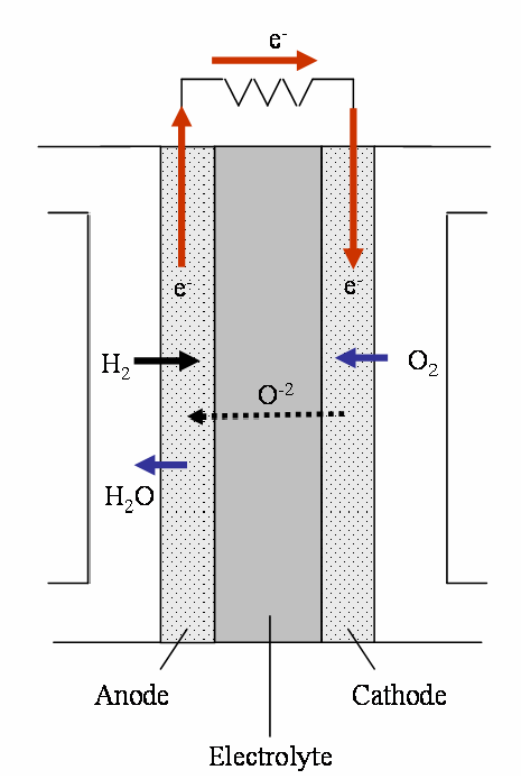

Fig.1-5 Schematic diagram of a SOFC.

Tab.1-1 Comparisons of various fuel cells

	MCFC	PAFC	PEMFC	SOFC
Electrolyte	Molten carbonate salt	Liquid phosphoric acid	Ion exchange membrane	Solid metal oxide
Operating tempt.	600~1000°C	150~200°C	60~100°C	600~1000°C
Reforming	External/Internal	External	External	External/Internal
Oxidant	CO_2/O_2/Air	O_2/Air	O_2/Air	O_2/Air
Efficiency	45~60%	35~50%	35~50%	45~60%
Max. Efficiency	85%	80%	60%	85%
Max. power output	2MW	1MW	250kW	220kW
Waste heat uses	High pressure stream	Space heating or water heating	Space heating or water heating	Heating water or stream

1.3 Direct methanol fuel cell

Direct methanol fuel cell (DMFC) is a kind of PEMFCs; we separate it from PEMFC and discuss in detail. Most fuel cells are powered by hydrogen, which can be fed to the fuel cell system directly or can be generated within the fuel cell system by reforming hydrogen-rich fuels such as methanol, ethanol, and hydrocarbon fuels. Direct methanol fuel cell, however, is powered by pure methanol, which is mixed with steam and fed directly to the fuel cell anode. Direct methanol fuel cells do not have many of the fuel storage problems typical of some fuel cells since methanol has a higher energy density than hydrogen. Methanol is also easier to transport and supply to the public using our current infrastructure since it is a liquid, like gasoline. Fig.1-5 shows the schematic diagram of a DMFC. The anode, the negative post of the fuel cell, has several jobs. It conducts the electrons that are freed from the hydrogen molecules so that they can be used in an external circuit. It has channels etched into it that disperse the hydrogen gas equally over the surface of the catalyst. The cathode, the positive post of the fuel cell, has channels etched into it that distribute the oxygen to the surface of the catalyst. It also conducts the electrons back from the external

circuit to the catalyst, where they can recombine with the hydrogen ions and oxygen to form water. The electrolyte is the proton exchange membrane. This specially treated material only conducts positively charged ions and blocks electrons. The catalyst is a special material that facilitates the reaction of oxygen and hydrogen. It is usually made of platinum powder very thinly coated onto carbon paper or cloth. The catalyst is rough and porous so that the maximum surface area of the platinum can be exposed to the hydrogen or oxygen. The platinum-coated side of the catalyst faces the proton exchange membrane.

Because methanol is fed directly into the fuel cell, complicated catalytic reforming is unneeded, and storage of methanol is much easier than that of hydrogen because it does not need to be done at high pressures, as methanol is a liquid. The energy density of methanol is orders of magnitude greater than even highly compressed hydrogen. However, efficiency is low, due to the high permeation of methanol through the membrane, and the dynamic behavior is sluggish. Methanol is also poisonous. As a result of these strengths and problems, DMFCs are limited in the power they can produce, but can still store much energy in a small space. This means they can produce a small amount of power over a long period of time which makes them well suited to power consumer electronics such as cell phones and laptops but rules them out of automotive applications. The DMFC relies upon the oxidation of methanol on a catalyst layer to form carbon dioxide. Water is consumed at the anode and is produced at the cathode. Protons (H^+) are transported across the proton exchange membrane to the cathode where they react with dioxygen to produce water. Electrons are transported via an external circuit from anode to cathode providing power to external devices.

The half reactions are:

Anode: $CH_3OH + H_2O \rightarrow CO_2 + 6H^+ + 6e^-$

Cathode: $1.5O_2 + 6H^+ + 6e^- \rightarrow 3H_2O$

Net reaction: $CH_3OH + 1.5O_2 \rightarrow CO_2 + 2H_2O$

Because water is consumed at the anode in the reaction, pure methanol cannot be used without provision of water via either passive transport such as back diffusion, or active transport such as pumping. The need for water limits the energy density of the fuel.

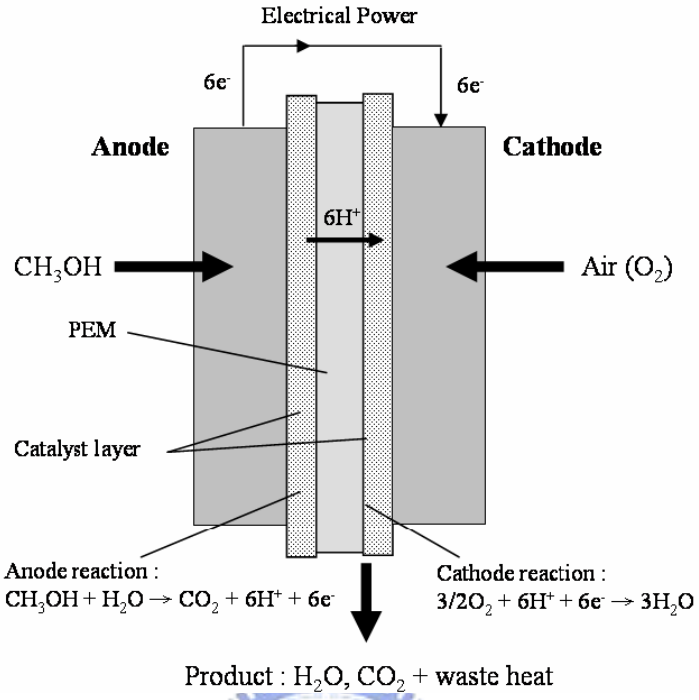

Fig.1-6 Schematic diagram of a DMFC.

1.4 Problems of DMFC

The problems of DMFC restrict the commercialization of DMFC at present, which include:

1. Low temperature- poor kinetics at anode and cathode
2. Needs Ru co-catalyst- Pt poisons otherwise
3. Methanol cross-over through membrane to cathode

One of the most important limitations of direct methanol fuel cell is low catalytic activity of the electrodes, especially the anodes and at present, there is no practical alternative to Pt based catalysts. High noble metal loadings on the electrode [2, 3] and the use of perfluorosulfonic acid membranes significantly contribute to the cost of the devices. An efficient way to decrease the loadings of precious platinum metal catalysts and higher utilization of Pt particles is by better dispersion of the desired metal on the suitable support [4]. In general, small particle size and high dispersion of platinum on the support will result in high electrocatalytic activity. Carbon materials possess suitable properties for the design of electrodes in electrochemical devices. Carbon is an ideal material for supporting nano-sized

metallic particles in the electrode for fuel cell applications. No other material except carbon material has the essential properties of electronic conductivity, corrosion resistance, surface properties, and the low cost required for the commercialization of fuel cells. In general, the conventional supports namely carbon black is used for the dispersion of Pt particles

1.5 Catalyst support for fuel cells

For improving the utility of catalysts, the material with high surface area, high electron conductivity is required as the catalyst support. However, the high chemical resistance to acid or alkaline media and the possibility to control, up to certain limits, the porosity and the surface chemistry made carbon based materials a preferred choice for catalyst supports. Carbon possesses unique electrical and structural properties that make it a suitable material for use in fuel cells. Various forms of carbon, such as graphite, carbon black and other composite materials have been chosen for catalyst supports. Among them, carbon nanotubes represent a distinctive class of catalyst supports, exhibiting a high surface area and many available adsorption sites. Typically, the total surface area of as-grown single-walled carbon nanotubes ranges between 400 and 900 m2/g, whereas for as-produced multi-walled carbon nanotubes values are ranging between 200 and 400 m^2/g. In a single-walled carbon nanotube, bundle adsorption sites are represented either by the interior of a nanotube, the interstitial channels between tubes, the outer surface of the bundle or the grooves formed at the contact between adjacent tubes. For multi-walled carbon nanotubes, adsorption can occur in the aggregated pores, inside the tube or on the external walls. Besides these catalyst-related structural properties, carbon nanotubes are more stable to oxidation, feature an increased wear-resistance and possess a good thermal stability. Their metallic character promotes them as good support candidates for metal particles, but chemically functionalized nanotubes can support other catalysts as well, such as bimetallic nanoparticles and organo-metallic complexes. There are three other advantages presented by carbon nanotubes as catalyst supports. First, the high purity of the material prevents self-poisoning, a common problem of conventional catalysts, which gradually wear out. Secondly, the mere nature of these supports can be of interest for liquid-phase reactions, thus limiting the mass transfer. Finally, the catalytic activity and its selectivity can directly benefit from the existence of specific metal–support interactions. As an overall result of all of the above features, the catalytic studies conducted on carbon nanotube-based systems have confirmed an increased loading

and a good dispersion of the catalyst particles with respect to values available on other supports, which naturally translates into better performance of the catalysts. For instance, platinum support for proton exchange membrane fuel cells, carbon nanotubes with 12 wt% platinum deposition give 10% higher voltage than carbon black with 29 wt% platinum deposition. When used as a catalyst support, carbon nanotubes lead to atypical activity and selectivity in several catalytic reactions such as hydrogenation of olefins and nitrobenzene into aniline, or selective hydrogenation of the double carbon bond in an unsaturated aldehyde. Also of interest are hydroformylation of olefins to aldehydes, and partial dehydrogenation reactions. Another range of applications targets catalysts for redox reactions and catalytic decompositions.

1.6 Motivation of this thesis

Carbon black (Vulcan XC-72R) which has high surface area (about 240 m^2g^{-1}) is commonly used as the catalyst supports for increase the uniformity of platinum catalysts. However, the platinum particles are covered by carbon blacks easily result in the low oxidation reduction rate of methanol [5] (see Fig.1-7).

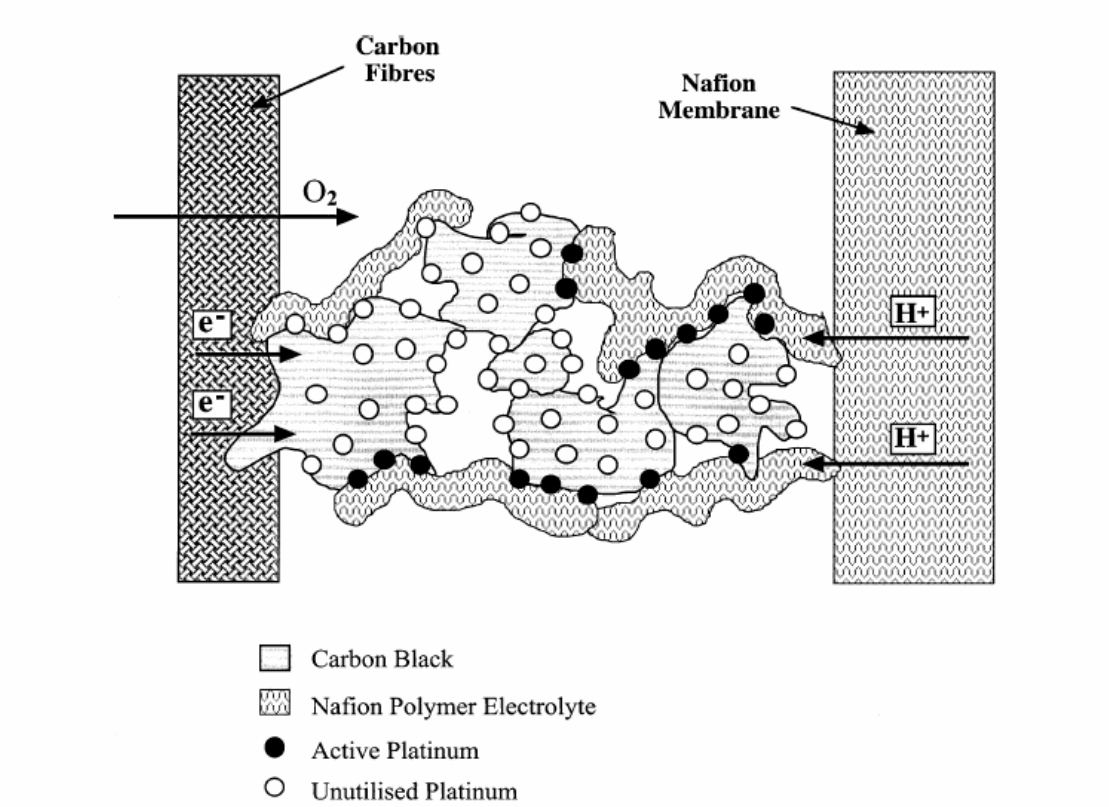

Fig.1-7 Poor utility of Pt catalysts by using carbon black as catalyst supports

In this thesis, we would like to combine the novel and amazing materials --- carbon nanotubes with the direct methanol fuel cell technologies to overcome the drawbacks of catalyst layers in a DMFC. The schematic diagram of DMFC with carbon nanotubes based electrodes was shown in Fig 1-8. Therefore, the motivations of this thesis are:

1. We want to enhance the utility of catalysts by introducing CNTs to replace the carbon black as the catalyst supports.
2. We want to simplify the fabricating processes of MEA by directly synthesizing CNTs on GDL.
3. We want to find out the better way to disperse catalysts on CNTs for improving the performance of a DMFC.
4. We want to realize the influence of surface modifications of CNTs for further applications.

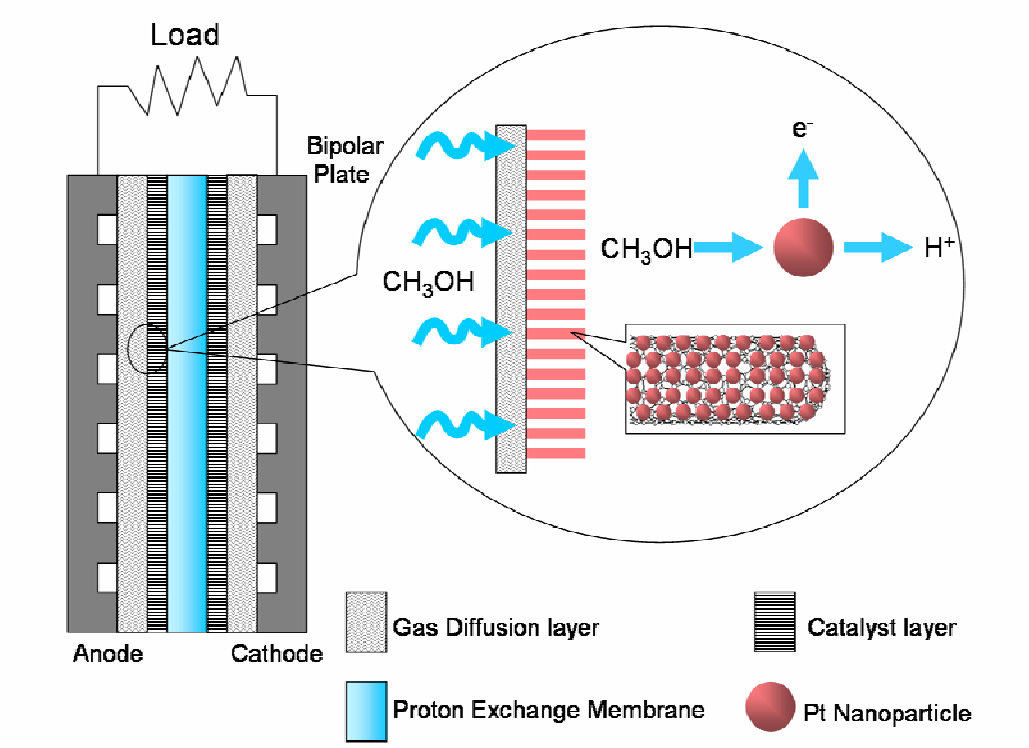

Fig.1-8 Schematic diagram of a direct methanol fuel cell and MWNT-based electrode

Chapter 2

Literature review

2.1 History of fuel cell

The fuel cell can trace back to the 1800's discovered by Sir William Robert Grove, a Welsh born, Oxford educated barrister. Grove realized that if electrolysis, using electricity, could split water into hydrogen and oxygen then the opposite would also be true. Combining hydrogen and oxygen, with the correct method, would produce electricity. The overall reaction is:

$H_2O \rightarrow 2H_2 + O_2 \qquad E^0 = 1.23V$

For improving his hypothesis, Sir William Robert Grove built a device that would combine hydrogen and oxygen to produce electricity, the world's first fuel cell. His invention was a success, and Grove's work advanced the understanding of the idea of conservation of energy and reversibility. In 1899, a fuel cell with power density of 104 km h^{-1} was held by an electric vehicle, the “Jamais Contente”. In 1900 in the USA, there were 1681 steam-driven vehicles, 1575 electric vehicles and only 936 driven by petrol engines. All electric vehicles were powered by lead-acid batteries. A fuel tank is lighter than a lead-acid battery and can be recharged more rapidly. A tank of fuel gives a much longer range than a fully charged battery- current target of 300 km still remains elusive. The advent of the self-starter, which powered by a lead-acid battery finally, clinched the relegation of electric vehicles to milk floats and fork-lift trucks. In the late 19th and early 20th centuries, coal was the major power source. But all attempts to make coal fuel cells failed, and fuel cells fell out of favour until the 1960’s, due to interest from an out of this world source.

2.2 Principle and structure of DMFC

2.2.1 The Proton Exchange Membrane (PEM)

Direct methanol fuel cell is a kind of Proton Exchange Membrane fuel cells. As the name implies, a PEMFC employs a proton exchange membrane (PEM). The PEM serves as a physical barrier between the anode and cathode gases and also as the electrolyte (hence it is also known as a solid polymer electrolyte). Today, the most common PEM is Nafion, a perfluorosulfonic acid membrane developed by E.I. DuPont de Nemours & Co. The structure of Nafion is shown in Fig.2-1. The values of x and y can be varied to create materials with

different equivalent weights and the most common equivalent weight is 1100. Although Nafion is similar in structure to polytetrafluoroethylene (PTFE or Teflon), it has excellent mechanical strength, water insolubility, and chemical and thermal stability. The sulfonated side chains endow Nafion with high proton conductivity and cation exchange capacity. Nafion has found numerous applications, such as liquid and gas separations, fuel cells, and the chloro-alkali industry.

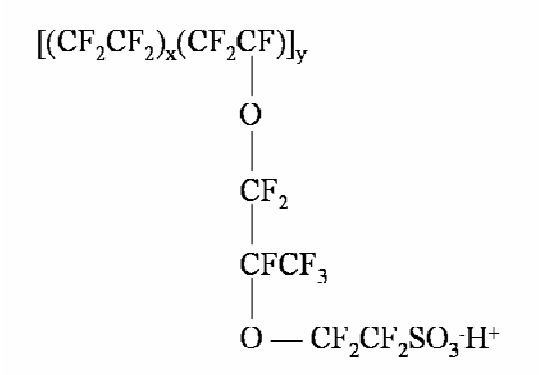

Fig.2-1 The structure of Nafion.

Structurally, Nafion is a fascinating polymeric material. The exact structure of Nafion is not known but there have been several models proposed to describe the way in which ionic groups aggregate within Nafion membranes. These models include the Mauritz-Hopfinger Model [6], the Yeager Three-Phase Model [7], the Eisenberg-Hird-More Model of Hydrocarbon Ionomers [8], and the Gierke Cluster Network Model [9]. Each of these models attempts to predict the fundamental features of equilibrium ionic selectivities and ionic transport. Electrostatic interactions cause the ionic groups to aggregate and form tightly packed regions referred to as clusters [10]. These electrostatic interactions enhance the intermolecular forces and considerably influence the properties of the parent polymer. Small angle X-ray scattering (SAXS) and neutron scattering experiments clearly indicate that ionic clustering is present in Nafion [11]. Although no one model has been found to provide a complete explanation of the properties and selectivities found, several models base these properties and selectivities on an extensive micro-phase separated morphology [12, 13]. Yeager's model describes Nafion as consisting of three regions: a fluorocarbon region (A), an interfacial zone (B) and an ionic cluster region (C). These regions are depicted in Fig.2-2.

Region A consists of the fluorocarbon backbone and is quite hydrophobic. Region C consists of clusters of pendant sulfonate groups. This region is quite hydrophilic, most absorbed water and counterions exist in this region. Gierke has proposed that these ionic clusters are spherical and exist as a network interconnected by smaller channels [14]. Region B is an interfacial region containing the pendant side chain material and sulfonate groups that are not clustered. Hence, only part of the absorbed water and counterions exist in this region.

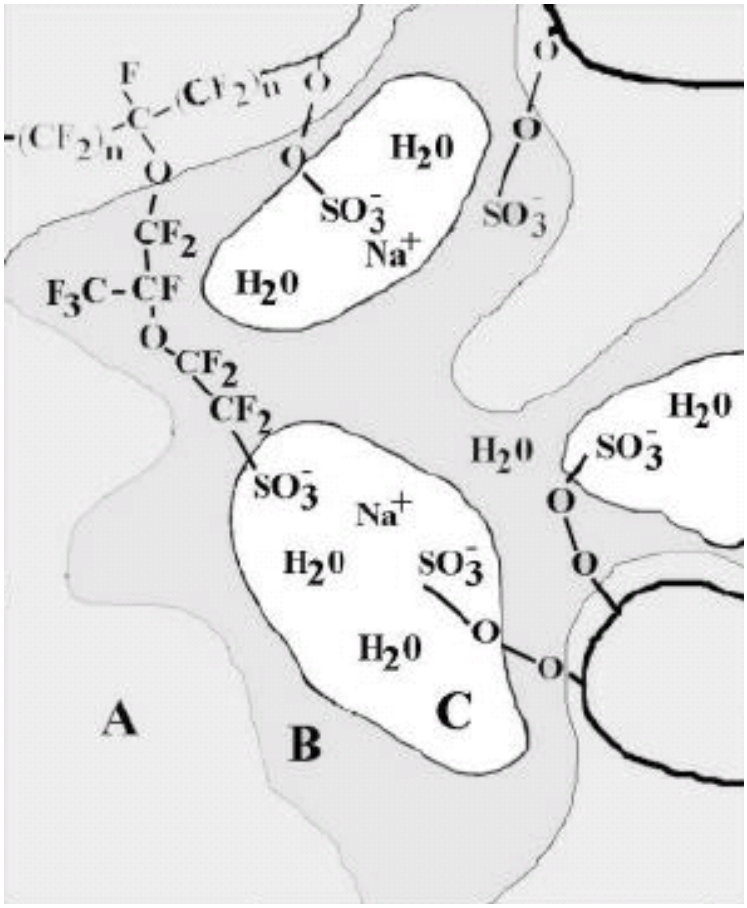

Fig.2-2 Yeager's three-phase model of Nafion; a fluorocarbon region (A), an interfacial zone (B) and an ionic cluster region (C).

The proton conductivity of Nafion is dependant on its hydration state. In the dry state, Nafion is a poor ion conductor, but ionic conductivity increases sharply with water content [15]. Because of this, reactant gases are often humidified before they enter a PEMFC. However, this can induce water management issues at the cathode. This also limits the operational temperature of Nafion based PEMFCs to under around 100^{o}C since sufficient

liquid water must be present for good conductivity. However, if too much water is present, electrode pores and flow fields are filled by water, leading to mass transport issues. This is often referred to as flooding. Therefore, water management is often a delicate balance that is critical to good performance. Companies such as Dow, Aciplex, Gore and Ballard have developed other membranes. The scientific community has studied these membranes in less detail since they are proprietary to the companies that developed them. Generally, they have similar sulfonated perfluorocarbon structures.

2.2.2 DMFC Electrodes

DMFC electrodes are complex three-dimensional structures consisting of a number of different materials in a heterogeneous mix. Much skill and art have been developed to produce structures with improved performances. Usually a 10-50 m thick layer, consisting of carbon-supported Pt catalyst bonded with recast Nafion and/or PTFE is applied onto a gas diffusion backing. The backing is typically carbon fiber paper or carbon cloth that serves as a current collector and gas conduit. The backing is often treated to aid water management within the cell. The recast Nafion in the catalyst layer originates from a Nafion solution that can be mixed with the catalyst before electrode preparation or added once the catalyst layer has been formed. Its primary purpose is to provide a medium for proton conduction within the catalyst layer, because only those Pt sites that are in ionic contact with the membrane can be active for oxidation or reduction of the fuel or oxidant. The purpose of PTFE is to bind together the electrode particles and to aid in water management. The catalyst, Nafion and PTFE are typically mixed together with water and alcohol(s) to form an ink. This ink is then spray-applied, brush-applied or even screen printed onto the backing [16]. Several proprietary methods have been reported where the catalyst mixture is applied directly onto the membrane [17, 18]. Typically, electrodes are hot-bonded to each side of the membrane to form the membrane and electrode assembly (MEA). An MEA is shown in Fig.2-3. The thin size and low mass of the MEA is the main advantage of a DMFC. This allows for the formation of compact lightweight stacks. A fuel cell stack consists of several MEAs electrically connected in series by bipolar plates. The bipolar plate serves as an electrical connection between the MEAs and also physically separates the reactant gases. A schematic diagram of a single cell DMFC is shown in Fig. 2-4. Bipolar plates have flow fields machined onto each side to distribute the reactant gases throughout the entire area of the

electrode. The most common flow field shapes are serpentine and interdigitated.

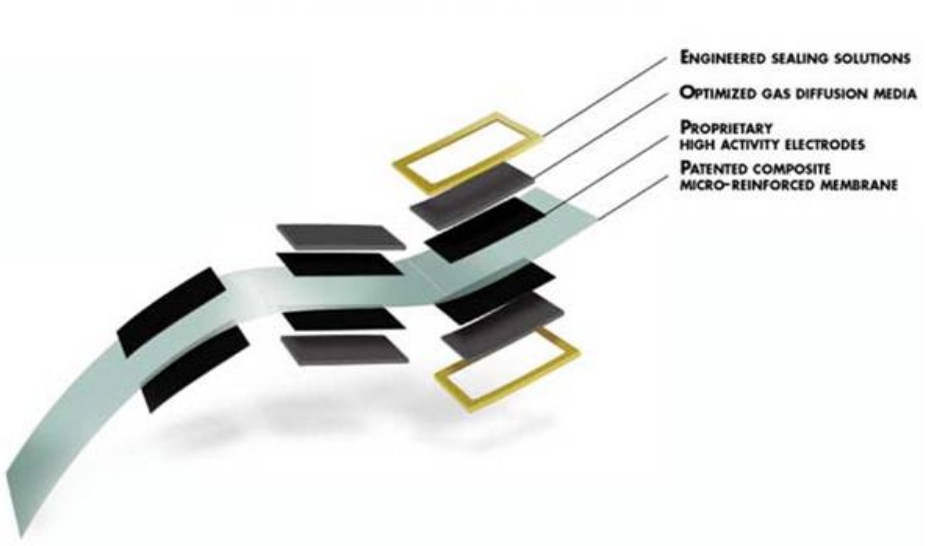

Fig.2-3 Membrane and electrode assembly (MEA).

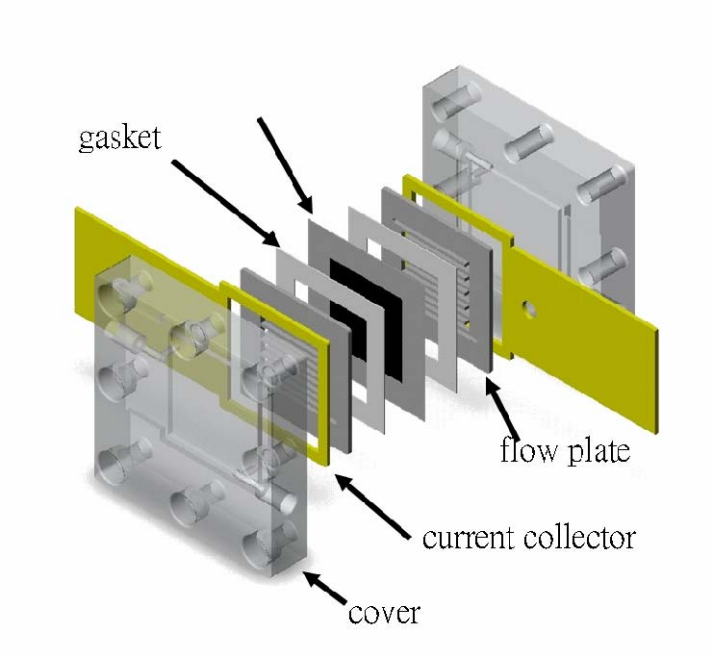

Fig.2-4 Exploded view of a DMFC.

2.2.1 DMFC Anodes

DMFC anodes typically consist of a Pt catalyst, either Pt black or Pt on a carbon support. These anodes perform very well when pure hydrogen is used, but storage and infrastructure issues make hydrogen an inconvenient fuel to supply. To circumvent these issues, hydrogen can be replaced by methanol. However, DMFC has a major drawback, that is, CO poison.

CO poisons a Pt catalyst by adsorbing strongly onto its surface, blocking active sites for hydrogen electro-oxidation, resulting in losses of electrical current. There is an unacceptable performance loss when as little as 10 ppm of CO is present in the fuel mixture. Obviously, a CO tolerant catalyst is desired. Pt is easily poisoned but bi-metallic Pt/X co-catalysts (X = Ru, Mo, Sn) have been shown to be more tolerant to CO. The second metal is deposited with Pt and will either reduce poisoning or decrease the potential at which CO is removed. Ru has been shown to be the most effective.However, adding Ru further increases the cost of the anode. Operating at higher temperatures can also decrease the effect of CO poisoning.

2.2.2 DMFC Cathodes

The oxygen reduction reaction (ORR) is a multi-electron process consisting of numerous elementary steps, involving both series and parallel pathways. It is generally accepted that oxygen reduction on Pt occurs via dissociative adsorption of O_2 followed by protonation of the adsorbed species, with the former being the ratedetermining step. There have been several models that attempt to describe these pathways [19-21]. Several models successfully interpret the same data due to their similarity. One such model is the bridge model of the ORR on Pt in acid, illustrated in Fig. 2-5. Because of the bridging oxygen system, it is obvious that optimal Pt particle spacing is of critical importance.

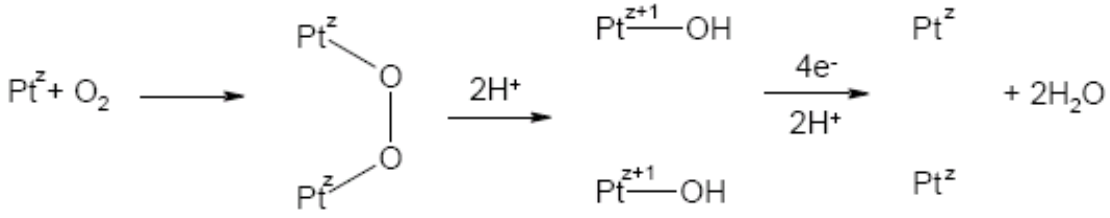

Fig. 2-5 The bridge model of oxygen reduction on Pt (z represents the oxidation state).

The complicated pathway of the ORR results in slow electrochemical kinetics. One measure of the rate of an electrochemical reaction is its exchange current density, j_o. j_o for the ORR on Pt is 10^5 less than j_o for hydrogen oxidation at Pt. It is because of this huge difference that the activity at the cathode most influences hydrogen/air cell fuel cell performance. Therefore, enhancing the cathode activity has been a major focus for PEMFC electrode development. In order to increase cathode activity, one must increase catalyst utilization. This will not only increase performance but can also lead to a lowering of the

required Pt loading. In order for a catalyst site to be electrochemically active, a pathway for electron, proton and gas transport must all be present. The active area of Pt is typically measured using cyclic voltammetry (CV) in acid electrolyte. Specifically, the area under the hydrogen adsorption/desorption peaks is determined as shown in Fig.2-6. Regions of oxide formation (Q_A) and reduction (Q_C) as well as formation of hydrogen (H_A) and its reduction (H_C) are indicated. A larger area per mass of Pt indicates a larger active area. One very successful method to increase catalyst utilization is to employ a carbon supported Pt catalyst. Typically, Pt particles (3-10 nm) are dispersed onto the electronically conducting carbon particles, about 30-50 nm. The ideal carbon support should possess high chemical stability, good electronic conductivity, high surface area and suitably pore size distribution. The type of carbon that appears to be best suited to be a fuel cell catalyst support is carbon black. There are several types of commercial carbon blacks that are have been studied for use with fuel cells, Vulcan XC72 is the most common. Although carbon is an excellent electronic conductor, it is a very poor proton conductor. This is mainly because carbon is hydrophobic. However, the carbon surface does consist of some hydrophilic moieties. Carbon-oxygen complexes, such as phenol, carbonyl, carboxyl, quinone and lactone groups can all be found on the carbon surface. Typically, exposing the carbon to an oxidizing agent forms these complexes.

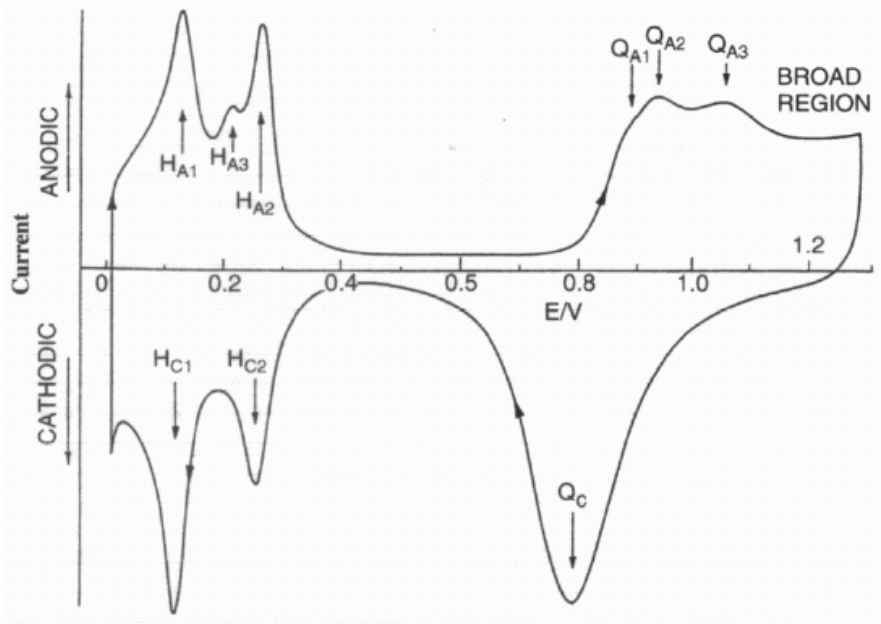

Fig.2-6 CV of a platinum electrode in 0.5M $H_2SO_{4(aq)}$.

One serious issue with Pt/carbon catalysts is the sintering of the Pt particles [22]. Sintering occurs when Pt particles become larger over their lifetime. This decreases the Pt surface area, and ultimately leads to a decline in performance throughout the lifetime of operation. Ideally, a catalyst support material that is both electronically and ionically conductive is desired. Pickup et al. have studied such a material, a conducting polymer composite [23]. The composite consists of polyprrole and polystyrenesulfonate, which are electronically conductive and proton conductor, respectively. This material was tested as a replacement for carbon and reasonable performance was achieved. However, low Pt utilization and polymer stability are still issues [24]. Another method to increase catalyst utilization is to add a proton-conducting polymer (such as Nafion) into the catalyst layer. Pt catalyst near or directly in contact with the Nafion membrane is utilized most efficiently. However, utilization drops off deeper into the catalyst layer, largely due to the limited proton conductivity of the catalyst layer. Nafion solution can be applied onto preformed electrodes or directly mixed with the catalyst during ink preparation. This increases the proton conductivity of the catalyst layer. In 1986, Raistrick was able to demonstrate that carbon-supported Pt catalyst mixed with Nafion could outperform conventional Pt black electrodes that had ten times the Pt loading [25]. This was a major breakthrough in fuel cell development in that it made the cost of Pt required much more feasible. When designing an electrode using carbon-supported catalyst and Nafion, they must be mixed in proper proportions to form a stable three-phase boundary where the gas, ion conductor and catalytically active electronically conducting phase are all present. This requirement limits the amount of Nafion that can be added since the morphology, low gas permeability, and poor electronic conductivity of Nafion disrupts this boundary and adversely affects cell performance. Because of this, and the high cost of Nafion, alternative methods for providing proton conductivity in the catalyst layer are of interest. Another approach to increase Pt utilization is to simply deposit Pt only in the areas of the electrode where it would be electroactive. This can be done by sputter deposition where layers as thin as 2 nm can be deposited. There have been many studies that use sputter deposition to localize Pt catalyst at the front surface of the electrode or even directly onto the membrane surface. Srinivsan et al. applied a 50 nm thick layer of Pt onto an uncatalyzed gas diffusion layer (GDL) by sputter deposition and achieved a 10-fold reduction in Pt loading (from 4 mg/cm^2 to 0.4 mg/cm^2)

without a loss in performance [26]. Hirano et al. later showed that electrodes prepared by sputter deposition with a Pt loading of 0.1 mg/cm^2 could perform the same as those prepared using standard materials (Pt/C) at a 0.4 mg/cm^2 Pt loading [27]. Cha and Lee have further reduced the Pt loading to 0.04 mg/cm^2 by alternating sputter deposited Pt layers and painted Nafion/Carbon ink layers, with successively lower amounts of Pt in each layer [28]. This leads to very efficient utilization of Pt. sputter deposition is promising for fuel cells since a larger percentage of Pt is electrochemically active. Also, it allows for the fabrication of very thin active layers, which decrease ohmic and mass transport overpotentials in the catalysts layer. Also, sputter deposition is a well established industrial technique in areas such as thin films and integrated circuits and it is anticipated that this technique could be readily applied to micro-fuel cell applications.

2.3 Introduction of carbon nanotubes

Carbon nanotubes, long, thin cylinders of carbon, were discovered in 1991 by S. Iijima [29]. These are large macromolecules that are unique for their size, shape, and remarkable physical properties. They can be thought of as a sheet of graphite rolled into a cylinder. These intriguing structures have sparked much excitement in the recent years and a large amount of research has been dedicated to their understanding. Currently, the physical properties are still being discovered and disputed. What makes it so difficult is that nanotubes have a very broad range of electonic, thermal, and structural properties that change depending on the different kinds of nanotube. To make things more interesting, besides having a single cylindrical wall (SWNTs), nanotubes can have multiple walls (MWNTs)--cylinders inside the other cylinders. Much research has been devoted to the study of the equilibrium structure of carbon nanotubes. Currently, some information is still begin disputed, but I have compiled recent data on the most basic and neccessary aspects of single-walled carbon nanotubes (SWNT).

2.3.1 Basic structure of carbon nanotubes

Carbon nanotubes exist as a macro-molecule of carbon, analagous to a sheet of graphite rolled into a cylinder. Graphite is a tessellation of hexagonal rings of carbon. When graphite coiled, the carbon arrangement becomes very strong. Carbon nanotubes have been known to be up to one hundred times as strong as steel and almost two millimeters long. [30] These nanotubes have a hemispherical cap at each end of the cylinder. They are light, flexible, thermally stabile, and are chemically inert. They have the ability to be either metallic or

semi-conducting depending on the twist of the nanotube. Carbon nanotubes are classified as single-walled and multi-walled carbon nanotubes according to the numbers of graphite layers. The formation of CNTs over one graphite layer we called it multi-walled carbon nanotube.

2.3.2 Types of SWCNTs

SWCNTs form different types, which can be described by the chiral vector (n, m), where n and m are integers of the vector equation $R = na_1 + ma_2$. The chiral vector is determined by the diagram at the left. Imagine that the nanotube is unraveled into a planar sheet. Draw two lines along the tube axis where the separation takes place. In other words, if you cut along the two blue lines and then match their ends together in a cylinder, you get the nanotube that you started with. Now, find any point on one of the blue lines that intersects one of the carbon atoms (point A). Next, draw the armchair line, which travels across each hexagon, separating them into two equal halves. Now that you have the armchair line drawn, find a point along the other tube axis that intersects a carbon atom nearest to the Armchair line (point B). Now connect A and B with our chiral vector, R. The wrapping angle is formed between R and the Armchair line. If R lies along the Armchair line ($\theta=0°$), then it is called an "Armchair" nanotube. If $\theta=30°$, then the tube is of the zigzag type. Otherwise, if $0°<\theta<30°$ then it is a "chiral" tube. The vector a1 lies along the zigzag line. The other vector a2 has a different magnitude than a1, but its direction is a reflection of a1 over the Armchair line. When added together, they equal the chiral vector R. [31] The values of n and m determine the chirality, or twist of the nanotube. The chirality in turn affects the conductance of the nanotube, it's density, it's lattice structure, and other properties. A SWNT is considered metallic if the value n - m is divisible by three. Otherwise, the nanotube is semiconducting. Consequently, when tubes are formed with random values of n and m, we would expect that two-thirds of nanotubes would be semi-conducting, while the other third would be metallic, which happens to be the case [32]. Given the chiral vector (n,m), the diameter of a carbon nanotube can be determined using the relationship

$d = (n^2 + m^2 + nm)^{1/2}\ 0.0783\ nm$

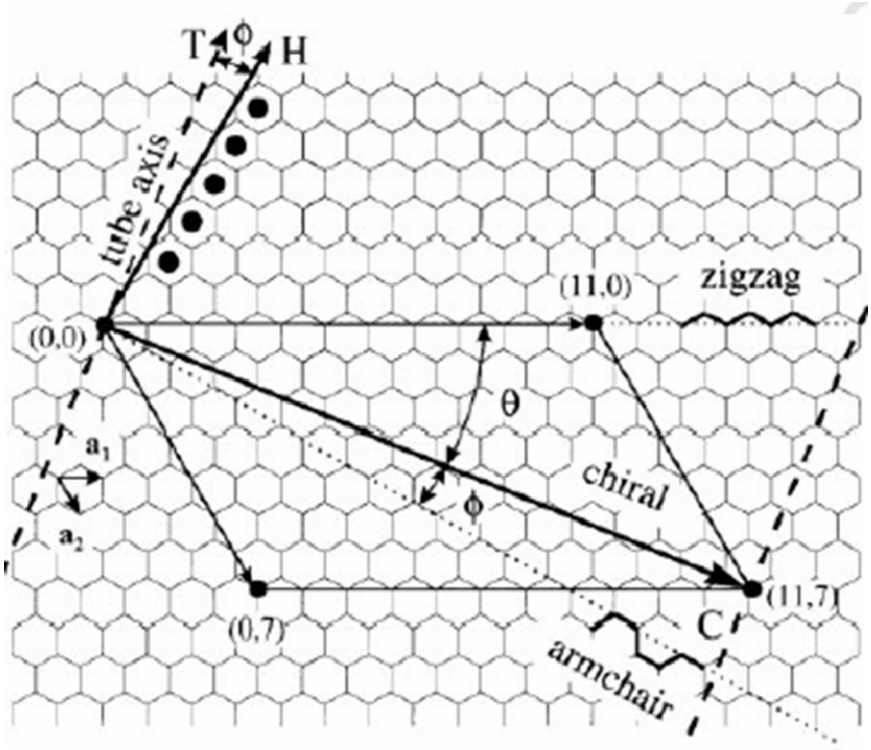

Fig.2-7 Structure of a carbon nanotube

2.3.3 Detailed Structure

The average diameter of a SWNT is 1.2 nm [32]. However, nanotubes can vary in size, and they aren't always perfectly cylindrical. The larger nanotubes, such as a (20, 20) tube, tend to bend under their own weight [33]. The diagram at right shows the average bond length and carbon separation values for the hexagonal lattice. The carbon bond length of 1.42 Å was measured by Spires and Brown in 1996 [32] and later confirmed by Wilder et al. in 1998 [31]. The C-C tight bonding overlap energy is in the order of 2.5 eV. Wilder et al. estimated it to be between 2.6 eV - 2.8 eV while at the same time, Odom et al. estimated it to be 2.45 eV [34]. A (10, 10) Armchair tube was found to have C_{5V} symmetry [35] which has the following character table:

2.3.4 Ropes of Carbon Nanotubes

In 1996, Thess et al. measured the properties of ropes of carbon nanotubes [35]. As shown in the diagram at right, ropes are bundles of tubes packed together in an orderly manner. They found that the individual SWNTs packed into a close-packed triangular lattice with a lattice constant of about 17 Å. This was later confirmed by Gao, Cagin, and Goddard in 1997 [36]. In addition, they concluded that the density, lattice parameter, and interlayer

spacing of the ropes was dependent on the chirality of the tubes in the mat. (10, 10) Armchair tubes had a lattice parameter of 16.78 Å and had a density of 1.33 g/cm^3. Zigzag tubes of the chirality (17, 0) had a lattice parameter of 16.52 Å and a density of 1.34 g/cm^3. Mats made of (12, 6) chiral SWNT's had a lattice parameter of 16.52 Å and a density of 1.40 g/cm^3. The space between the tubes was also dependent on chirality. Armchair tubes had a spacing of 3.38 Å, zizzag tubes had a spacing of 3.41 Å, and (2n, n) chiral tubes had a interlayer spacing value of 3.39 Å. Compare these values to the spacing between the layers of graphite sheets, and the spacing between the variant walls of a MWNT, both about 3.4 Å[37]. As a good estimate, the lattice parameter in CNT ropes is d + 0.34 nm, where d is the tube diameter given above. The eletrical transport properties of SWNTs has been recently studied has raised some controversy. The conductance of a tube is quantized, and a nanotube acts as a ballistic conductor. Nanotubes also have a constant resistivity, and a tolerance for very high current density.

2.3.5 Ballistic Conductance

In 1998, Stephan Frank et al. experimented on the conductance of nanotubes [38]. Using a SPM, he carefully contacted nanotube fibers with a mercury surface. His results revealed that the nanotube behaved as a ballistic conductor with quantum behavior. The MWNT conductance jumped by increments of 1 G_0 as additional nanotubes were touched to the mercury surface. The value of G_0 was found to be 1/12.9 kΩ^{-1}, where $G_0 = 2e^2/h$. The coefficent of the conductance quantum was found to have some suprising integer and non-integer values, such as 0.5 G_0. Later, in 1999, Sanvito, Kwon, Tománek, and Lambert, used a scattering technique to calculate the ballistic quantum conductance of MWTNs [39]. They found that their results explained these unexpected conductance values found by Frank in 1998. Sanvito et al. stated that some of the quantum conductance channels were blocked by interwall reactions. Also, the interwall reactions of MWNTs were found to redistribute the current over individual tubes across the structure nonuniformly.

2.3.6 Resistivity and Maximum Current Density

Relatively early in the research of nanotubes, Thess et al. calculated the resistivity of ropes of metallic SWNTs to be in the order of 10^{-4} Ω-cm at 300 K [35]. They did this by measuring the resistivity directly with a four-point technique. One of their values they measured was 0.34 x 10^{-4}, which they noted would indicate that the ropes were the most

highly conductive carbon fibers known, even factoring in their error in measurement. In the same study his measurements of the conductivity, Frank et al. was able to have reach a current denisty in the tube greater than 107 A/cm^2 [38].

2.3.7 Thermal Conductivity

There seems to be some disagreement into the exact nature of the thermal conductivity of carbon nanotubes, although most agree that thermal conductivity seems to change depending on temperature, and possible also on current and vacancy concentration. In 1999, J. Hone, M. Whitney, and A. Zettle found that the thermal conductivity was temperature dependent, and was almost a linear relationship [40]. They suggested that the conductivity was linear in temperature from 7 K to 25 K. From 25 K to 40 K, the line increases in slope, and it arises monotonically with temperature to above room temperature. They proposed a model to explain the low temperature behavior, which is:

$$k_{zz} = \Sigma C v_z^2 \tau \qquad (2\text{-}1)$$

Where k_{zz} is the slope of the line on the graph, C is the heat capacity, ν is the sound velocity, and τ is the relaxation time, which is approximately 10^{-11} s. They also found that the thermal conductivity for a single rope at room temperature could vary between 1800 - 6000 W/m-K. Also that year, Che, Cagin, and Goddard numerically calculated the thermal conductivity of a (10, 10) nanotube to approach 2980 W/m-K as the current applied to it is increased [41]. In 2000, Berber, Kwon, and Tomànek determined the thermal conductivity of carbon nanotubes and its dependence on temperature [42]. They confirmed the suggestion of Hone et al. in 1999 by suggesting an unusually high value of 6,600 W/m-k for the thermal conductivity at room temperature. They theorized that these high values would be due to the large phonon mean free paths, which would concur with Hone's model suggested above. Both groups stated that these values for thermal conductivity are comparable to diamond or a layer of graphite. However, Berber et al. suggested that the graphs of the temperature dependence of thermal conductivity looked much less linear than previously proposed by Hone et al. Instead of a near-linear graph with a positive slope, their graph showed a positive slope from low temperatures up to 100K, where it peaks around 37,000 W/m-K. Then, the thermal conductivity drops dramatically down to around 3000 W/m-k when the temperature approaches 400 K.

Chapter 3

Experimental setups

3.1 Bias-assisted microwave plasma chemical vapor deposition system

Fig.3-1 schematically depicts the layout of the MPECVD system. A quartz tube is vertically attached to a rectangular waveguide used as deposition chamber. The microwave from a magnetron source (model IMG 2502-S, IDX Tokyo, Japan) is supplied to the quartz tube through an isolator, and a power meter. Then the microwave power is coupled to the quartz tube through an aluminum waveguide with a hole drilled through from top to bottom face. Aluminum tubes extend out from both holes; the tube extensions are water-cooled as well. A sliding short circuit is then attached at the end of the waveguide. The lower position of the quartz tube is connected a stainless steel multi-port chamber equipped with a rotary pump. The substrates are positioned in the middle of the quartz tube waveguide intersection and held vertically by a substrate holder which is 20mm in diameter, made of molybdenum. Under the holder, attached a tantalum wire which is connected to the bias system; it was used as the lower electrode in the bias treatment stage. A quartz protector under the holder to protect the plasma not attracted to the tantalum wire attached to the molybdenum. The upper electrode, a molybdenum plate of 20mm in diameter which is placed 35 mm above the substrate, also attached to a tantalum wire. The controlled amount of the source gases was introduced into the chamber by mass flow controllers (model 647B, MKS instrument, Inc., USA) from the upper end of the quartz tube. A small window was cut in the waveguide at the center of the plasma cavity, allowing direct observation of the plasma.

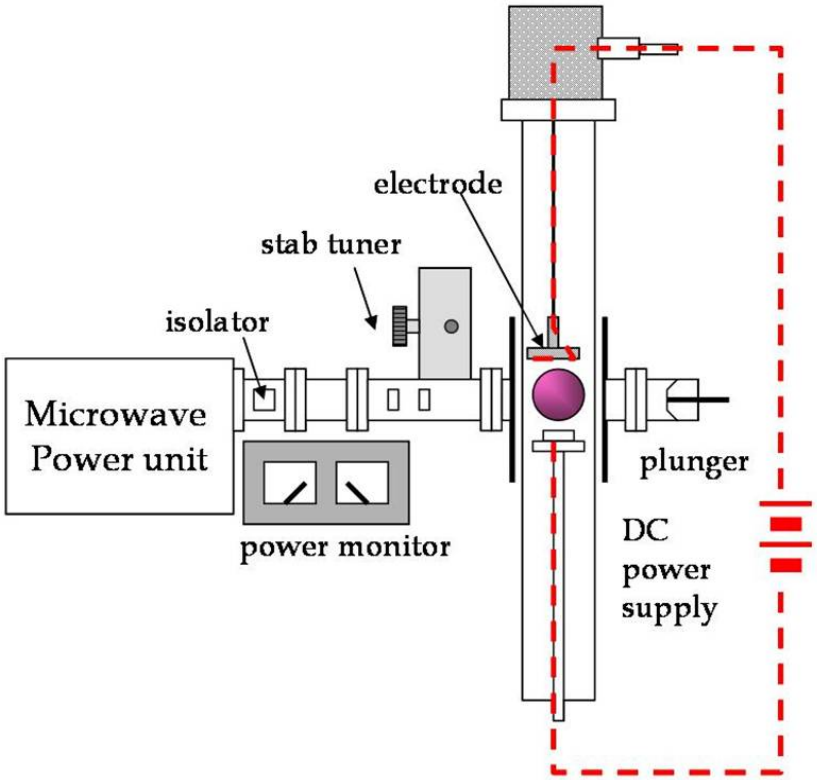

Fig.3-1 Schematic diagram of MWPECVD

3.2 Analysis Instruments

3.2.1 Scanning Electron Microscopy (SEM)

Scanning electron microscopy is used to observe the surface morphology of wide range kinds of objects. It has the advantage of rather easy sample preparation, high image resolution, large depth of field, and high magnification. A common SEM contains an electron gun to generate electron beams, which will be accelerated under 0.4-40kV voltage. By deflecting the incident beams with the focusing coils, a two dimensional image can be obtained by detect the reflected secondary electrons and the backscatter electrons. The model we use here is JEOL 6500, with field emission electron source and 15kV accelerate voltage.

3.2.2 Transmission Electron Microscopy (TEM)

Transmission electron microscopy (TEM) is by far the most important technique for studying defects in great detail. Much of what was stated before about defects would be speculative theory, or would never have been conceived without TEM. In a typical TEM a static beam of electrons at 100-400kV accelerating voltage illuminate a region of an electron

transparent specimen which is immersed in the objective lens of the microscope. The transmitted and diffracted electrons are recombined by the objective lens to form a diffraction patter in the back focal plane of that lens and a magnified image of the sample in its image plane. A number of intermediate lenses are used to project either the image or the diffraction patter onto a fluorescent screen for observation. The screen is usually lifted and the image formed on photographic film for recording purposes. A simple diagram of typical TEM instrument is shown in Fig. 3-2.

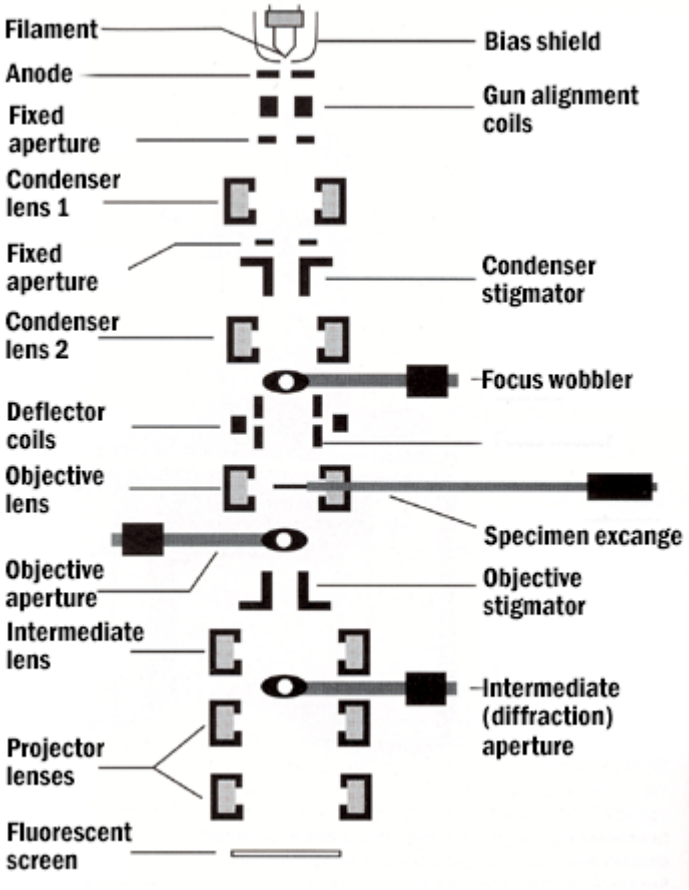

Fig.3-2 Schematic diagram of a TEM.

3.2.3 Raman Spectroscopy

A powerful and nondestructive method to determine nanotube structure is Raman spectroscopy, which is widely used to study the vibrational modes of carbon-based graphitic nanostructures. While photons illuminate a molecule or a crystal, they react with the atoms accompany with momentum change or energy exchange. By collecting the scatter photons,

we can obtain a sequence of spectrum, including Raman scattering (inelastic scattering) and Reyleigh scattering (elastic scattering). The photon of Raman scattering can be classified into two kinds, Stoke side which photons loss energy or the molecules gains energy, and anti-Stoke side, which photons gains energy or molecules loss energy. Generally, Stoke side is used to characterize the material. As Raman spectrum provides information of crystallinity and bonding, it has become the most direct and convenient way to identify carbon related materials. The instrument we use is HORIBA Jobin Yvon, HR800. The source we use is He-Ne laser with wavelength of 632.82nm and power of 12mW. The spectral slit width is $0.4cm^{-1}$.

3.3.4 Energy Dispersive X-ray Analysis (EDX)

EDX is a microanalytical technique that uses the characteristic spectrum of x-rays emitted by the specimen after excitation by high-energy electrons to obtain information about its elemental composition. The ranges of elements detectable by EDX and electron energy loss spectroscopy (EELS) are somewhat complementary; EDX is generally better suited to detecting elements of high atomic number (Z) whereas EELS can readily detect low-Z elements. Unlike EELS, EDX does not provide chemical information (except through quantitative analysis in some cases). Compared to EELS, EDX is a relatively simple technique and provides rapid qualitative microanalysis of the specimen. The spatial resolution is determined by the probe size, beam broadening within the specimen, and the effect of backscattered electrons on the specimen around the point of analysis.

3.3.5 X-ray Diffraction (XRD)

XRD is a useful tool to analyze the crystallography of specimen. Also, we could determine the mean particle size of particles by XRD. When X-ray radiation passes through matter, the radiation interacts with the electrons in the atoms, resulting in scattering of the radiation. If the atoms are organized in planes and the distances between the atoms are of the same magnitude as the wavelength of the X-rays, constructive and destructive interference will occur. This results in diffraction where X-rays are emitted at characteristic angles based on the spaces between the atoms organized in crystalline structures called planes. Most crystals can have many sets of planes passed through their atoms. Each set of planes has a

specific interplanar distance and will give rise to a characteristic angle of diffracted X-rays. The relationship between wavelength, atomic spacing (d) and angle was solved as the Bragg Equation. If the illuminating wavelengh is known and the angle can be measured then the interplanar distance can be calculated from the Bragg equation: $n\lambda = 2d\sin\theta$. A set of 'd-spaces' obtained from a single compound will be represent the set of planes that can be passed through the atoms and can be used for comparison with sets of d-spaces obtained from standard compounds.

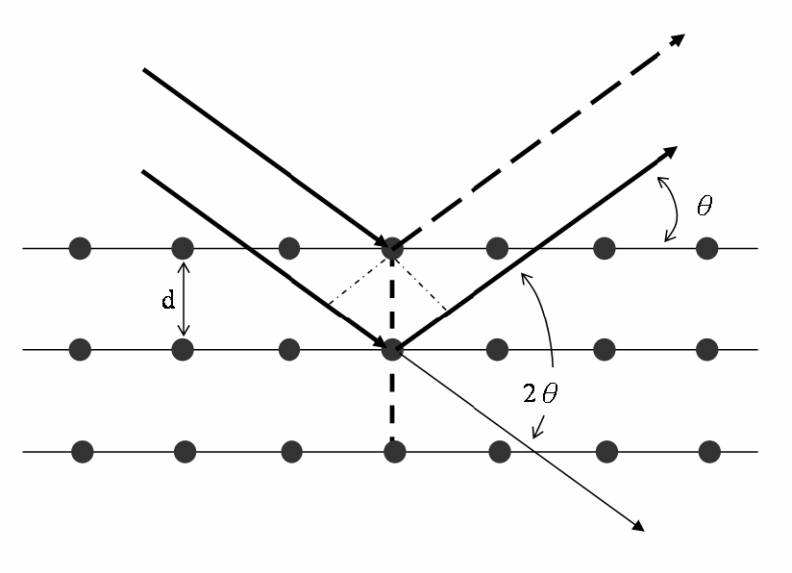

Fig. 3-3 Schematic diagram of Bragg's law.

3.2.6 Cyclic Voltammetry (CV)

Cyclic voltammetry is the most widely used technique for acquiring qualitative information about electrochemical reactions. The power of cyclic voltammetry results from its ability to rapidly provide considerable information on the thermodynamics of redox processes and the kinetics of heterogeneous electron-transfer reactions, and on coupled chemical reactions or adsorption processes. A simple potential wave form that is often used in electrochemical experiments is the linear wave form i.e., the potential is continuously changed as a linear function of time. The rate of change of potential with time is referred to as the scan rate (v).A more commonly used variation of the technique is cyclic voltammetry, in which the direction of the potential is reversed at the end of the first scan. Thus, the waveform is

usually of the form of an isosceles triangle. This has the advantage that the product of the electron transfer reaction that occurred in the forward scan can be probed again in the reverse scan. In addition, it is a powerful tool for the determination of formal redox potentials, detection of chemical reactions that precede or follow the electrochemical reaction and evaluation of electron transfer kinetics. Fig.3-4 is the experimental setup of our cyclic voltammetry measuremsnt. Cyclic voltammetries were recorded by CH Instrument 614B potentiostat using a three-electrode cell. A platinum wire served as the counter electrode and a saturated calomel electrode (SCE), was used as the reference electrode. The working electrode is a Pt wire attached with a 0.25 cm^2 thin Pt foil, which is used to contact with the testing sample.

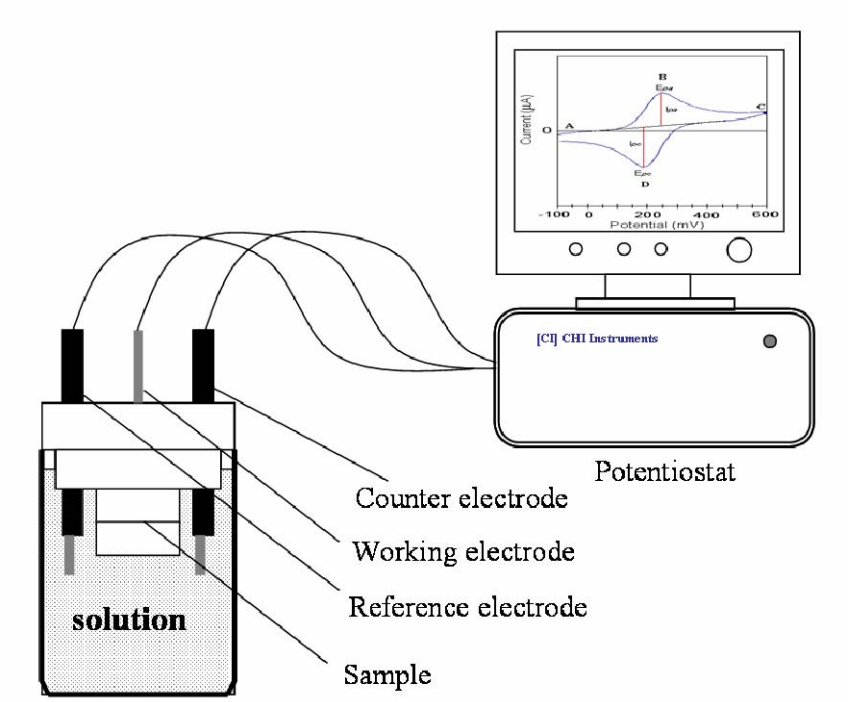

Fig.3-4 Schematic diagram of a cyclic voltammetry experiment.

3.2.7 Single Cell testing

The MEA (membrane electrode assembly) for the DMFC test cell was made by hot-pressing pretreated Nafion 117 together with an anode sheet and a cathode sheet at 500 kgf/cm^2. The anode sheet was a carbon cloth (E-TEK) with carbon nanotube-supported Pt catalyst layer. The cathode sheet was a carbon cloth with a carbon-supported 40 wt% Pt catalyst layer supplied by E-TEK. Polarization curves were obtained by the fuel cell testing

system (BEAM 75M FC system) using a commercial single cell with a working area of 1 cm^2. The fuel was 2 M CH_3OH delivered at 2 ml/min by a micropump and oxygen flow was regulated by a flowmeter at 500 cm^3/min.

Chapter 4

Dispersion of Pt nanoparticles on MWCNTs by different routes

4.1 Directly fabricating carbon nanotubes on carbon cloth (GDL) and dispersion of Pt nanoparticles on carbon nanotubes based electrodes by sputtering

4.1.1 Introduction

Carbon nanotubes and related materials have been investigated as catalyst supports for fuel cell applications in the past decades. The dispersions of Pt or Pt-Ru catalysts on CNTs have been widely reported recently, and shown the improvement of electrocatalytic properties by using CNTs as catalyst supports [43-49]. However, conventional dispersion approaches of Pt on CNTs based on wet impregnation and chemical reduction of the metallic precursors, which require a series of complex procedures and a lot of time. Also, the remove of chemical solvents and other contaminants is a crucial step for preventing the degradation of cell performance. It is everyone's expectation to find out a simple and convenient way for fulfilling the needs of catalysts deposition.

In this sction, a fast, convenient and simple way to disperse Pt on CNTs supports is demonstrated by using a rf-magnetron sputtering system.

4.1.2Experimental procedures

Multi-wall carbon nanotubes were fabricated directly on carbon cloth (E-TEK) by bias assisted microwave plasma enhanced chemical vapor deposition (see Fig.3-1). Iron was first deposited on the carbon cloth with area of 1cm^2 by ion beam sputtering deposition for 10 min. It was mainly used as the catalyst for synthesizing carbon nanotubes. The reactive gas species were methane and hydrogen with a ratio of 1/4. The microwave power and the working pressure were set at 300W and 10Torr, respectively. The additive bias was adjusted from 0V to -200V. All of the experimental conditions for synthesizing MWCNTs are listed in Tab. 4-1. An optical pyrometer was used to monitor the substrate temperature which was about 600^oC.

The deposition of platinum nanoparticles on carbon nanotubes was carried out by means of a rf-magnetron sputtering (SYSKEY rf-magnetron sputtering), which is shown in Fig.4-1. The experimental conditions of deposition of Pt nanoparticles by rf-magnetron sputtering are listed in Tab. 4-2. The metal loading of Pt/CNTs catalyst can be easily

controlled by varying sputtering time, which depicts in Fig.4-2. The metal loading was measured by TGA and EDX. Based on MWCNTs will totally burn away at 900^{o}C in O_2 atmosphere, and the residues should be Pt nanoparticles. Therefore, we can identify the metal loading of Pt by TGA.

Polarization curves were obtained by the fuel cell testing system (BEAM 75M FC system) using a commercial single cell with a working area of 1 cm^2. 2M methanol solution was fed to the anode side at a flow rate of 3 ml min^{-1}. Oxygen was fed to the cathode side at a flow rate of 500 ml min^{-1}. The single cell was operated at 70^{o}C. The details of the operation condition are shown in Tab.4-2.

Table 4-1 Growth condition of MWCNT by MWCVD

Metallic catalyst	Fe
Microwave power	300W
Reactive gas	CH_4, H_2
Base pressure	10^{-3} Torr
Working pressure	10 Torr
Growth time	20 min
Additive bias	0 ~ -200 V

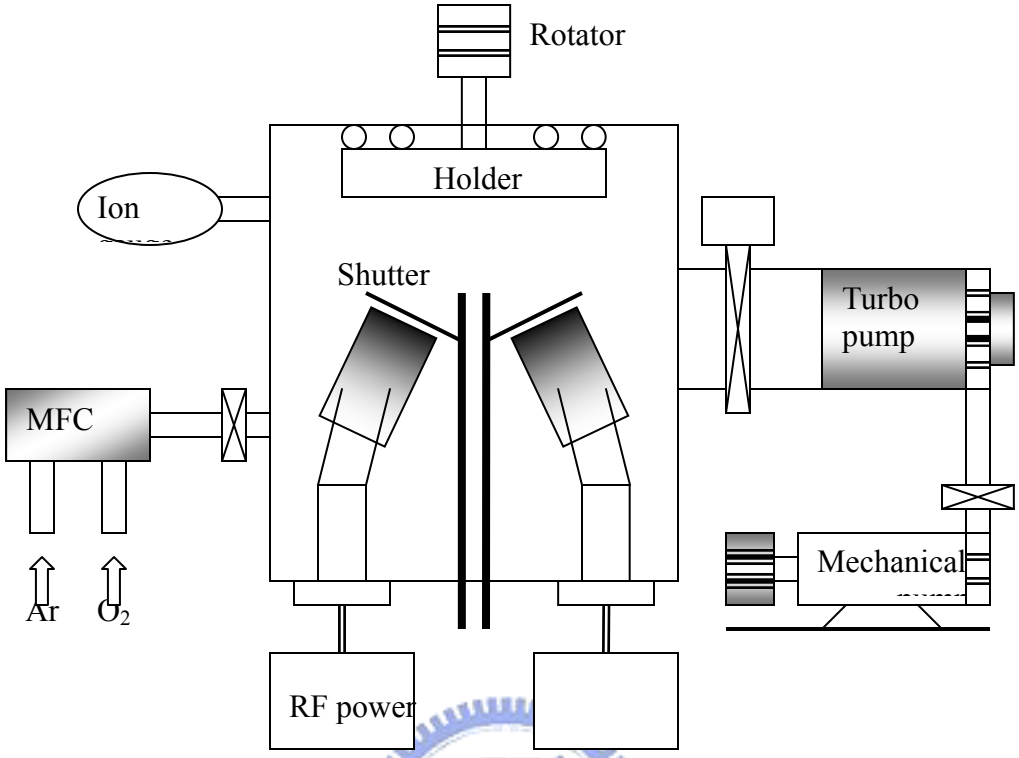

Fig.4-1 Schematic diagram of a rf-magnetron sputtering system

Tab.4-2 Experimental conditions of deposition of Pt

Target	Pt
Working pressure	10 mTorr
Power	40W
Base pressure	6 x 10^{-6} Torr
Sputtering time	0 ~ 20 min
Etching gas	Ar 12 sccm

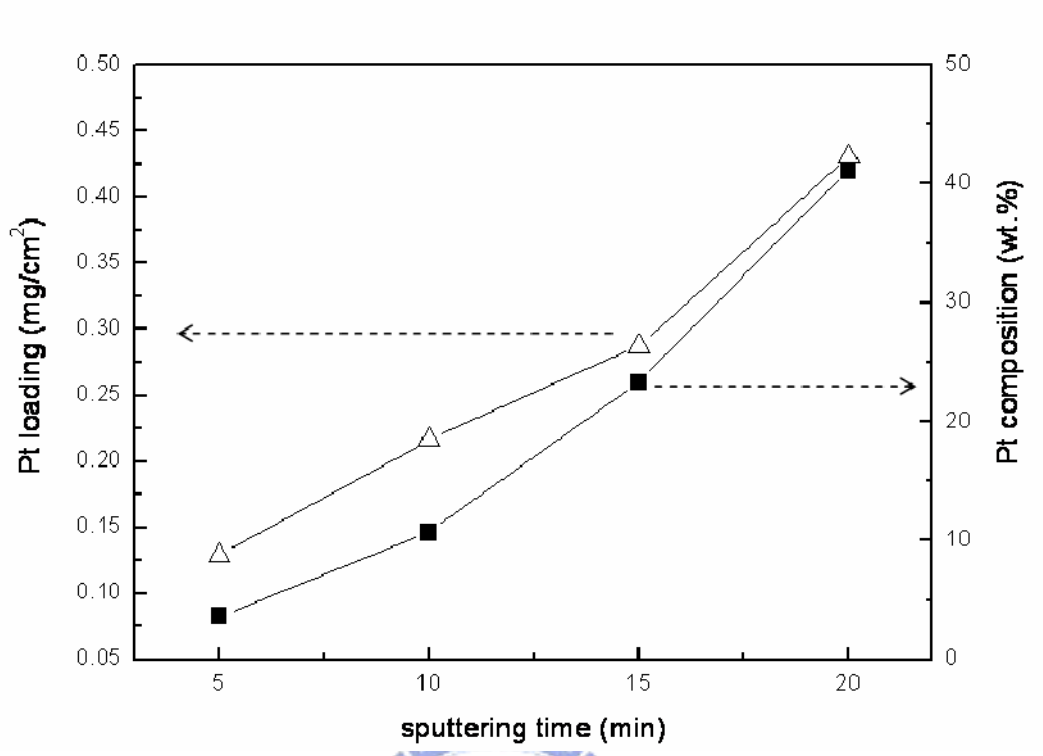

Fig.4-2 The metal loading and wt.% of sputtered Pt/CNTs

Table 4-3 Operation conditions of single cell test

Cathode	Pt / MWCNTs
Anode	E-TEK(Pt-Ru 0.4 mg/cm2)
Cathode feed	O_2
Anode feed	CH_3OH
Operation tempt.	70°C
Activation time	3 h
O_2 flow rate	500 sccm
CH_3OH flow rate	50 sccm

4.1.3 Result and discusions

Fig.4-3 shows the carbon nanotubes were directly grown on carbon cloth by MWCVD under different additive bias. Fig.4-3 (a) is the image of carbon nanotubes grown without applying bias. Fig.4-3 (b), (c),and (d) are images of carbon nanotubes grown on carbon cloth with applying negative bias of -100V,-150V and -200 V, respectively. It is easy to find that the length of CNTs is enlarged with the increasing negative bias voltage. It has been reported generally that applying negative bias could enhance the nucleation density of diamond [50-52].This might enhance the growth rate of carbon nanotubes result in the elongation of tube's length. However, the distance between carbon nanotubes under -200V is very small. This is difficult to deposit noble catalysts onto the surface of carbon nanotubes uniformly by sputtering. On the contrary, carbon nanotubes grown without applied bias shown poor growth rate. Therefore, we choose the condition of applied -100V as the optimal bias voltage for growing CNTs on carbon cloth in this section. The BET surface area of the CNT samples, determined by N2 physisorption at 77 K, was about 90.31 2 m^2/ g. The nano-structure of the carbon nanotube grown under -100V is shown in Fig.4-4. The outer and inner diameter of carbon nanotubes are about 20 nm and 10nm, respectively. It is found that the amount of amorphous carbon around the outer shell of nanotube is very small; this indicates that the crystallinity of these carbon nanotubes is good.

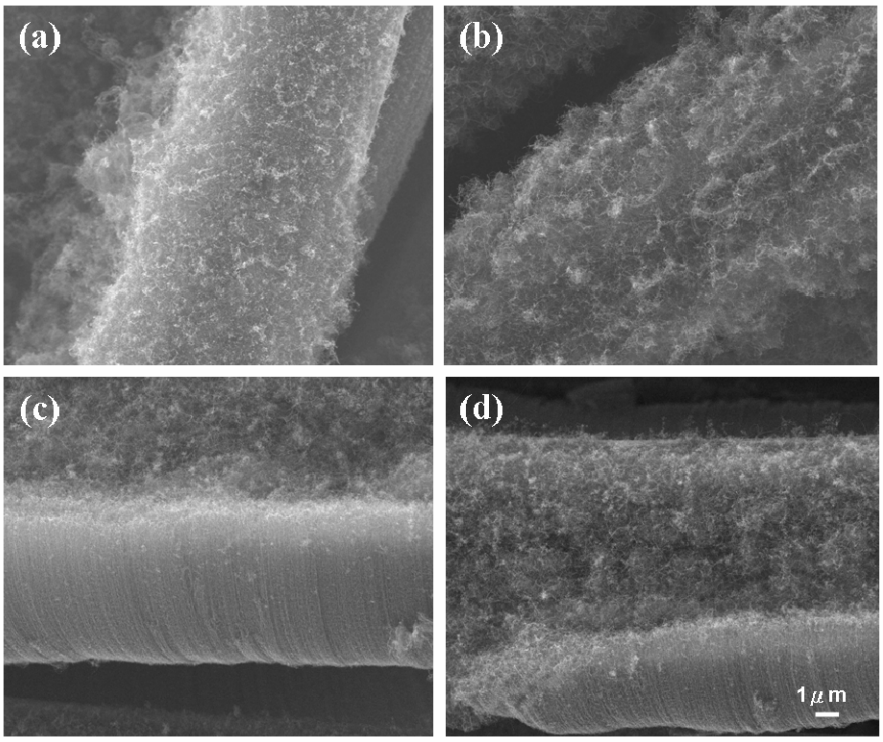

Fig.4-3 SEM images of different negative bias for synthesizing carbon nanotubes on carbon cloth: (a) 0V,(b)-100V,(c)-150V,and(d)-200V.

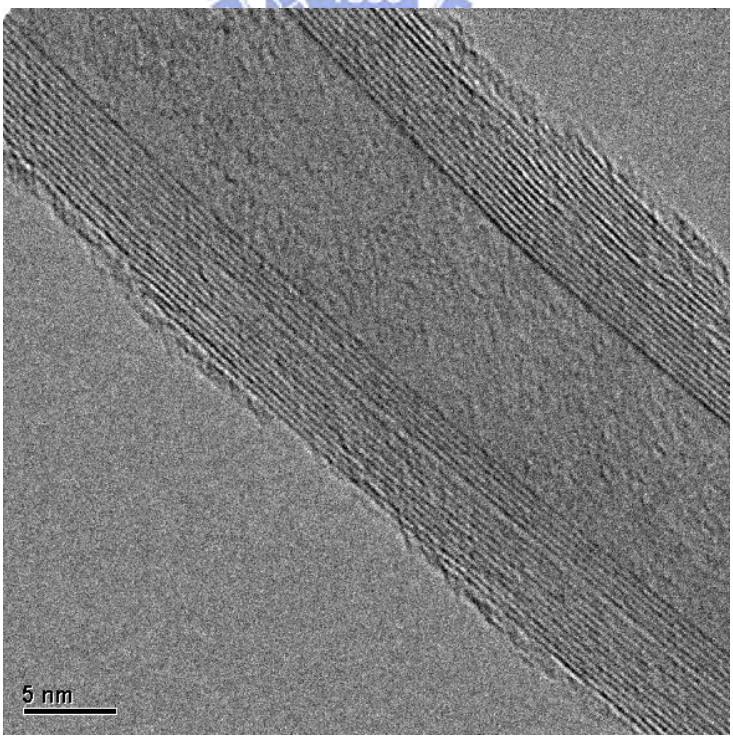

Fig.4-4 TEM images of carbon nanotubes growth with applied -100V.

The metal loading of Pt/CNTs catalyst was controlled by varying sputtering time. For the purpose of specificity and convenience, Pt5/CNTs, Pt10/CNTs, Pt15/CNTs and Pt20/CNTs were denoted as Pt nanoparticle deposited on carbon nanotubes supports by sputtering for 5 minutes, 10 minutes, 15 minutes and 20 minutes, respectively. The morphologies of sputter-deposited Pt/CNTs under various sputtering time observed by SEM were given in Fig.4-5. The Pt particles become large from several nanometers to dozen of nanometers with the increasing sputtering times. It can be seen that Pt particles will aggregate when the sputtering times is over 10 minutes. Fig.4-6. depicts the histogram of Pt nanoparticles distribution of sputter deposited Pt/MWCNTs, which was made by randomly calculating 100 grains of Pt nanoparticles from TEM micrograph. This indicates that sputter deposited Pt/MWCNTs shows a narrow size distribution from Fig.4-6 and average diameter of Pt nanoparticle is 3.4 nm.

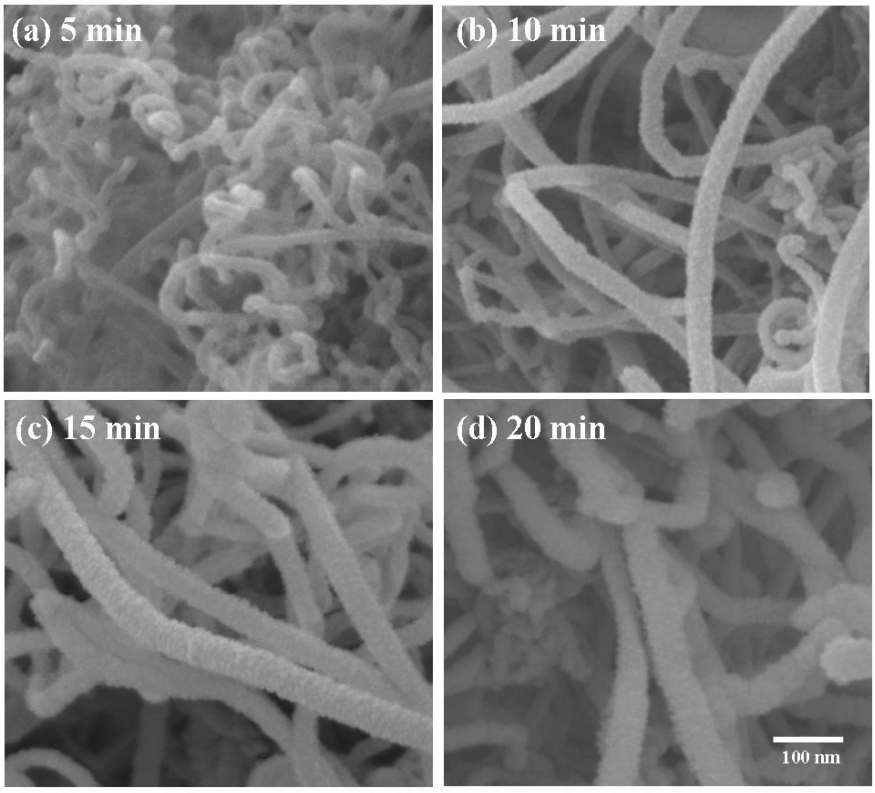

Fig.4-5 SEM images of platinum catalysts deposited on carbon nanotubes by sputtering for (a) 5min, (b) 10 min, (c)15 min and (d) 20 min.

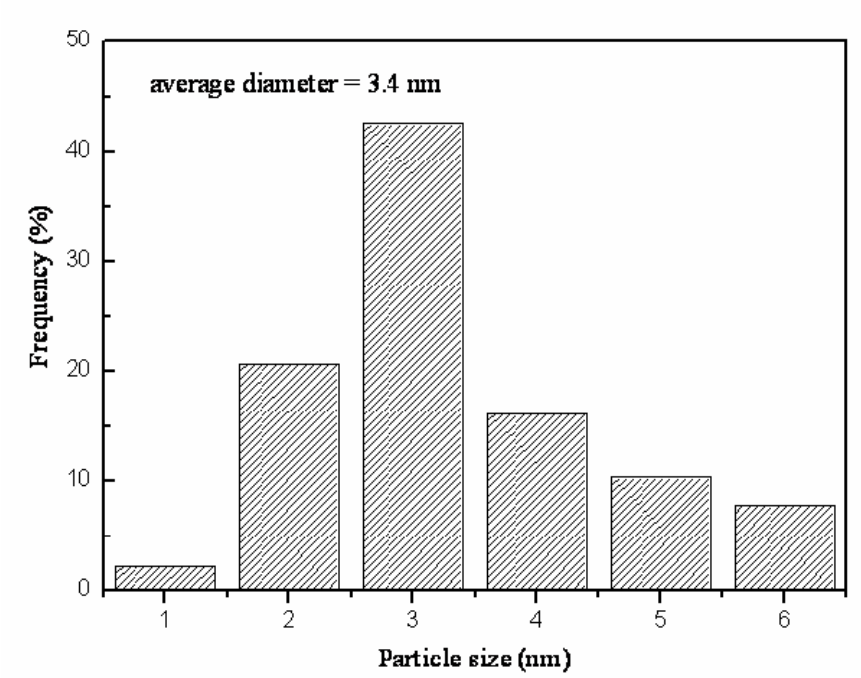

Fig. 4-6 Histogram of Pt nanoparticle diatribution of sputter deposited Pt/MWCNTs

Fig.4-7 shows CVs of Pt5/CNTs, Pt10/CNTs, Pt15/CNTs and Pt20/CNTs immersing in deaerated 1M H_2SO_4 solutions. Two peaks, corresponding to weak H-adsorption and strong H-adsorption are observed during cathodic potential sweep between 0.4 and 0.05 V. The strong, medium and weak H-desorption peaks between 0.4 and 0.05 V are also observed under anodic sweep [53]. By using the charge passed for H-adsorption QH, surface area of Pt (S_{Pt}) can be estimated from the equation below [54].

S_{Pt} /cm^2= QH/210 ($\mu C/cm^2$) (4-1)

The constant 210 in equation 4-1 is surface charge density of Pt. Each electrode was taken with a triangular potential sweep (50 mVs-1) between 0 and 1.0 V (vs. SCE) in 1 M H_2SO_4 solution for the determination of the surface area of Pt. Obviously, the great improvement of electrochemical property can be seen after using carbon nanotubes as the catalyst support. The H-adsorption peak has stronger intensity for Pt/CNTs due to the better dispersion and smaller particle size when compared with Pt/CC.

Characteristics of the Pt/CNTs in methanol solution, which were performed by cyclic voltammetry were measured in a deaerated 1M CH_3OH + 1 M H_2SO_4 solution between 0 and 1.0 V with a scan rate of 50 mVs-1. Methanol-oxidation current peaks are clearly observed at

0.8 V in the anodic sweep and at 0.6 V in the cathodic sweep from all samples, which represent the reactions of equation 4-2 and 4-3 [55].

$$Pt\text{-}(CH_3OH)ads \rightarrow Pt\text{-}(CO)ads + 4H^+ + 4e^- \quad (4\text{-}2)$$

$$Pt\text{-}CO + Pt\text{-}OH \rightarrow 2Pt + CO_2 + H^+ + e^- \quad (4\text{-}3)$$

From Fig.4-8, the peak current density of all CNTs supported electrocatalysts is obviously higher than that of Pt10/CC. The improvement in electrocatalytic activity was attributed to the present of carbon nanotubes supports, the small size distribution and good dispersion of Pt on carbon nanotubes. Pt20/CNTs exhibits the maximum current density, which is about 18.3 mA cm^{-2} according to the highest Pt loading of all Pt/CNTs samples. However, Pt10/CNTs shows higher mass efficiency than Pt15/CNTs and Pt20/CNTs, which could be observed in Tab.4-4. The degradation of the electroactivity of Pt15/CNTs and Pt20/CNTs can be explained as the aggregation of Pt nanoparticles during long sputtering times. Various electrochemical properties of these samples are listed in Tab.4-4. Tab.4-4 listed various calculated values of Pt loading (L_{Pt}, mg), working surface area of Pt (S_{Pt}, cm^2), methanol oxidation current density at 0.8V (i, mA cm^{-2}) of samples and mass efficiency of Pt (Me, mA mg^{-1} Pt). The polarization curves and power density curves of the MEA with sputtered Pt/MWCNTs cathode catalyst layer were show in Fig.4-9 and Fig.4-10, respectively. Obviously, the power density is increasing with the increasing of sputtering times. However, the power density of Pt20/MWCNTs cell is slightly higher than Pt15/MWCNTs cell, which is consistent with the results of CVs.

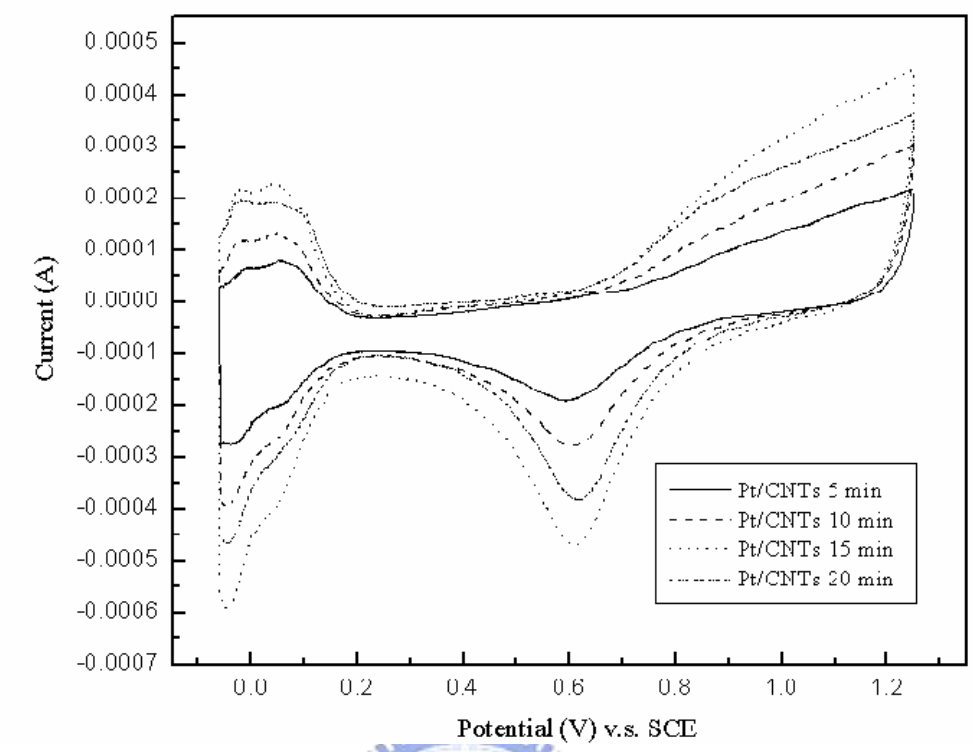

Fig.4-7 Cyclic votammograms of Pt/CNTs electrode with different sputtering times in 1.0 M H_2SO_4 aqueous solution.

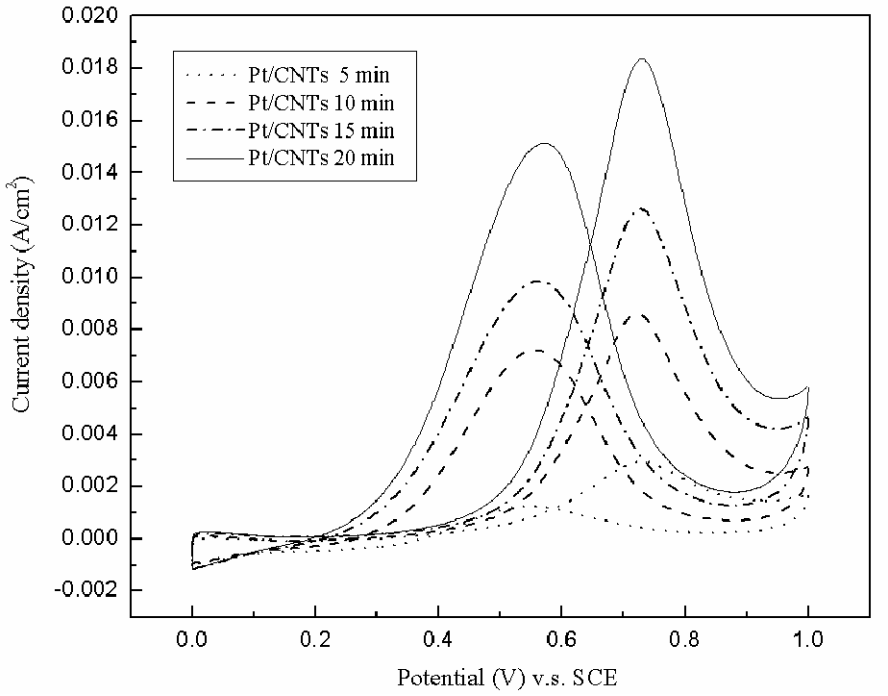

Fig.4-8 Cyclic votammograms of Pt/CNTs electrode with different sputtering times (a)5 min, (b)10 min, (c)15 min and (d)20 min in 1.0 M H_2SO_4 + 1.0 M $CH_3OH_{(aq)}$.

Tab.4-4 Electrochemical properties of sputtered Pt/CNTs

Sample	Power (W)	Time (min)	Loading (mg/cm^2)	S_{Pt} (cm^2)	$I_{0.8V}$ (mA)	ECS (m^2/g)	ME (mA/mg^2)
Pt5/CNTs	20	5	0.08	0.45	3.0	0.56	37.5
Pt5/CNTs	20	10	0.15	0.66	8.7	0.44	58.0
Pt5/CNTs	20	15	0.27	1.44	12.7	0.53	47.7
Pt5/CNTs	20	20	0.42	1.91	18.3	0.45	43.6

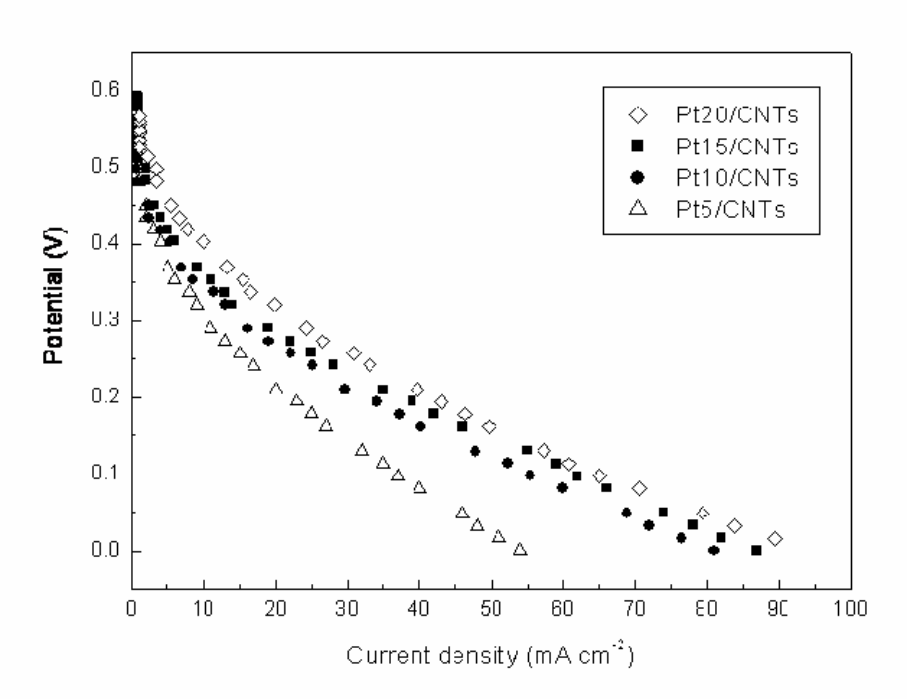

Fig.4-9 Polarization curves of the Pt/CNTs in $1cm^2$ single cell with CH_3OH/O_2 at flow rates of 50/500 sccm and 70°C

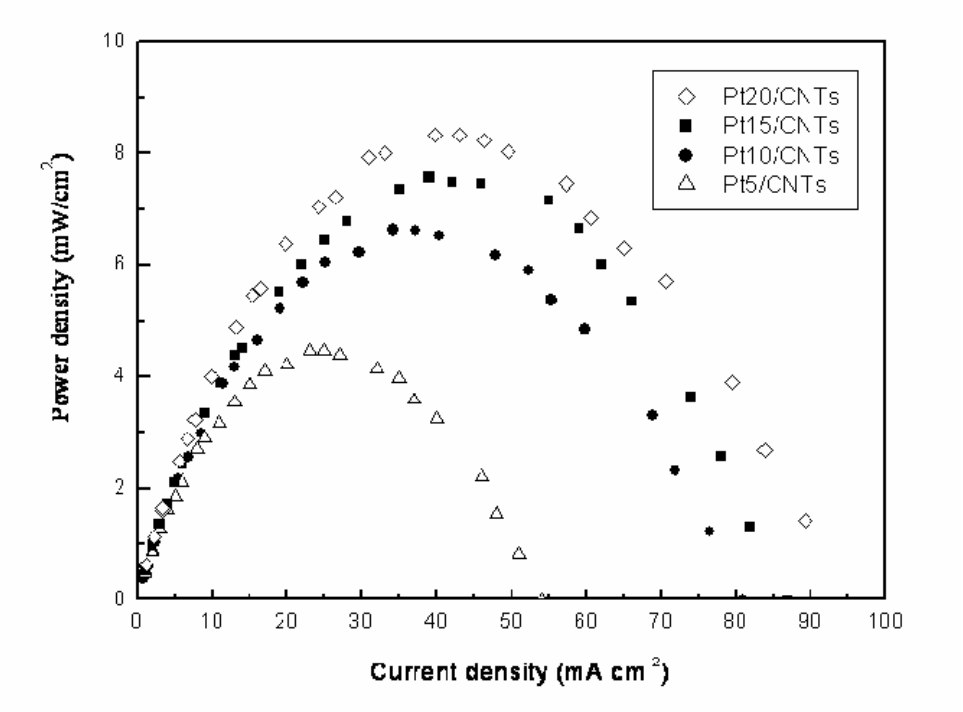

Fig.4-10 Power density curves of the Pt/CNTs in 1cm^2 single cell with CH_3OH/O_2 at flow rates of 50/500 sccm and 70°C.

4.1.4 Conclusions

Platinum nanoparticles were uniformly dispersed by sputtering on carbon nanotubes support as the cathode for a DMFC. The platinum surface area measured from the H-adsorption charge obtained by cyclic voltammetry has a maximum surface area of 1.91 cm^2 at 0.42 mg cm^{-2} Pt loading. The maximum current density is considered to be based on the surface area of Pt, which is 18.3 mA cm^{-2} from the measurement of cyclic voltammetry. The improvement in electrocatalytic activity was attributed to the present of carbon nanotubes supports, the small size distribution and good dispersion of Pt on carbon nanotubes. These results show that sputtering deposition is a feasible and convenient method for dispersing the electrocatalysts on catalyst support. However, the calculated mass efficiency (Me) of methanol oxidation at 0.8 V on different Pt/CNTs are listed in Table 4-4. Pt10/CNTs shows highest mass activity than the others, suggesting a higher utilization of the Pt nanoparticles. The mass efficiency of Pt/CNTs first increases with the increasing sputtering time and then decrease after sputtering over 10 min. It can be explained that although the longer sputtering time can get the higher methanol oxidation current density, the mass

efficiency will gradually decrease due to the aggregation of Pt nanoparticles after long time deposition. This is because Pt catalysts only deposited on the upper layers of carbon nanotubes, which results in the low utilization of catalyst. The shield effect restricts the further applications of dispersing Pt nanoparticle on catalyst supports by sputtering method.

4.2 Synthesis and dispersion of Pt nanoparticles on carbon nanotubes based electrodes by wet impregnation

4.2.1 Introduction

According to the shield effect of sputtering method, we focus on synthesizing and dispersing Pt on MWCNTs by polyol process and wet impregnation method in this section. A general method applied successfully for the synthesis of metallic nanoparticles is polyol process. Chemical reduction of metal species in liquid polyols under different reaction conditions is the basis of the polyol process. In this process, the metallic salts are dissolved in a liquid polyol (mostly ethylene glycol) and controlled heating is done, all in the absence of air, to obtain fine nanoparticles of the bimetallic nanoparticles. The experimental conditions have a large impact on the product and the particle size. The polyol solution is heated to reduce the metal(s) to a zero valence state. Typically, the heating temperature will range from 20^{o}C to 300 ^{o}C and the heating period will range from 1 minute to 5 hours. A high surface area conductive support material can be mixed with the polyol solution to form the supported catalysts for fuel cell applications. Carbon black (Vulcan XC-72) [56-59], activated carbon [60], carbon nanotubes [61-63] and porous metal oxide having a surface area from 20 to 2000 m^2 /g, are support materials.

In this section, we synthesized Pt nanoparticles by polyol process first and then dispersed on MWCNTs supports by a wet impregnation method for improve the distribution and uniformity of Pt nanoparticles.

4.2.2 Experimental procedures

The Pt nanoparticles were synthesized by the polyol processes and then dispersed on MWCNTs/CC sample. Initial materials of polyol process included metallic complex salts of $H_2PtCl_6 \cdot 6H_2O$ (SHOWA, 98 wt. %), polymer protector agent PVP-40 [FW~ 38000-40000, poly (vinyl pyrrolidone)) (Sigma, 99 wt. %)], and the solvent Ethylene Glycol (E.G.) (SHOWA, 99.5%). Polymer (PVP) is the protection agent to limit metal particle growth spacing. This method were expected a uniformly homogeneous nucleation and growth mechanism of nanoparticle. The reaction dominates by temperature control and solvent plays as reductant as well. By differing experimental time could obtain various Pt loadings. Detail chemical reduction mechanism of the solvent was introduced in other reports [64, 65]. Pt (IV) metal ion concentration was fixed at 10mM. Reaction chamber was pre-heated under 160^{0}C

for thermodynamic stabilization and reactants dipping rate was 2 ml min^{-1} till exhausted. After dipping, the entire reaction system was kept under 160 ^{o}C for 3h under N_2 flux 25 cm^3 min^{-1}. The whole reaction system was kept under 120 rpm magnetic stirring by temperature programmed hotplate and reaction temperature was kept within ± 1^{o}C. After acetone dilution, dark brown gelation precipitate formed as polymer and Nanoparticle composites. Residual sample re-dispersed into EtOH and further centrifuged at 15000 rpm for 5h. The experimental flow chart of synthesis of Pt nanoparticles by polyol method is presented in Fig.4-10. TEM image of Pt nanoparticles which were synthesized by polyol process is shown in Fig.4-11. The particles size ranges between 5 and 10 nm. Fig.4-12 depicts the histogram of polyol synthesized Pt nanoparticles distribution, which was made by randomly calculating 100 grains of Pt nanoparticles from TEM micrograph. After synthesis, the MWCNTs/CC was directly impregnated into Pt-PVP/EtOH solution and dried in a furnace under 200^{o}C for removing contaminants.

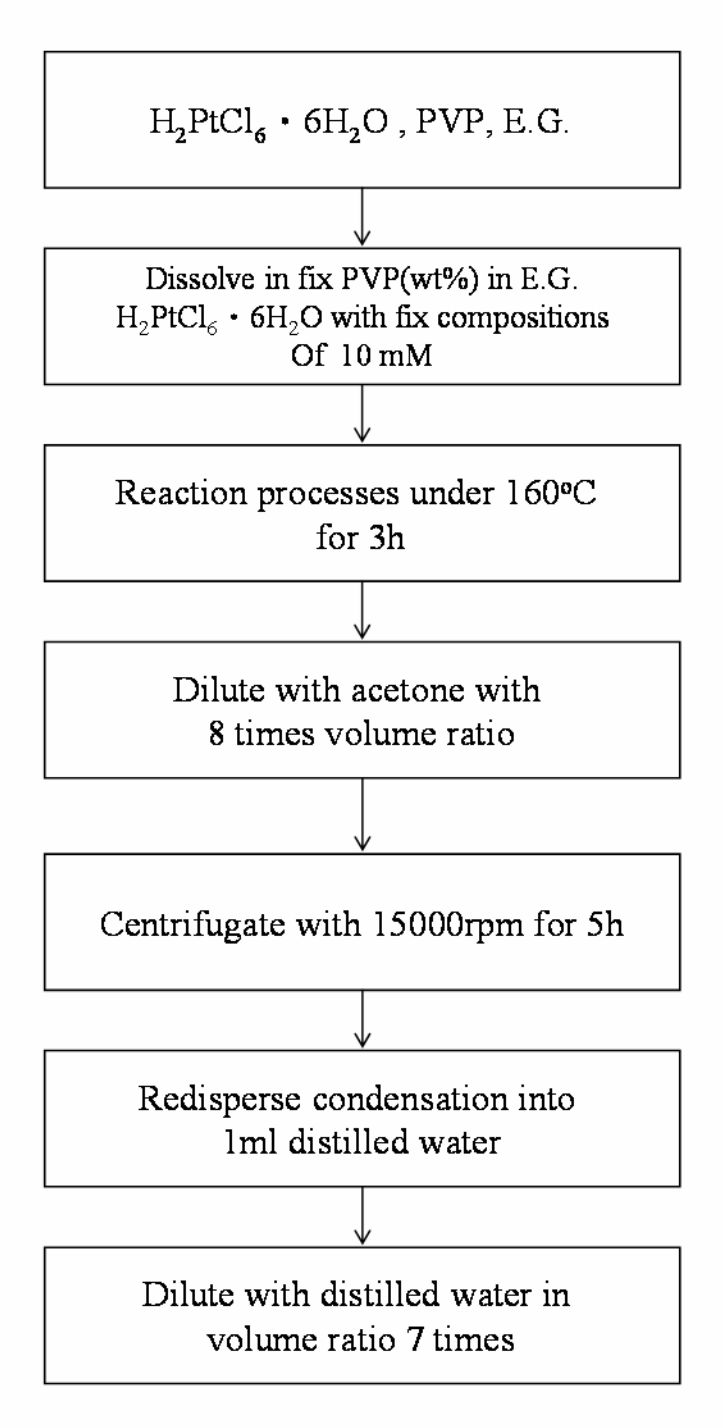

Fig.4-11 Experimental flow charts for synthesis of Pt nanoparticles.

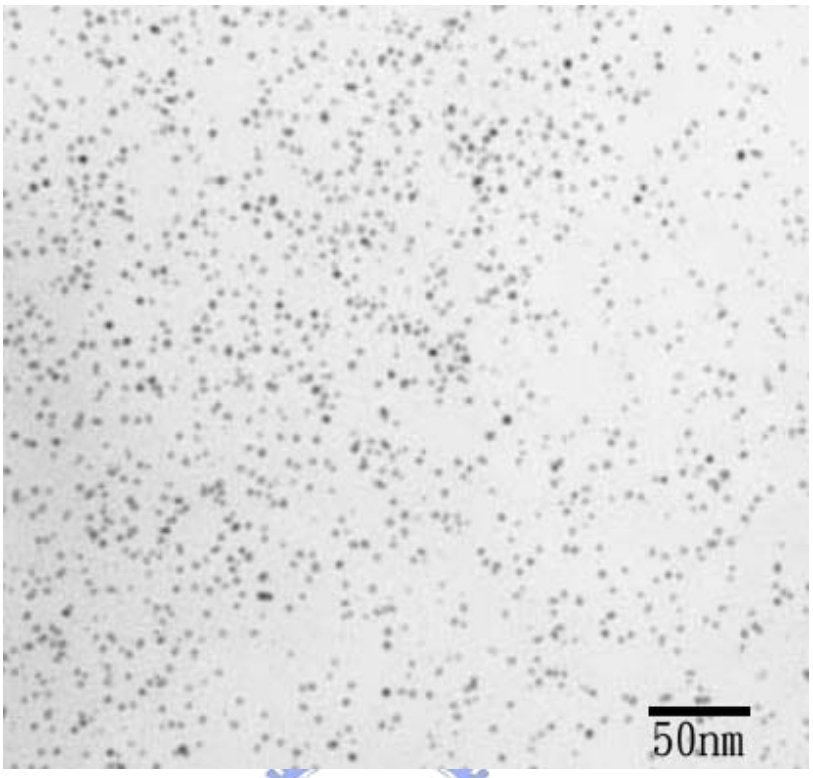

Fig.4-12 TEM image of Pt nanoparticles synthesized by polyol process

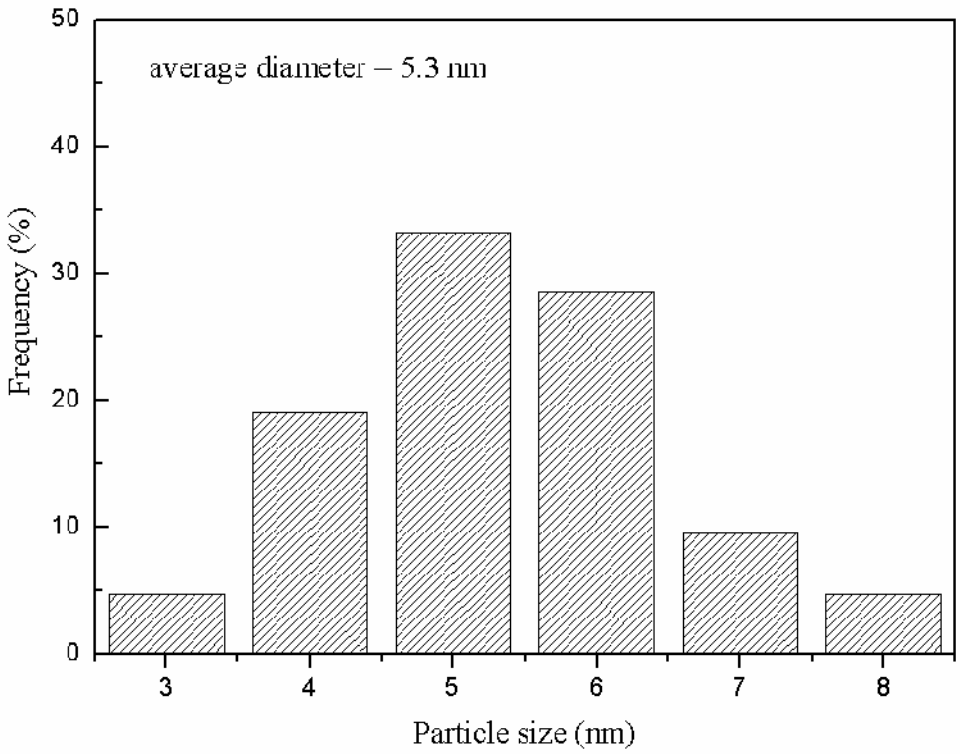

Fig.4-13 Histogram of polyol synthesized Pt nanoparticle distribution.

4.2.3 Result and discussion

Fig.4-13 are the SEM images of Pt/MWCNTs, the Pt nanoparticles were dispersed by wet impregnation. Fig.4-13 (b) is a higher magnification SEM image. Therefore, Pt nanoparticles can uniformly disperse on MWCNTs even the MWCNTs of the lower layers. The electrochemical properties of Pt/MWCNTs were investigated by cyclic voltammetry. Fig. 4-14 depicts the CVs of Pt/CC and Pt/MWCNTs in 1M H_2SO_4 with a scan rate of 50 mV/s. The real surface area of Pt/MWCNTs which we have discussed in chapter 4 is much larger than Pt/CC. This could be attributed to the presence of CNT supports greatly improved the uniformity and surface area of Pt. The electrooxidation of methanol of wet impregnated Pt/MWCNTs in 1M H_2SO_4 + 1M CH_3OH is characterized by CV in Fig.4-15. The current density of Pt/CNTs at 0.8V is much higher than Pt/CC, which is about 28 mA/cm^2. This can be explained that increased electrochemical surface area resulted from increased interfacial area between catalyst particles and thus it increased the catalytic surface area available for methanol oxidation reaction. Steady state polarization curve was measured by the fuel cell testing system (BEAM 75M FC system) under operating conditions comprising of a 2M methanol solution as the fuel and pure oxygen as the oxidant at a cell temperature of 70^oC. The details of the operation condition are same as Tab.4-3.

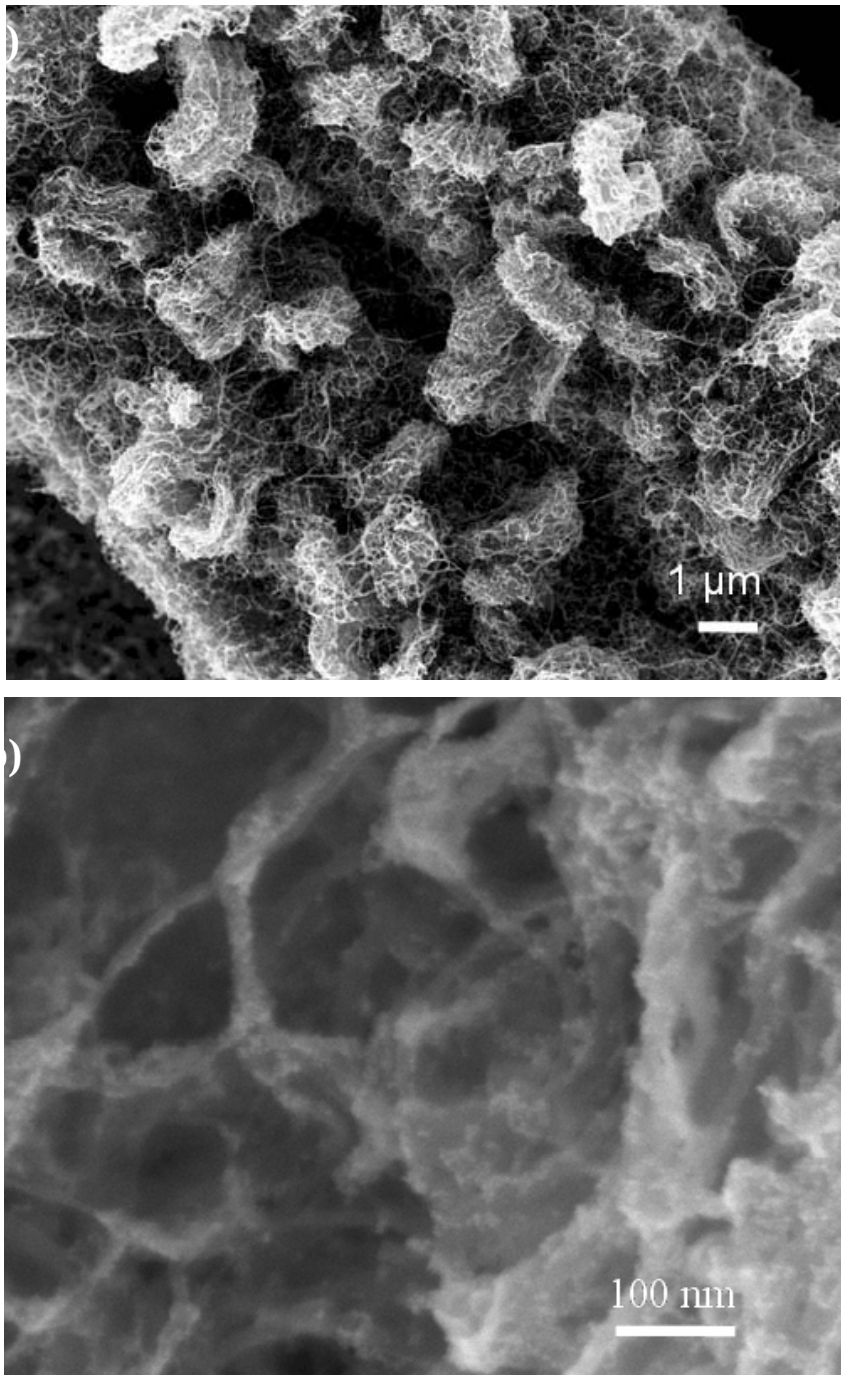

Fig.4-14 SEM images of Pt nanoparticles disperse on MWCNTs by wet impregnation.

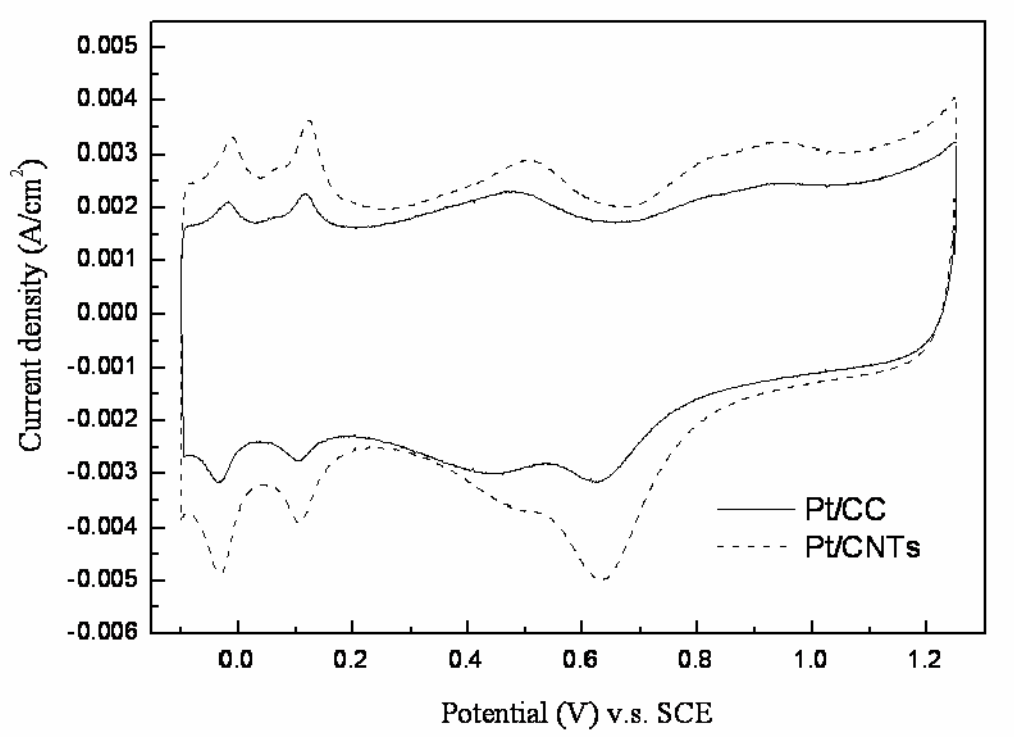

Fig.4-15 Cyclic votammograms of Pt/CNTs electrode in 1.0 M H_2SO_4 aqueous solution.

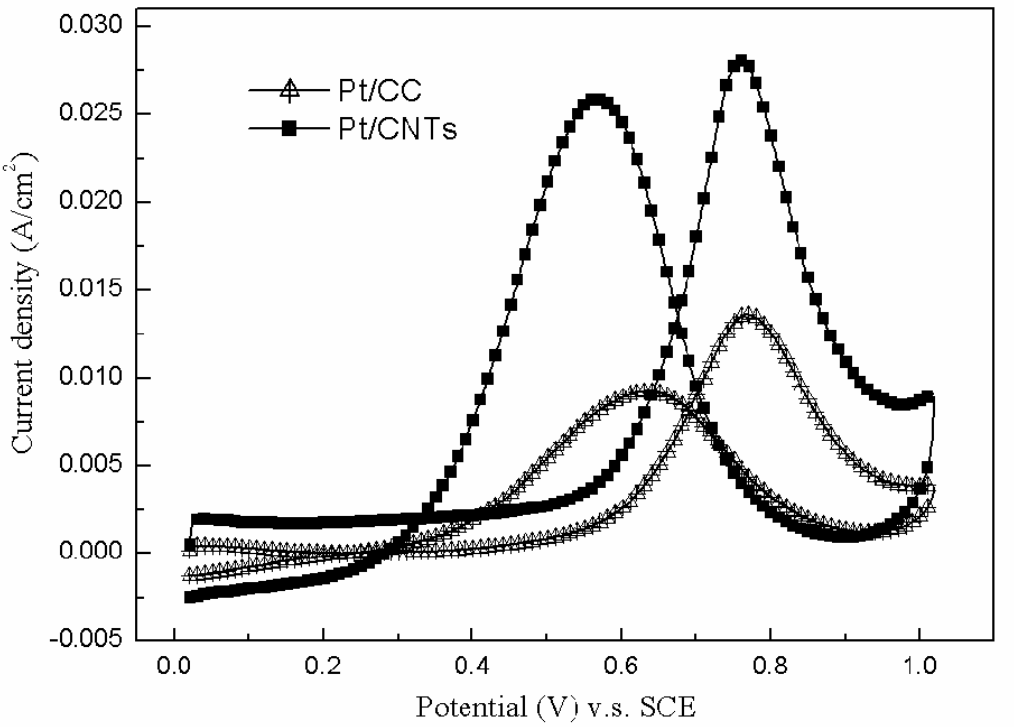

Fig.4-16 Cyclic votammograms of Pt/CNTs electrode in 1.0 M H_2SO_4 + 1.0 M CH_3OH aqueous solution.

Fig. 4-17 shows the performance of single cells with Pt/MWCNTs catalyst layer. The catalyst loading of the cathode is 0.4 mg/cm^2. The performance and power density of single fuel cell is much lower than the sputter deposited Pt/CNTs electrode. It could be ascribed to two reasons. First, the polyol synthesized Pt nanoparticles have larger particles than the sputter deposited. Secondary, due to the hydrophobic and chemical inert features of CNTs, dispersion of Pt nanoparticles on pristine CNTs results in the agglomeration of Pt nanoparticles. TEM image of the agglomeration of Pt nanoparticles on pristine MWCNTs is shown in Fig.4-18. It could be clearly seen that the diameter of polyol synthesized Pt nanoparticles is about 7 nm, but agglomerate to form a cluster with a diameter over 20 nm. Surface modification of MWCNTs is needed for resolving the agglomeration of Pt nanoparticles. The single cell performance of MWCNTs based DMFC with high Pt loading of 2.0 mg/cm^2 is presented in Fig.4-19. The power density of MWCNTs based DMFC is only 27.4 mW/cm^2. This shows that the agglomeration of Pt nanoparticles greatly degrades the electrocatalytic ability of Pt catalysts.

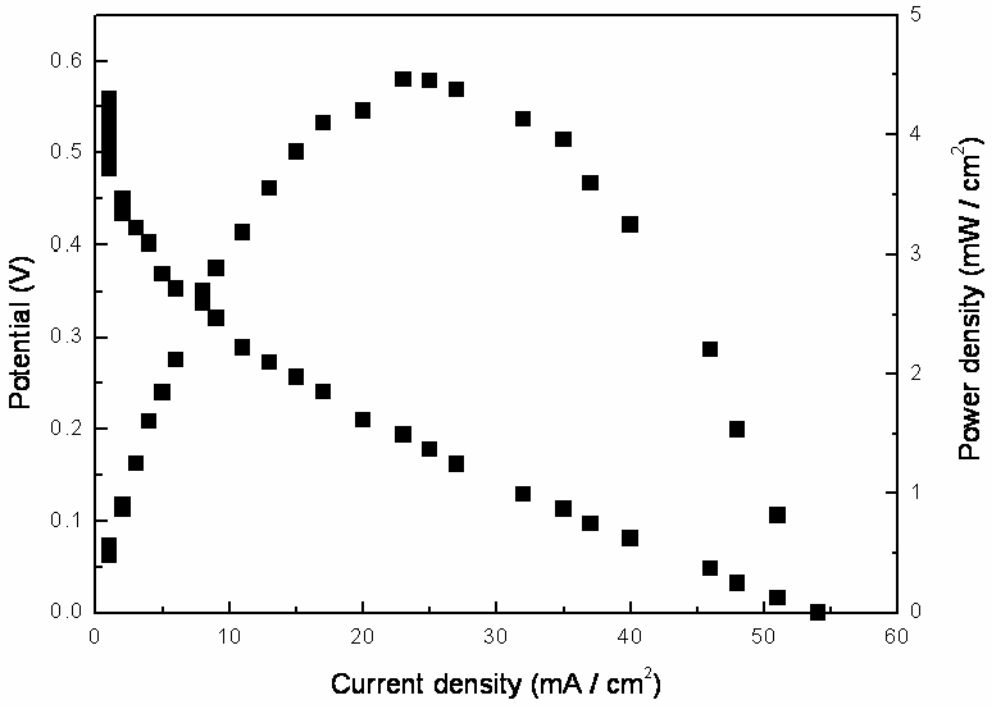

Fig.4-17 Polarization curves of the Pt/CNTs in 1cm^2 single cell with CH_3OH/O_2 at flow rates of 50/500 sccm and 70^{o}C.

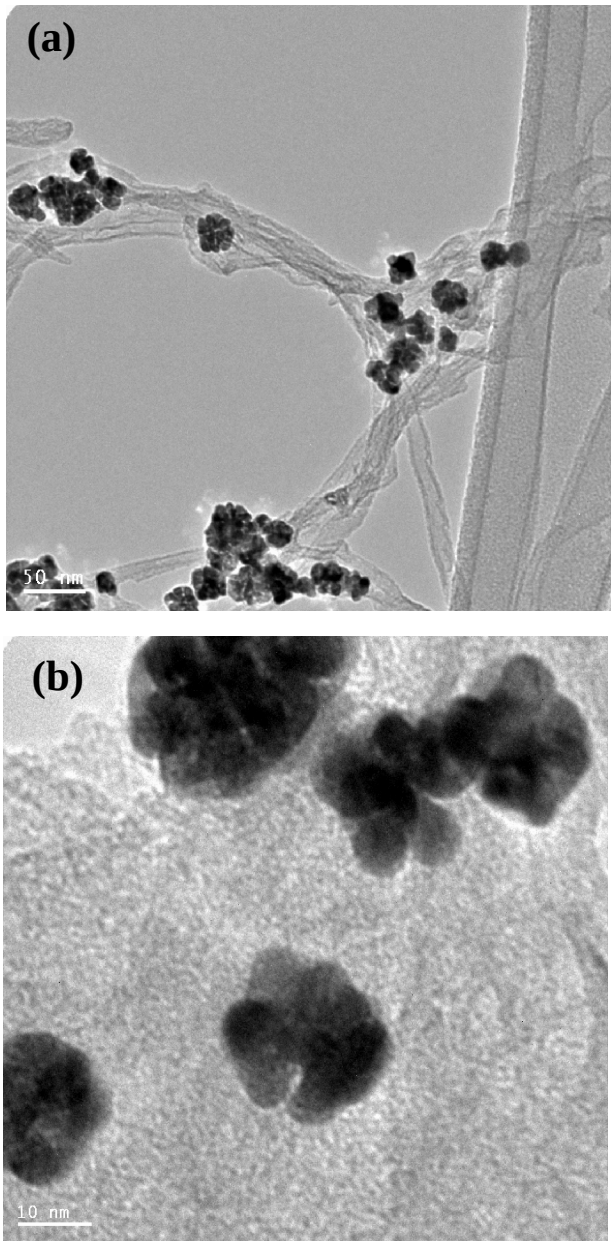

Fig.4-18 TEM images of Pt nanoparticles dispersion on pristine MWCNTs. (b) is an image with high magnification.

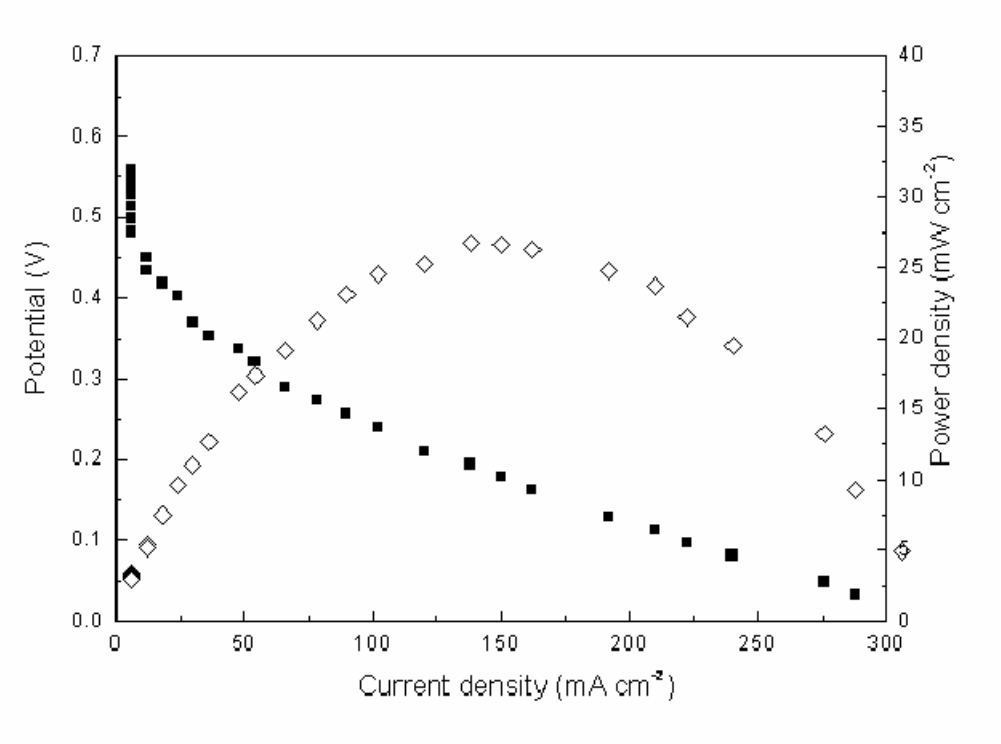

Fig.4-19 Polarization curves of the Pt/CNTs in 1cm^2 single cell with CH_3OH/O_2 at flow rates of 50/500 sccm and 70^{o}C. The Pt loading is 2.0 mg/cm^2.

4.2.4 Conclusion

In this section, we successfully synthesized Pt nanoparticles by polyol process and dispersed on MWCNTs by wet impregnation. The Pt particle size ranges from 5 to 10 nm, which is larger than the sputter deposited Pt nanoparticles. Dispersing Pt catalysts on MWCNTs by wet impregnation can solve the shield effect of sputtering method. However, lower methanol oxidation current density and poor single cell performance were found from the measurements of CVs and cell performance test. This could be attributed to that the surface of carbon nanotubes is chemically inert and difficult to support nanoparticles homogeneously. Therefore, the agglomeration of nanoparticles occurs, and this will result in the degradation of electrocatalytic ability of catalysts.

Chapter 5

Surface modification of CNTs

5.1 Surface modification of CNTs by refluxing in nitric acid

5.1.1 Introduction

Because the pristine surface of carbon nanotubes is relatively inert and difficult to support nanoparticles homogeneously, the agglomeration of nanoparticles usually occurs. This will result in the degradation of electrocatalytic ability of catalysts, which have been studied in previous chapter. Therefore, increasing the active site and improving the adhesion of carbon nanotubes surfaces is an important and necessary issue. The aromatic ring system of the CNTs can be disrupted by the application of extremely aggressive reagent, such as HNO_3 [66-68], H_2SO_4 [69], KOH [70-72], and therefore the CNTs can be functionalized with groups such as hydroxyl (-OH), carboxyl (-COOH) and carbonyl (>C=O). MWCNTs reflux in organic solvents produces dangling bonds that undergo further chemical reactions and provide the oxidative power necessary to incorporate acidic sites into CNTs.

5.1.2 Experimental procedures

A schematic diagram of the modification of MWCNTs is presented in Fig.5-1. MWCNTs were first immersed in 14M HNO_3 solution and refluxed at 80^{o}C for 18hr. The experimental setup is shown in Fig.5-2. The reasons for choosing 14M and 18 hr in this experiment will discuss later. And then, the sample was filtered with 0.1 mm PTFE (poly-(tetrafluoroethylene)) membrane in deionized water to functionalize with groups. Finally, the polyol synthesized Pt nanoparticles were dispersed on modified MWCNTs by wet impregnation. Here, we modified MWCNTs by HNO_3 solution with high concentration (14M) for anchoring more active sites. Fig.5-3 show the TEM images of Pt dispersed on MWCNTs modified by (a) 2M HNO_3 and (b) 14M HNO_3 solutions. It was found that the increase of the nitric acid concentration for surface modifications will create more anchoring sites for metal deposition, which means catalysts have smaller particles and more homogeneous dispersion. The same conclusions are also claimed by K. I. Han et al [73].

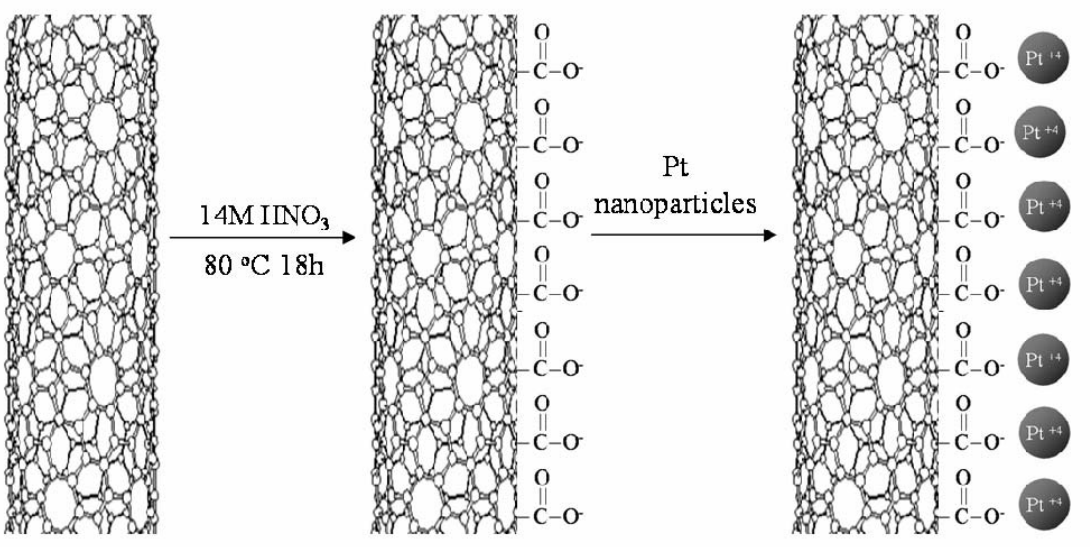

Fig.5-1 Schematic diagram of the modification of MWCNTs.

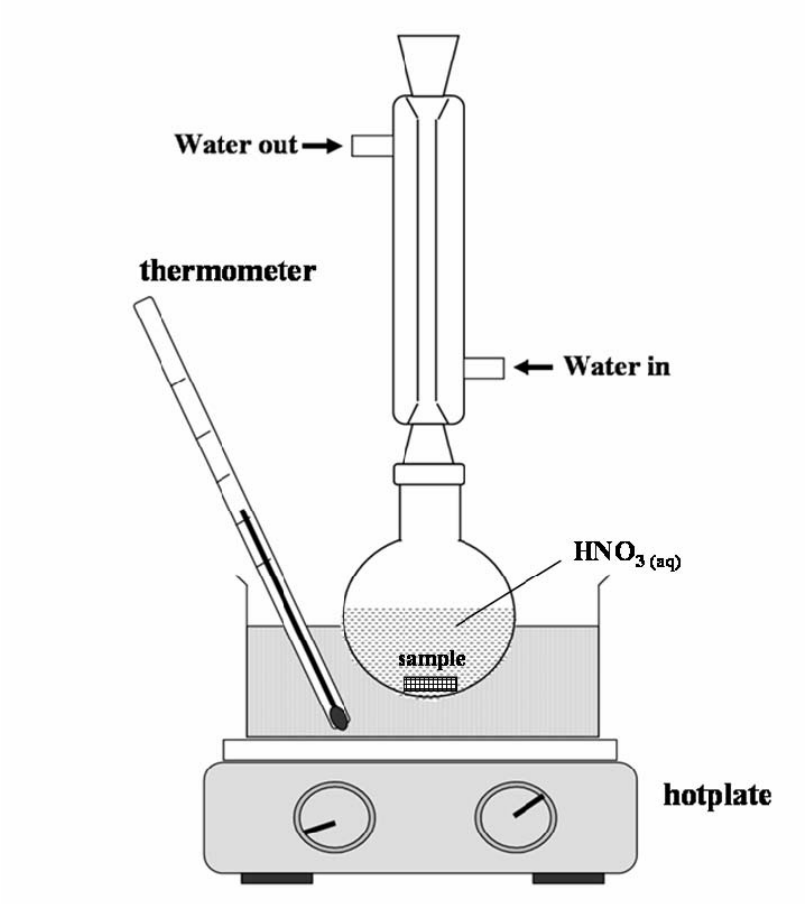

Fig.5-2 Schematic diagram of the experimental setup.

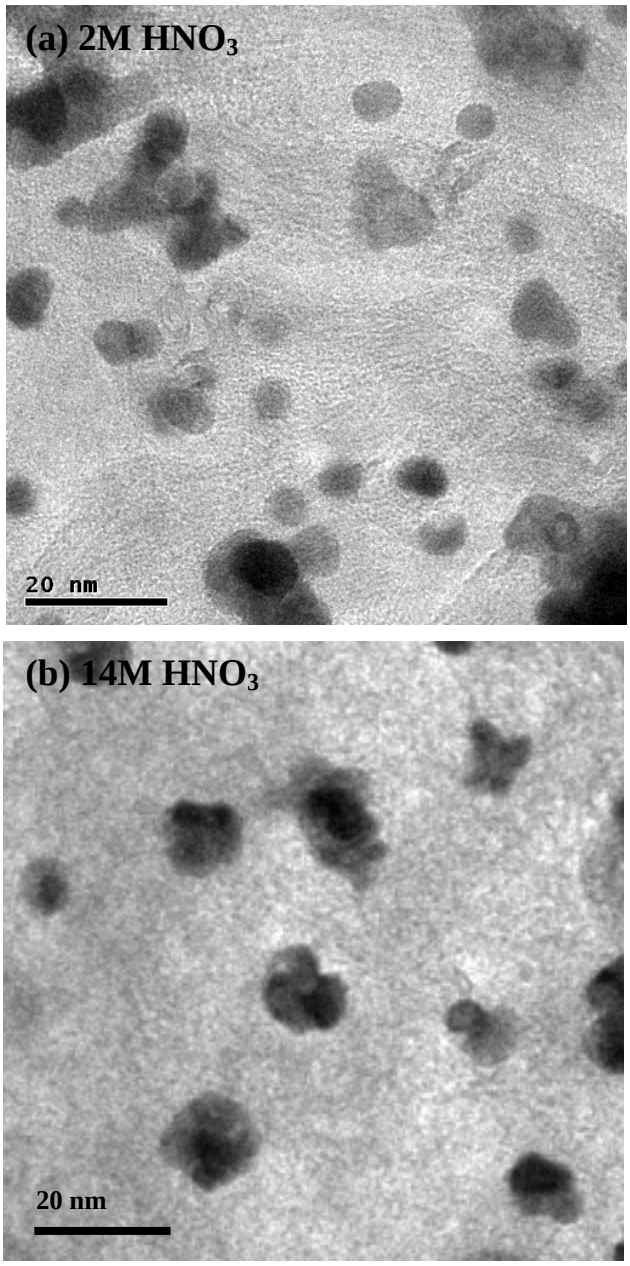

Fig.5-3 TEM images of Pt dispersed on MWCNTs modified by (a) 2M HNO_3 and (b) 14M HNO_3 solutions

5.1.3 Results and discussions

Raman spectroscopy is widely used for analyzing the structure of carbon nanotubes [74-77]. Raman spectra of MWCNTs with various acid-treatment times were shown in Fig.5-4. All samples of MWCNTs show a disorder-induced peak around 1350 cm^{-1}, which roughly corresponding to the D-line associated with disorder-allowed zone-edge modes of graphite. As the acid-treatment increase, a significant increase of the intensity of D-band can be observed in Raman spectra. This is because the perfect two-dimensional graphitization is altered to a more disordered structure by carboxylation. The I_D to I_G ratio of these samples was calculated by integrating the area of D-band and G-band. The calculated I_D/I_G ratios of MWCNTs with various acid treatment times were displayed in Fig.5-5. The high I_D/I_G ratio of MWCNTs indicates more functional groups on the surface of MWCNTs after modifications [78, 79]. The acid-treatment of MWCNTs depicts the highest I_D/I_G ratio show the optimum condition for modification. MWCNTs which modified in 14M HNO_3 solution for 18 hr show the highest I_D/I_G ratio from Fig.5-5. Therefore, it is the reason why we modified MWCNTs for 18hr. The FTIR spectra of untreated and nitric acid treated MWCNTs are presented in Fig.5-6. Several peaks can be observed, but we only focus on the peaks at about 1730 and 1590 cm-1 on FTIR spectra in Fig.5-6 (b) and (c).This suggested that carboxylic acid groups and carboxylate groups were presented on the surface for nitric acid treated MWCNTs.

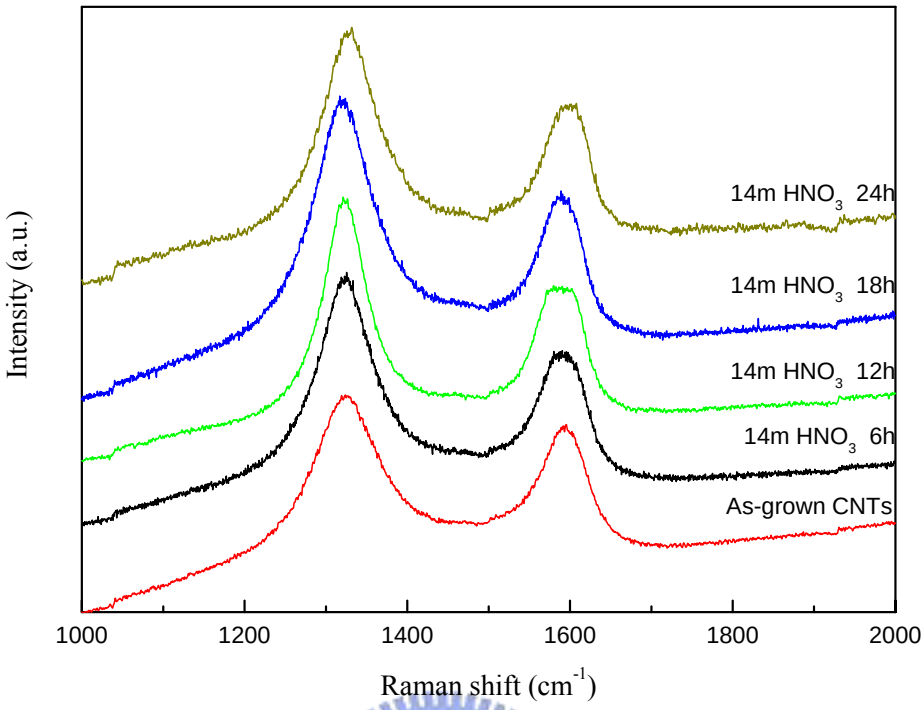

Fig.5-4 Raman spectra of various nitric acid-treatment times.

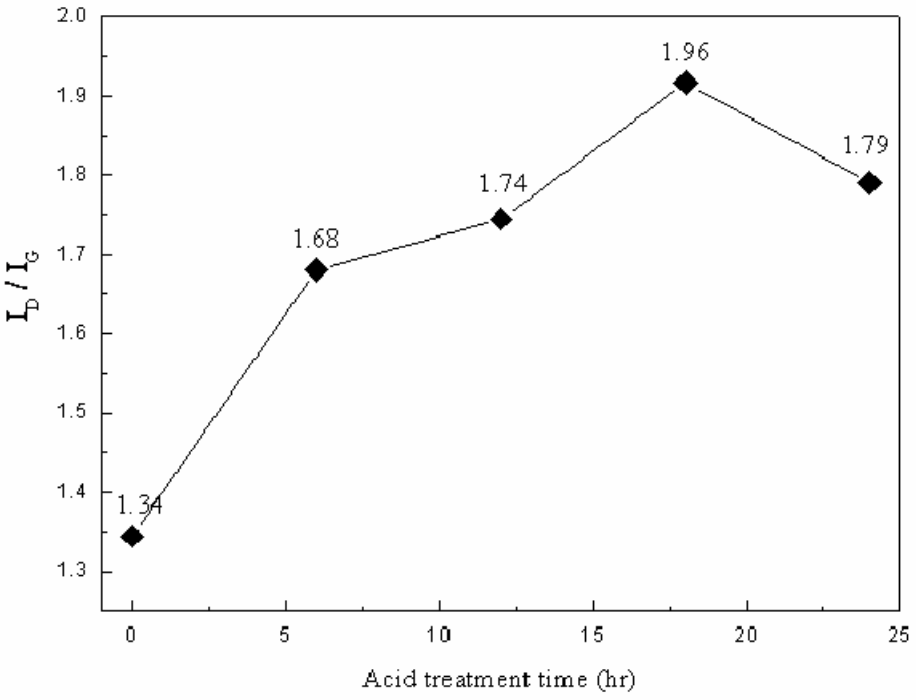

Fig.5-5 Relationship between I_D to I_G ratio and acid-treatment time.

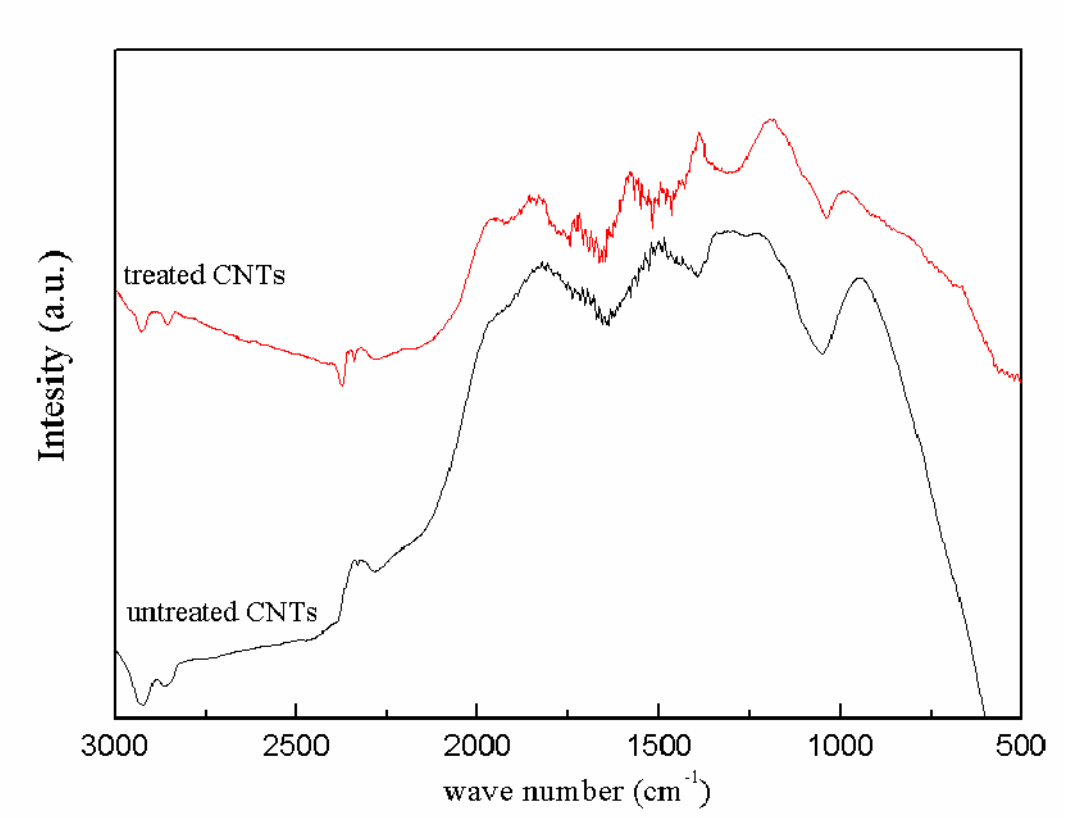

Fig.5-6 FT-IR spectrum of MWCNTs without and with nitric acid treatment.

Fig.5-7 depicts the HRTEM images of the nitric acid treated MWCNT and it can clearly be seen that the catalyst embedded in the tip of the MWCNT was removed. It is believed that the nitric acid destroyed the cap of MWCNT first and then eliminated the catalyst. However, the surface of nitric acid treated MWCNT was damaged after acidic treatment for 18h. The open-end MCNTs could provide extended surface area for supporting more catalysts [80]. The TEM images of Pt nanoparticles dispersed on pristine and functionalized MWCNTs were presented in Fig.5-8. Agglomeration of Pt nanoparticles was significantly improved after functionalized the surface of nanotubes. It could be contributed to the present of functional groups such as –COO and –OH can attract Pt ions, which greatly improved the uniformity and prevented the agglomeration of Pt nanoparticles. The XRD patterns for Pt/MWCNTs with and without nitric acid treatment are shown in Fig.5-9. The (2 2 0) reflections of Pt are used to calculate the average particle size according to the Scherrer's equation [81-83]:

$$L = 0.9\lambda_{K\alpha 1}/(B_{2\theta}\cos\theta_B) \qquad (5\text{-}1)$$

Where L is the average particle size, $\lambda_{K\alpha 1}$ is the X-ray wavelength (1.54056A ° for Cu $K_\alpha 1$ radiation), $B_{2\theta}$ is the peak broadening and θ_B is the angle corresponding to the peak maximum. The calculated mean particle size of Pt deposited on pristine and functionalized MWCNTs are 6.19 nm and 6.24 nm, respectively. The mean particle size of these two kinds of Pt/MWCNTs shows almost the same particle size. This means that it can't distinguish between the agglomeration and well distribution of Pt nanoparticles from XRD spectra. The electrochemical properties of Pt deposited on pristine and functionalized MWCNTs are investigated by cyclic voltammetry in 1M H_2SO_4 solution and 1M H_2SO_4 + 1M CH_3OH solution. Fig.5-10 is the CVs of these two samples in 1M H_2SO_4 solution with a scan rate of 50 mV/s. Adsorption peak of hydrogen in the cathodic potential sweep is used to determine the real surface area (working area) of Pt, which was already mentioned in previous chapter. The real surface areas of Pt on pristine MWCNTs and on functionalized MWCNTs are calculated by Eq.4-1. The electrocatalytic activity of Pt/pristine-MWCNTs and Pt/modified-MWCNTs were evaluated by the electrochemical oxidation of methanol. As shown in Fig.5-10, the peak current density of methanol oxidation on Pt/pristine-MWCNTs and Pt/modified-MWCNTs electrode is 30 mA/cm^2 and 58 mA/cm^2, respectively. The peak current density of methanol oxidation on Pt/modified-MWCNTs electrode is twice of that of Pt/pristine-MWCNTs. This was attributed to the better dispersion of Pt nanoparticles on MWCNT supports.

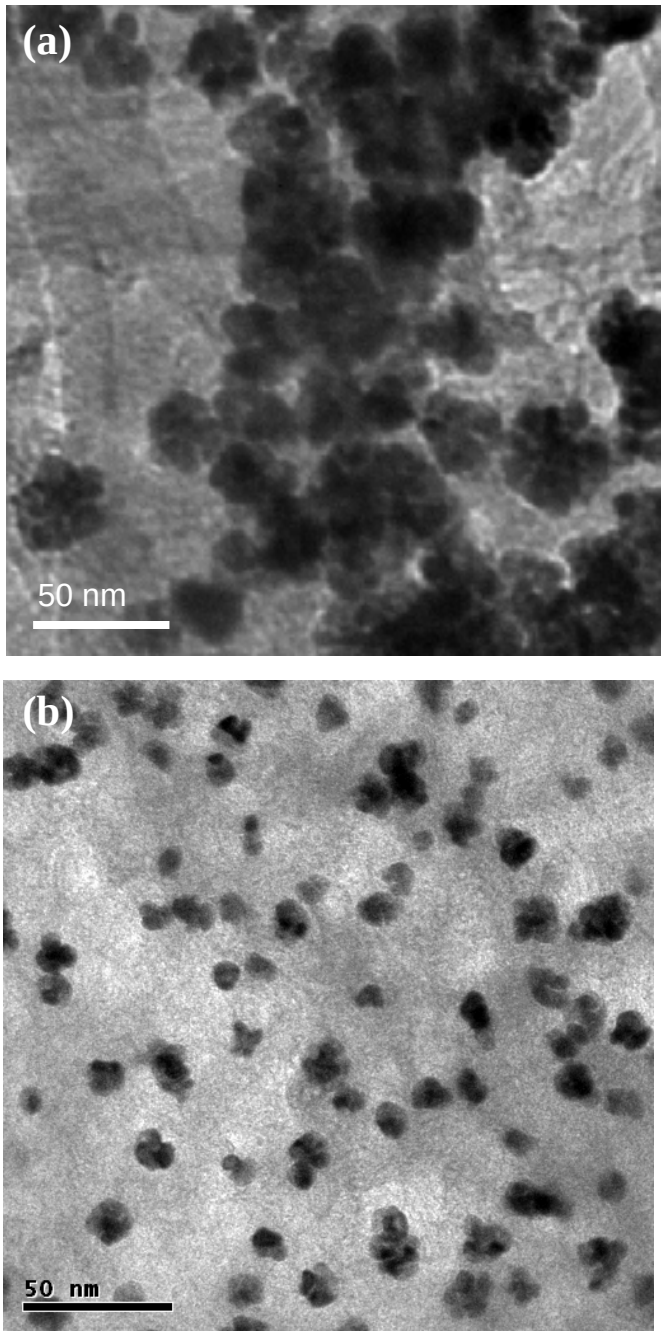

Fig.5-7 TEM images of Pt/MWCNTs (a) without and (b) with nitric acid treatment.

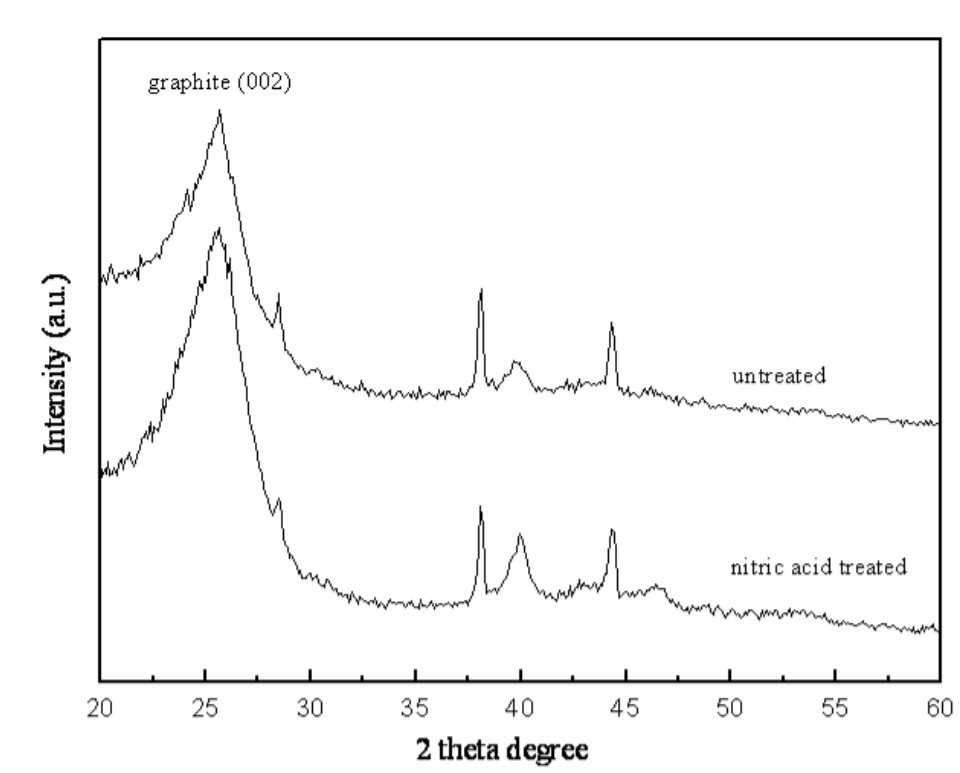

Fig.5-8 XRD patterns of Pt/MWCNTs without and with nitric acid treatment.

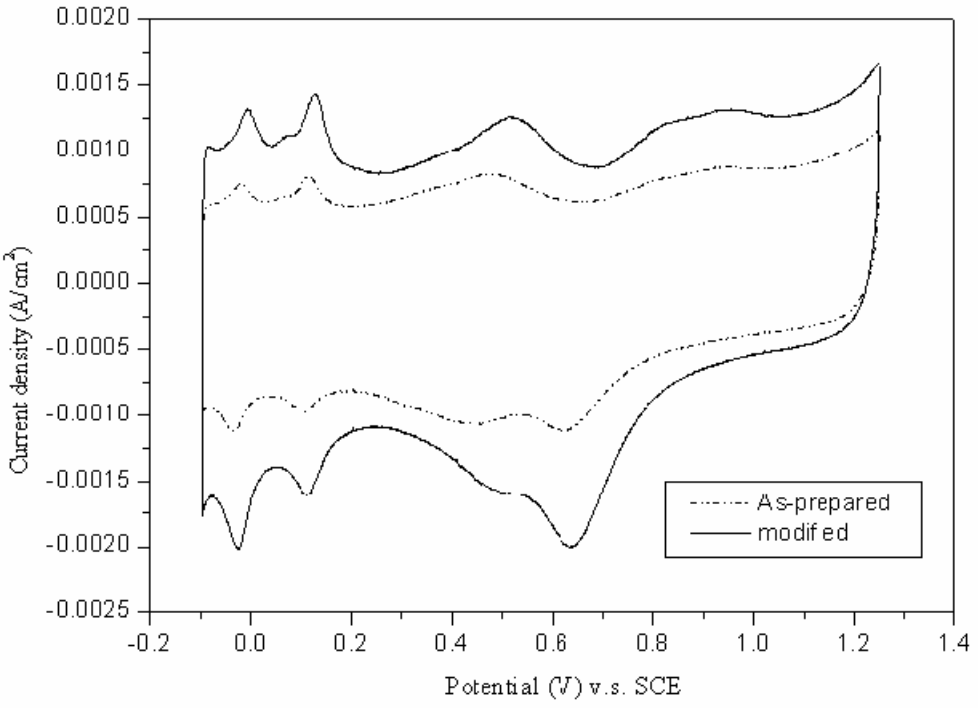

Fig.5-9 Cyclic votammograms of different Pt/CNTs electrodes in 1.0 M H_2SO_4 aqueous solution.

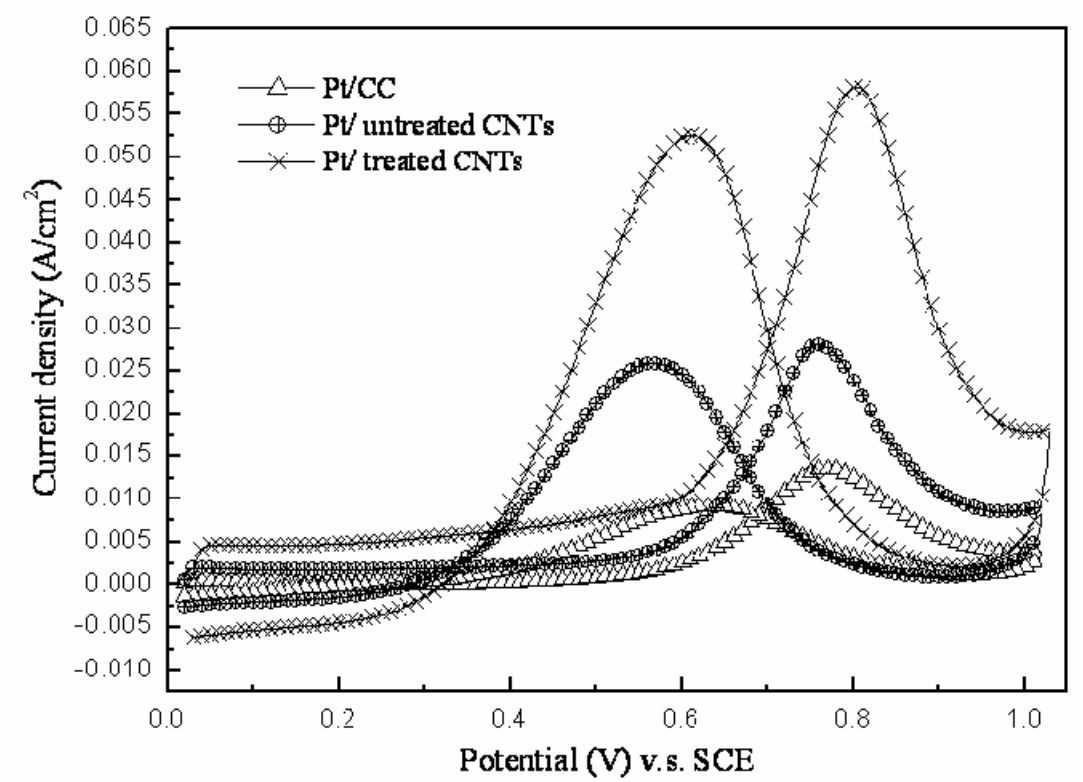

Fig.5-10 Cyclic votammograms of different Pt/CNTs electrodes in 1.0 M H_2SO_4 + 1.0 M CH_3OH aqueous solution.

Fig.5-11 shows a series of cell polarization and power density curves operated at different temperatures using 2M methanol solution with a flow rate of 3 ml min^{-1}. Pure oxygen was fed to the cathode side at a flow rate of 500 ml min^{-1}. The preparation of MEA and the operation conditions of single cell test are same as chapter 4. As can be seen from Fig.5-11(a), the polarization curves exhibit kinetic and ohmic control, while the mass transport limitation is not apparent. The maximum power density of the cell reaches 8.6 mW/cm^2 at 30 ˚C shown in Fig.5-11(b). The maximum power density is 12.6 mW/cm^2 when the temperature increased to 50 ◦C. This is because the kinetics of electrodes, particularly methanol oxidation at the anode, are enhanced at elevated temperatures. For the same reason, maximum power density is 15.8 mW/cm^2 at temperature of 70 ˚C. This trend demonstrates that the maximum power density nearly doubles when the cell temperature increases by 40 ˚C. Comparing with the Pt/pristine MWCNTs based cell in Fig.4-17, the power density of Pt/nitric acid treated MWCNTs based cell is higher almost triple times at 70^{o}C with a Pt

loading of 0.4 mg/cm^2. The significant improvement of cell performance could be observed between these two figures.

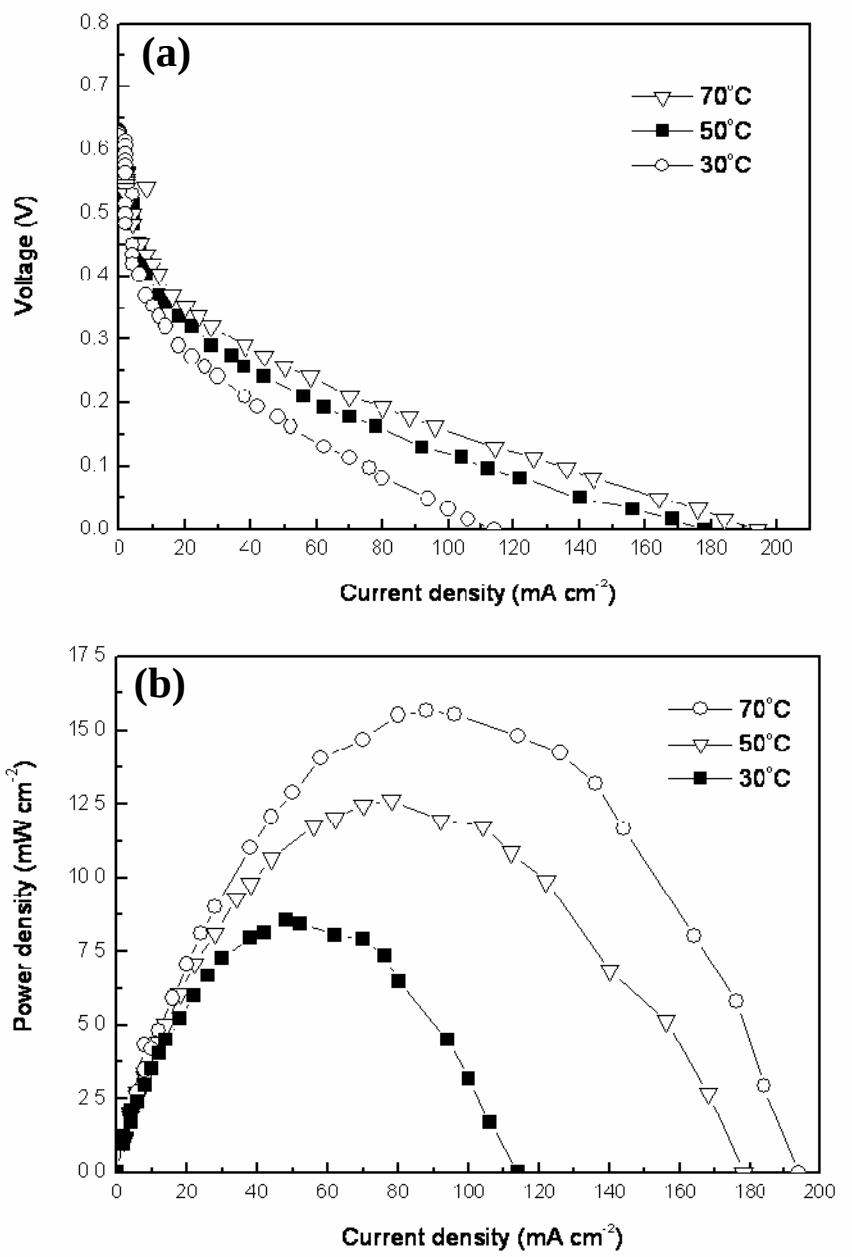

Fig.5-11 (a) polarization and (b) powder density curves of the Pt/CNTs in 1cm^2 single cell with CH_3OH/O_2 at flow rates of 50/500 sccm at different temperature.

5.1.4 Conclusions

The agglomeration of Pt nanoparticles can be greatly improved by functionalizing the surface of MWCNTs. The acid-treatment time of MWCNTs which depicts the highest I_D/I_G ratio shows the optimum condition for modification. Therefore, MWCNTs which modified in 14M HNO_3 solution for 18 hr show the highest I_D/I_G ratio. From the results of CVs and single cell test of Pt/MWCNTs electrodes, we can found the significant improvement of cell performance of DMFC after modifying MWCNTs. The power density of Pt dispersed on HNO_3 treated MWCNTs is 15.8, 12.6 and 8.6 mW/cm^2 at 70°C, 50°C and 30°C with 0.4 mg/cm^2 Pt loading ,respectively. This is much higher than the DMFCs with Pt/ pristine-MWCNTs and sputter deposited Pt/MWCNTs based cells.

5.2 Modification of CNTs by microwave digestion method

5.2.1 Introduction

Precious metals, such as Pt and Ru, are dispersed on carbon nanotubes and resulting materials for DMFC applications showed good electrocatalytic behaviors. Generally, electrocatalysts which supported on CNTs are synthesized by two steps. Raw CNTs were first refluxed with nitric acid and then metal precursors attached to functionalized CNTs surfaces. The step of refluxing CNTs in nitric acid not only opens the caps of CNTs, but functionalizes the surfaces of CNTs. However, conventional nitric acid treatments for modifying CNTs usually need to reflux CNTs for a long time and sometimes damage the structures of CNTs, which we have demonstrated in previous section.

Here, we report an efficient and undamaged method using microwave digestion system for modifying CNTs in a short time.

5.3.2 Experimental procedures

MWCNTs were modified utilizing a conventional nitric acid-treatment and a microwave digestion method. The MWCNTs immersed in 14M HNO_3 solution and refluxed at 80^{o}C for 18hr, which is the optimum condition for modifying MWCNTs in section 5.1. And then, the sample was filtered with 0.1 mm PTFE (poly-(tetrafluoroethylene)) membrane in deionized water as the conventional part. On the other hand, an alternative acidic treatment in microwave digestion system (Milestone Microwave Labstation ETHOSD) was used to modify MWCNTs. MWCNTs/CC was placed in a 100 ml Pyrex digestion tube. The MWCNTs immersed in 14M HNO_3 solution and refluxed at 80^{o}C for 18hr. And then, the sample was filtered with 0.1 mm PTFE (poly-(tetrafluoroethylene)) membrane in deionized water as the conventional part. On the other hand, an alternative acidic treatment in microwave digestion system (Milestone Microwave Labstation ETHOSD) was used to modify MWCNTs. 1 cm^2 of MWCNTs/CC was placed in a 100 ml Pyrex digestion tube. The first digestion step was to heat the system from room temperature to 210 ^{o}C within 20 min with 5 M HNO_3. The microwave power was set at 100 W. The second digestion step was to keep the temperature at 210^{o}C for 30min. After digestion; the sample was also filtered with 0.1 mm PTFE membrane in deionized water. The total modification time by microwave digestion method was less than 1 h.

5.3.3 Results and discussions

The FTIR spectra of untreated, conventional nitric acid treated and microwave digestion treated MWCNTs are presented in Fig.5-12. The peaks at about 1730 and 1590 cm-1 on FTIR spectra in Fig.5-12 (b) and (c) suggested that carboxylic acid groups and carboxylate groups and were presented on the surface for both conventional nitric acid treated and microwave digestion treated MWCNTs. The IR spectra of conventional nitric acid treated and microwave digestion treated MWCNTs show almost the same characteristic, which indicates the surface of microwave digestion treated MWCNTs were functionalized in a short time. XPS of microwave digestion treated MWCNTs is presented in Fig.5-13. The C 1s spectrum appears to be composed of graphitic carbon (284.8 eV) and C=O like species (285.82 eV). A small amount of surface functional groups of –CO (286.8 eV) and –COO (290.14eV) were also noted in the spectrum, which are the evidences of the functionalization of MWCNTs surface after acid-treatment by microwave digestion method. Raman spectra of pristine, nitric acid-treated, and microwave digestion treated MWCNTs were shown in Fig. 5-14. All samples of MWCNTs show a disorder-induced peak around 1350 cm^{-1}, which roughly corresponding to the D-line associated with disorder-allowed zone-edge modes of graphite. After modifications, a significant increase of the intensity of D-band can be observed in Raman spectra. The I_D to I_G ratio of these samples was calculated by integrating the area of D-band and G-band. The calculated I_D/I_G ratios of pristine, nitric acid-treated, and microwave digestion treated MWCNTs were 1.34, 1.96, and 2.21, respectively. The high I_D/I_G ratio of MWCNTs indicates more functional groups on the surface of MWCNTs after modifications.

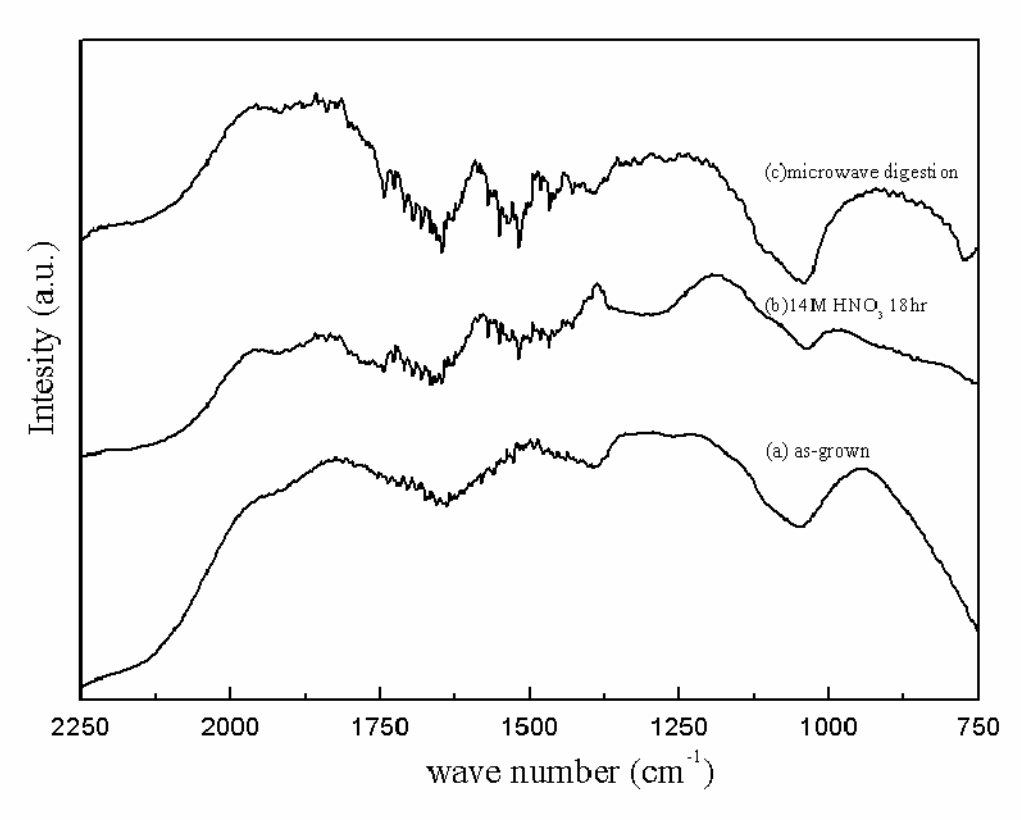

Fig.5-12 FT-IR spectrum of MWCNT with and without functionalization.

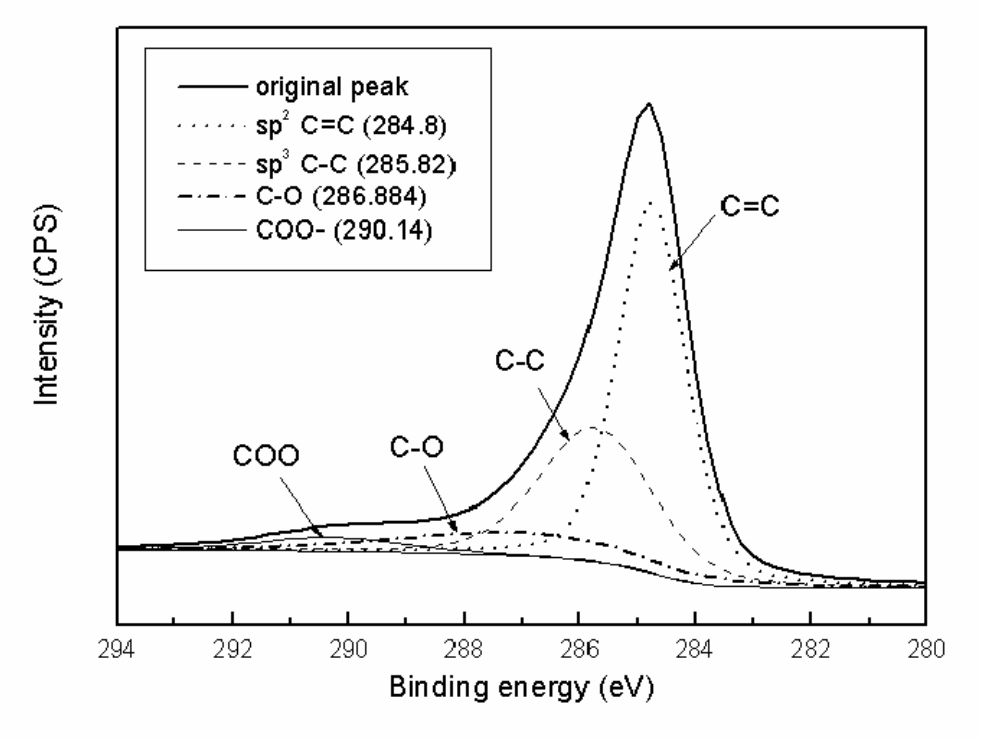

Fig.5-13 XPS of microwave digestion treated MWCNTs.

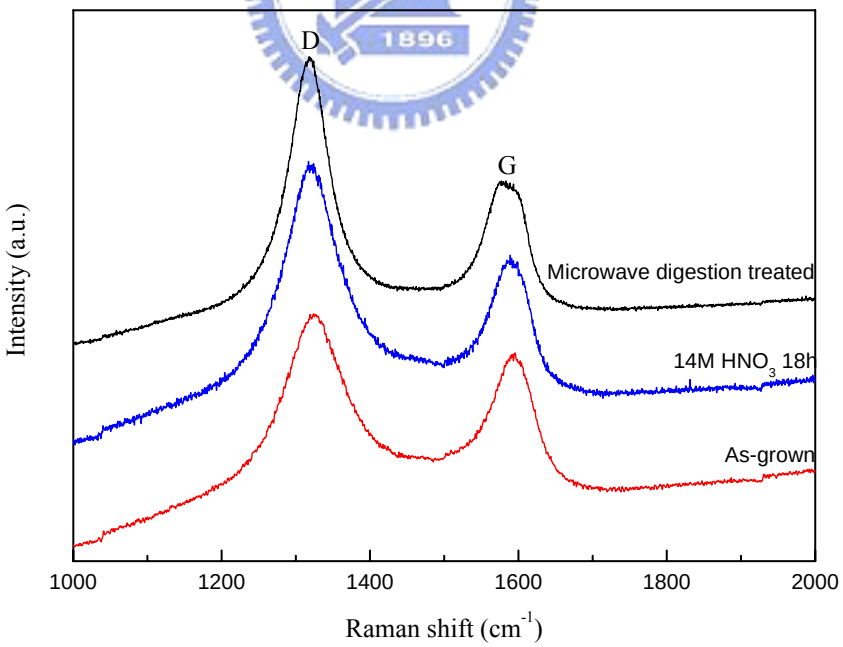

Fig. 5-14 Raman spectroscopy of nitric acid treated MWCNTs by different approaches

Fig.5-15 depicts the contact angle test of MWCNTs (a) without and (a) with modification by microwave digestion. The pristine MWCNTs show hydrophobic feature with contact angle of 107.10^{o}. After modification, the contact angle of MWCNTs is 9.28^{o}. This indicates that the MWCNTs become hydrophilic and is also the evidence of functionalization of nanotube surface. Fig.5-16 depicts the HRTEM images of the nitric acid treated and the microwave digestion treated MWCNT. It can clearly be seen that the catalyst embedded in the tip of the MWCNT was removed in both Fig.5-15 (a) and (b). It is believed that the nitric acid destroyed the cap of MWCNT first and then eliminated the catalyst. However, the surface of nitric acid treated MWCNT was damaged after acidic treatment for 18h. On the contrary, microwave digestion takes a tremendous advantage because the acid in this approach can absorb microwave energy rapidly and dissolve metal efficiently without damaging the wall structure and the processing time could be reduced. The catalysts were loaded by impregnated 1 cm^2 MWCNTs electrode into 2 mL precursor with 2mg metal loading. However, the actual Pt loading for pristine, nitric acid- treated and microwave digestion-treated Pt/MWCNTs samples are 0.18mg/cm^2, 0.24mg/cm^2 and 0.30mg/cm^2, which were determined by burning away the MWCNTs at 900^{o}C in O_2 atmosphere. We supposed that the nitric acid treated MWCNTs by both methods can supported more Pt catalysts because of the functionalized surface and open-end structure of MWCNTs. It is identical with Raman results. TEM micrographs of Pt nanoparticles disperse on (a) pristine MWCNTs and (b) microwave digestion treated MWCNTs are shown in Fig.5-17. The distribution of Pt nanoparticles on pristine MWCNTs is not uniform and large Pt clusters can be found. The significant agglomeration of Pt nanoparticles on MWCNTs is due to the chemically inert and hydrophobic surface of MWCNTs. However, a better dispersion of Pt nanoparticles on microwave digestiontreated MWCNTs is shown in Fig.5-17 (b). Although agglomeration of Pt nanoparticles still exists, the distribution of Pt nanoparticles on acid-treated MWCNTs by microwave digestion is greatly improved.

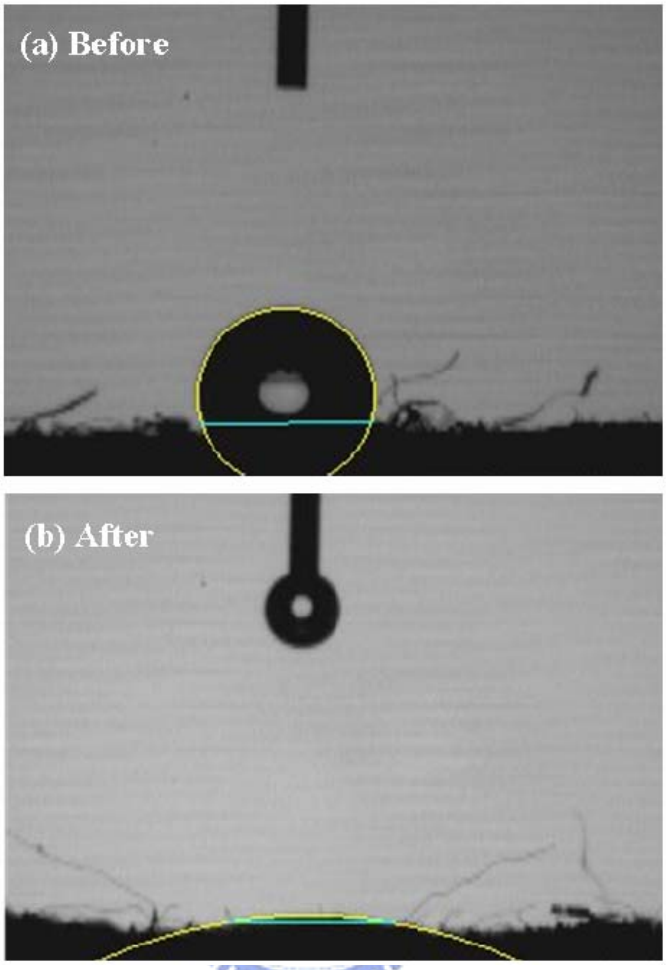

Fig.5-15 The photographs of contact angle test (a) before and (b) after modification in 5M HNO_3 by microwave digestion method.

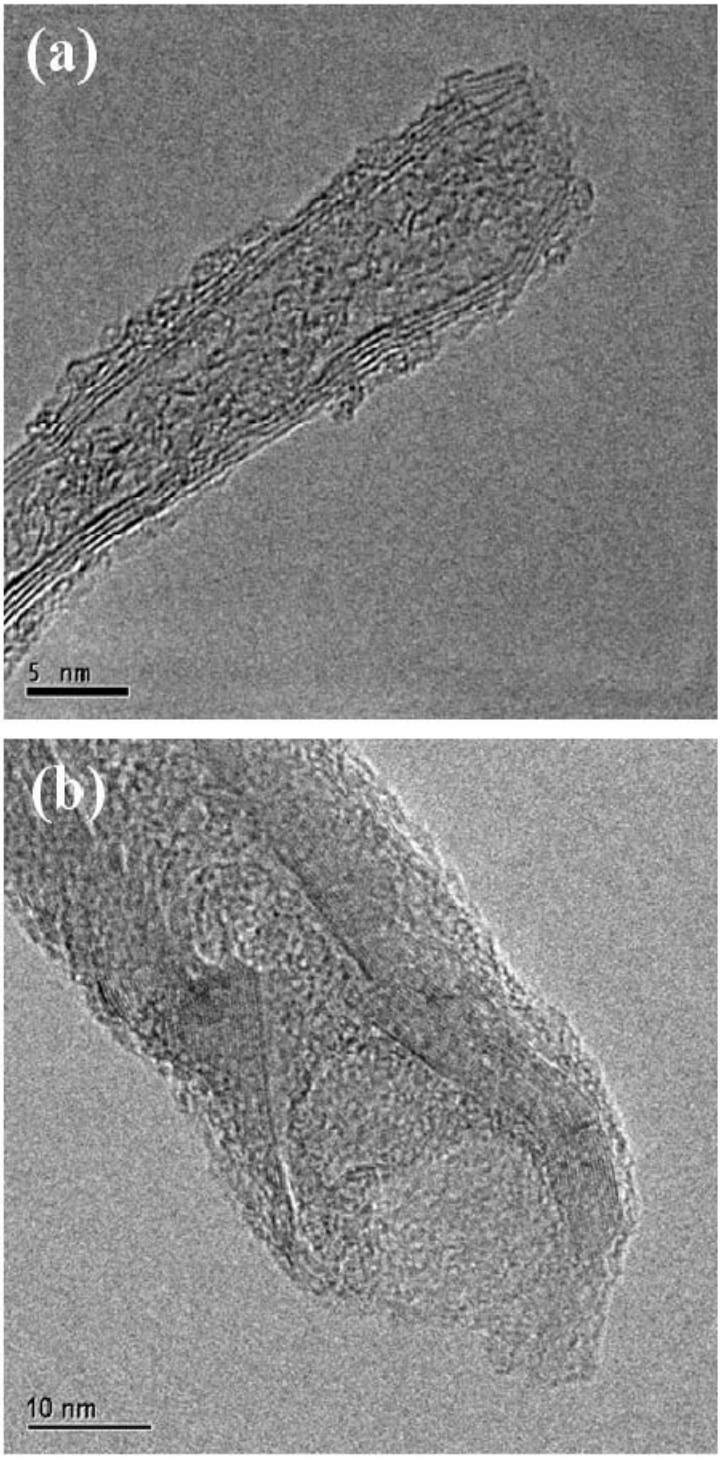

Fig.5-16 HRTEM images of open-end MWCNTs which were synthesized (a) by refluxing in 14M HNO_3 for 18 h and (b) by microwave digestion method in 5M HNO_3 solution.

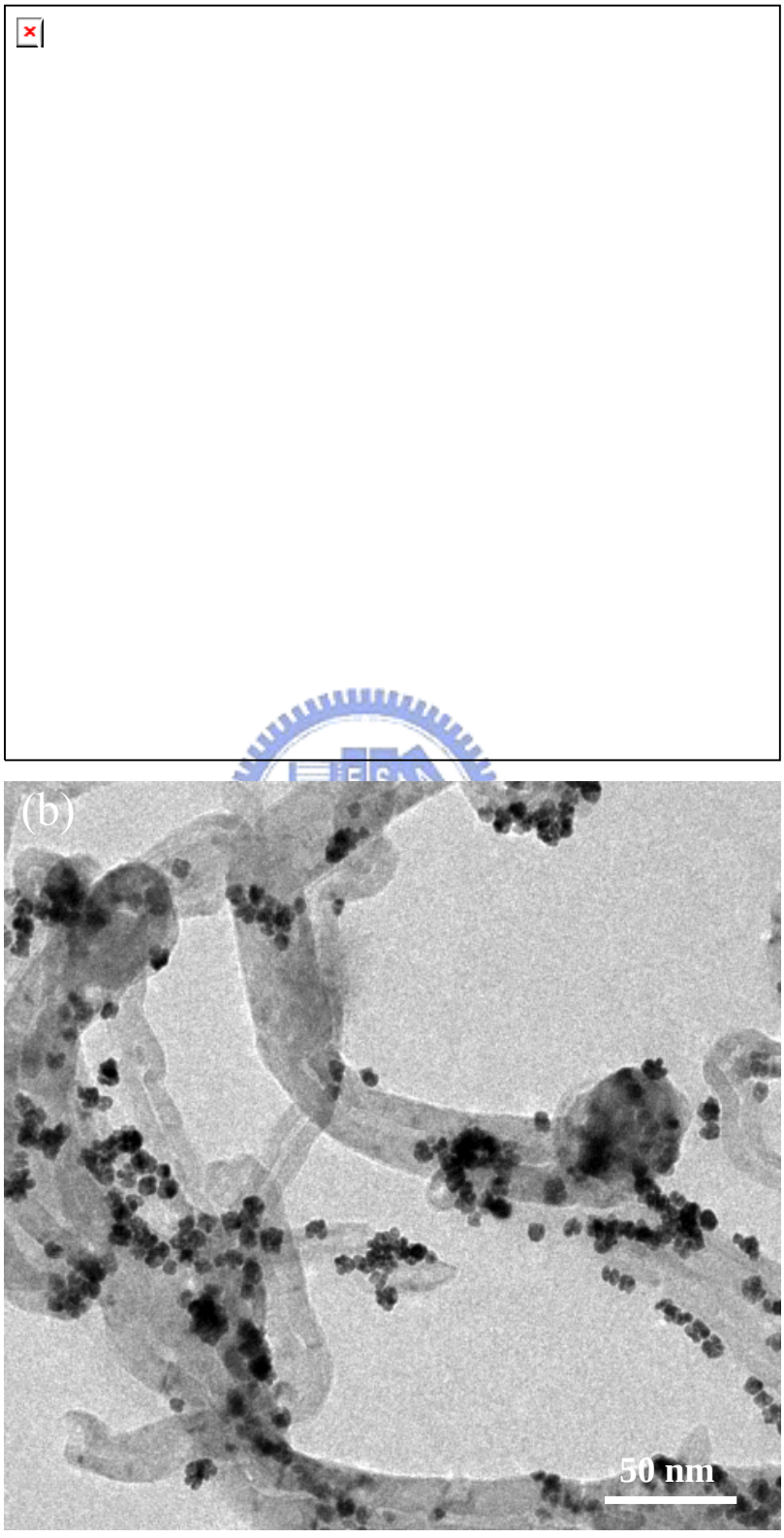

Fig.5-17 TEM images of Pt nanoparticles disperse on (a) pristine MWCNTs and (b) microwave digestion treated MWCNTs.

The electrocatalytic activity of Pt catalyst was tested by cyclic voltammetry (CV) in electrolyte of 1.0M H_2SO_4 with a scan rate of 50mVs^{-1} and is shown in Fig.5-18. the calculated active surface area of Pt from Fig.5-18 are 5.6, 20.1, and 23.9 cm^2 for the pristine, nitric acid-treated, and microwave digestion treated MWCNTs. The microwave digestion treated Pt/MWCNTs electrode has larger electrochemical Pt surface area than the others, which could be attribute to the more Pt amount attached on the MWCNTs. and uniform distribution of Pt nanoparticles. Various electrochemical properties of these samples are listed in Tab.5-1. Tab.5-1 listed various calculated values of Pt loading (L_{Pt}, mg), working surface area of Pt (S_{Pt}, cm^2), methanol oxidation current density at 0.8V (i, mA cm^{-2}) of samples and mass efficiency of Pt (Me, mA mg^{-1} Pt). Electrocatalytic activities of Pt/MWCNTs electrodes in methanol solution which were measured in a deaerated 1.0M CH_3OH + 1.0 M H_2SO_4 solution between 0 and 1.0 V with a scan rate of 50 mV/s are shown in Fig.5-19. The current density of methanol oxidation of microwave digestion modified Pt/ MWCNTs at 0.8V is 76 mA cm^{-2}, which is higher than conventional nitric acid treated sample and almost 2.5 times as high as the untreated Pt/MWCNTs sample. The Pt nanoparticles on modified MWCNTs show the higher utility than pristine MWCNTs from the comparison of mass efficiency in Tab.5-1. This may be attributed to the functionalized surface and the presence of open-end MWCNTs, which Pt nanoparticles can uniformly disperse on MWCNTs with larger amount.

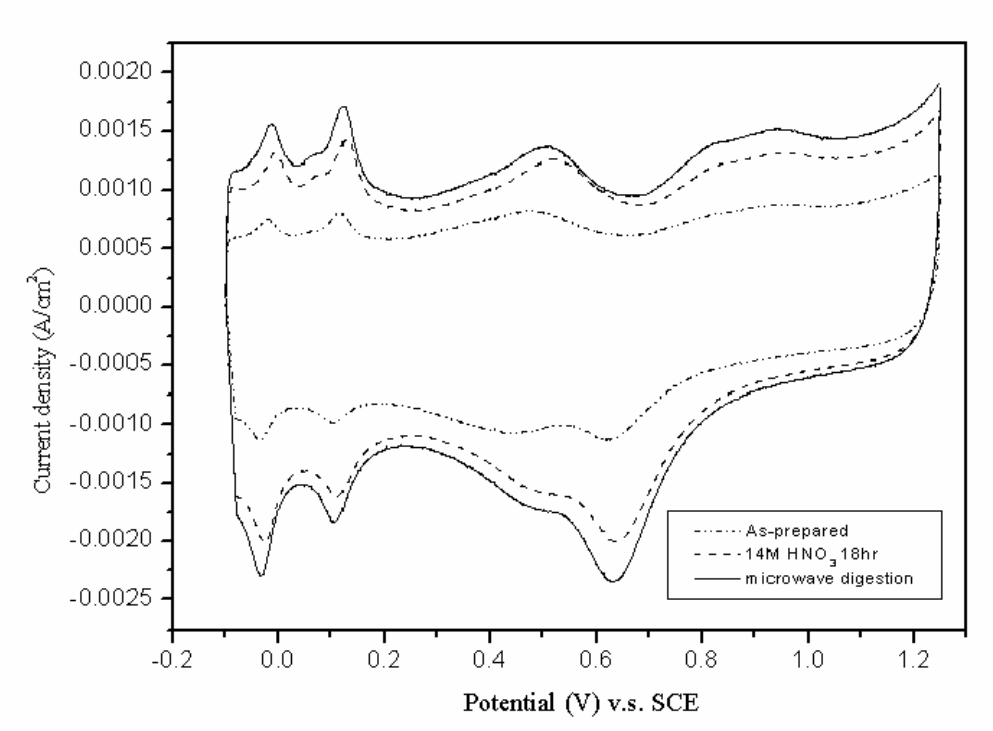

Fig.5-18 Cyclic votammograms of Pt/CNTs electrode in 1.0 M H_2SO_4 aqueous solution with a scan rate of 50 mVs^{-1}.

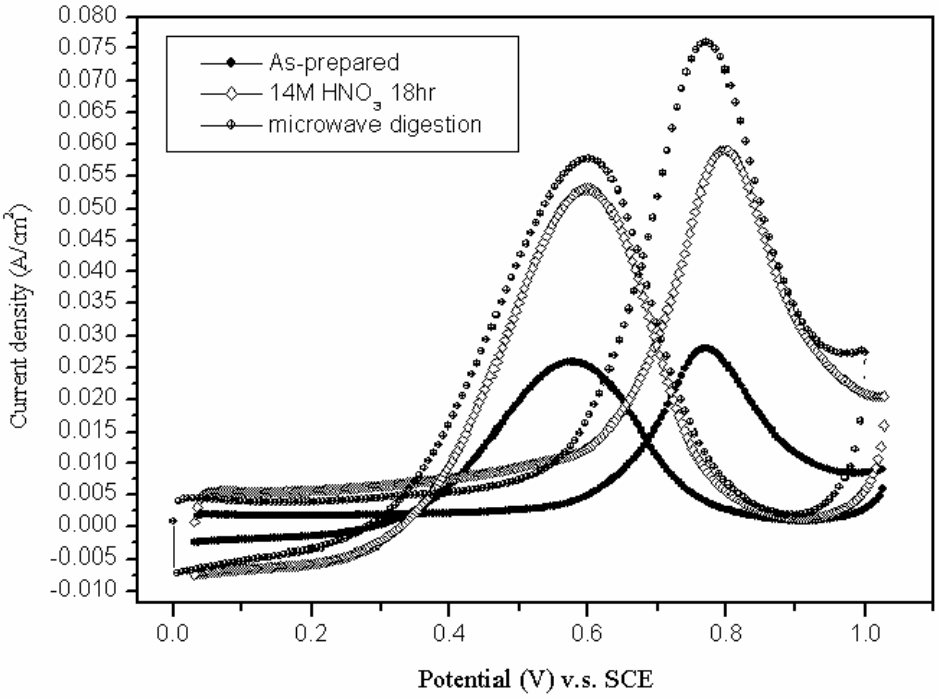

Fig.5-19 Cyclic votammograms of Pt/CNTs electrode in 1.0 M H_2SO_4 + 1.0 M CH_3OH aqueous solution with a scan rate of 50 mVs^{-1}.

Tab.5-1 Various electrochemical properties of samples

Sample	L_{Pt} (mg/cm^2)	S_{Pt} (cm^2)	$I_{0.8V}$ (mA/cm^2)	ME (mA/mg)
Pristine MWCNTs	0.18	5.6	28	156
14M HNO_3 18 h	0.24	20.1	59	246
Microwave digestion	0.30	23.9	76	253

5.2.4 Conclusions

A fast and effective way for modifying MWCNTs was demonstrated in this paper. TEM images reveal that the modification by microwave digestion method can obtain undamaged and open-end MWCNTs. The aggregation of Pt nanoparticles can be greatly improved by functionalizing the surface of MWCNTs using the microwave digestion method. The CVs results show that the microwave digestion modified Pt/MWCNTs electrode exhibits the larger electrochemical Pt surface area and higher current density of methanol oxidation than untreated and conventional nitric acid treated Pt/MWCNTs electrodes. This technique can be widely used for effective modifying CNTs and shorting the process time.

5.3 Surface modification of CNTs : Effects of functional groups

5.3.1 Introduction

We have discussed the effects of MWCNTs with nitric acid-treatment and optimized the acid-treatment condition in previous section. It is essential and interesting to realize the effects of different functional groups for supporting catalysts. The inert surface nature of CNTs due to a perfect graphene sheet structure has hindered the high dispersion of precious metal with uniform size distribution using the conventional impregnation method, in which the affinity of the carbon surface for the precursor solution exerts the dominant effect on dispersion in the deposition step [84]. To solve this problem, the surfaces of CNTs have been functionalized with functional groups like carboxyl [85–87], amine [88], and thiol [89] groups having a good affinity with precious metal, using various organic solution or electrochemical methods.

In this section, we would like to obtain highly dispersed Pt nanoparticles by introducing different functional groups like carboxyl, hydroxyl, and thiol groups on MWCNTs surfaces, using HNO_3, KOH, H_2SO_4 and C_2H_6SO solutions. The effects of MWCNTs modified in different solutions will also discuss in this section.

5.3.2 Experimental procedures

The MWCNTs which were synthesized on carbon cloth by MWPECVD were first modified by refluxing in 14M HNO_3 at 80^{o}C for 2 h. Then, the oxidized MWCNTs refluxed in various solutions such as HNO_3, H_2SO_4, KOH and C_2H_6SO for 18hr. The experimental conditions are listed in Tab.5-2. After modification, the samples poured into distilled water, and filtered with a 0.1 mm PTFE membrane as the pretreatment. However, the Pt nanoparticles were directly synthesized on MWCNTs/CC, which is different from wet impregnation in previous section. The electrode catalysts of Pt-deposited MWCNTs were prepared with $H_2PtCl_6 \cdot 6(H_2O)$. Then, MWCNTs/CC samples were heated and stirred with $H_2PtCl_6 \cdot 6(H2O)$ in ethylene glycol at 160^{o}C for 2 h. This solution was added into HNO_3 (14 M), dissoluted into 400 ml of distilled water, and filtered. The filtered water was almost as yellow as the H_2PtCl_6 solution. This procedure has often been applied for the Pt deposition on carbon supports [90–93].

Tab.5-2 Experimental conditions

Solution	HNO_3	H_2SO_4	KOH	C_2H_6SO
Concentration	14M	14M	14M	14M
Temperature	80°C	80°C	80°C	80°C
Time	6 hr	6 hr	6 hr	6 hr

5.3.3 Results and Discussions

The solutions which we choose for thiolation here were sulfur acid and 2-mercaptoethanol (C_2H_6SO). 2-Mercaptoethanol is a derivative of ethanol formed by replacement of one hydrogen by an thiol (-SH) group. 2-Mercaptoethanol is a reducing agent which can act as a biological antioxidant. It has higher flash point than H_2SO_4 and will hydrate with carboxylic group to form thiol group. Before MWNTs are thiolated, carboxylic groups should be introduced on the walls and ends of the MWNTs using various oxidizing agents [94-97]. HNO_3 is extensively used as oxidizing agent to attach carboxylic groups. The experimental flow charts of the thiolation of MWCNTs are shown in Fig.5-20. Raman spectra of MWCNTs treated with various solutions were shown in Fig.5-21. A significant increase of the intensity of D-band of HNO_3 and C_2H_6SO treated MWCNTs can be observed in Raman spectra. The I_D to I_G ratio of these samples was calculated by integrating the area of D-band and G-band were displayed in Tab.5-3. The high I_D/I_G ratio of MWCNTs indicates more functional groups on the surface of MWCNTs after modifications [78, 79]. MWCNTs which modified in C_2H_6SO solution show the highest I_D/I_G ratio.

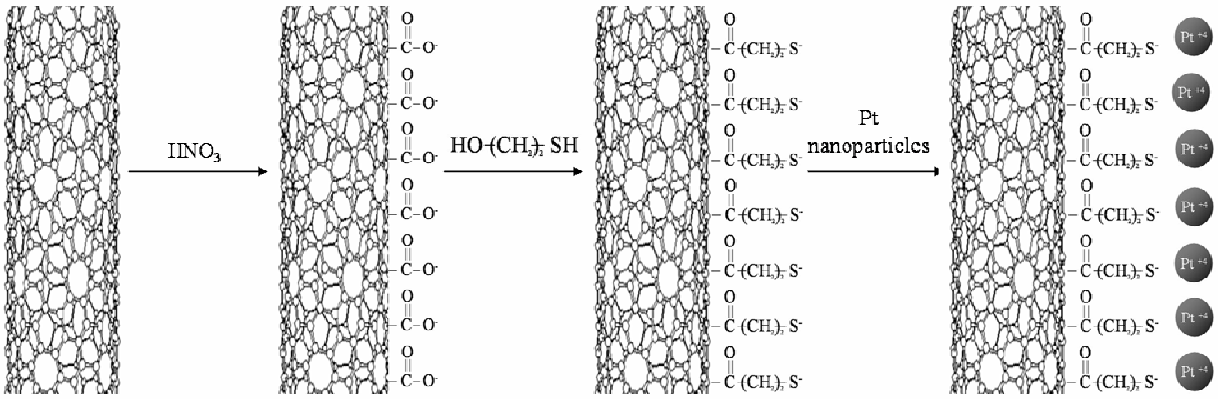

Fig.5-20 Experimental flow charts of thiolation of MWCNTs

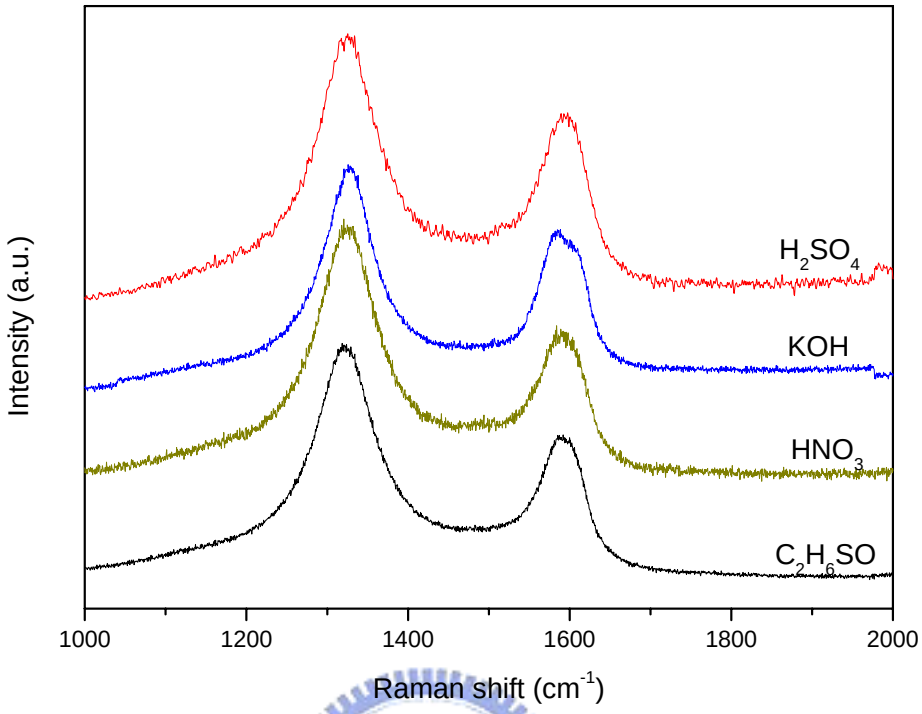

Fig.5-21 Raman spectra of MWCNTs modified by different solutions

Tab.5-3 I_D / I_G ratios of MWCNTs modified by different solutions

Solution	I_D / I_G
HNO_3	2.59
H_2SO_4	2.03
KOH	1.70
C_2H_6SO	2.67

Fig.5-22 is the FTIR spectra of (a) pristine, (b) oxidized and (c) thiolated MWCNTs. FTIR spectra of these three kinds of MWNT according to the sequence of surface thiolation of MWNT, meaning that oxidization with HNO_3 successfully introduced the carboxyl groups on the MWNT surfaces. After thiolation, the peak decreased, indicating the carboxyl groups were replaced by thiol groups. Fig. 5-23 shows the FTIR spectra of MWNTs modified with different solutions. The peak around 1725–1715 cm^{-1}, corresponding to the stretching of C>O in carboxyl groups, drastically increased. However, detection of thiol groups with FTIR

proved too difficult because of their weak response in the IR mode. For this reason, we used XPS to directly detect the sulfur atom and determine the surface oxidation states of the metals. Fig.5-24 shows the XPS survey patterns of Pt dispersed on modified MWCNTs by various solutions; i.e. HNO_3, H_2SO_4, KOH and C_2H_6SO. Notably, a weak S2p peak is seen for the MWCNTs modified in C_2H_6SO solution. This reveals the possibility of the functionalization of thiol groups on nanotube surface. The S2p spectra of XPS of MWCNTs modified in C_2H_6SO is shown in Fig. 5-25. Binding energy of S 2p3/2 is about 162.9 eV, with reference to C 1s at 284.6 eV [98]. According to the FTIR and XPS results, we can confidently say that the thiol groups were attached on the MWCNTs surface. The C 1s spectra of XPS of MWCNTs modified in HNO_3, KOH, H_2SO_4 and C_2H_6SO are shown in Fig. 5-26. The peak at 288.9eV shows that the surfaces of HNO_3, H_2SO_4 and C_2H_6SO are covered with carboxylic groups.

SEM images of Pt nanoparticles dispersed on MWCNTs which were modified by refluxing in different solutions are shown in Fig.5-27. It can found that the uniformity and agglomeration of Pt nanoparticles are improved after modifications. The XRD patterns for Pt/MWCNTs with different treatments are shown in Fig.5-28. The (2 2 0) reflections of Pt are used to calculate the average particle size according to the Scherrer's equation (Eq.5-1). The results of diffraction angle, half-width, and calculated mean particle size are shown in Tab.5-4. The calculated mean particle size of Pt dispersed on HNO_3, H_2SO_4, KOH and C_2H_6SO modified MWCNTs are 6.01 nm, 6.91, 6.15 and 5.21 nm, respectively. As shown in Tab.5-4, the effect of thiolated groups on the nanotube surface is seen for obtaining smaller particle size. According to Coulomb's law (Eq.5-2), the electrostat force is proportional to the reciprocal of the square of distance between two charges. Due to the radius of O atom is smaller than S atom, the electrostat force of O atom is larger than S atom. Therefore, the less Pt ions were attracted by S atom during the synthesizing process. This will result in particle size of Pt nanoparticles on thiolated-MWCNTs becomes smaller than oxidized-MWCNTs.

$$F = \frac{|Q_1 Q_2|}{4\pi\varepsilon_o r^2} \qquad (5\text{-}2)$$

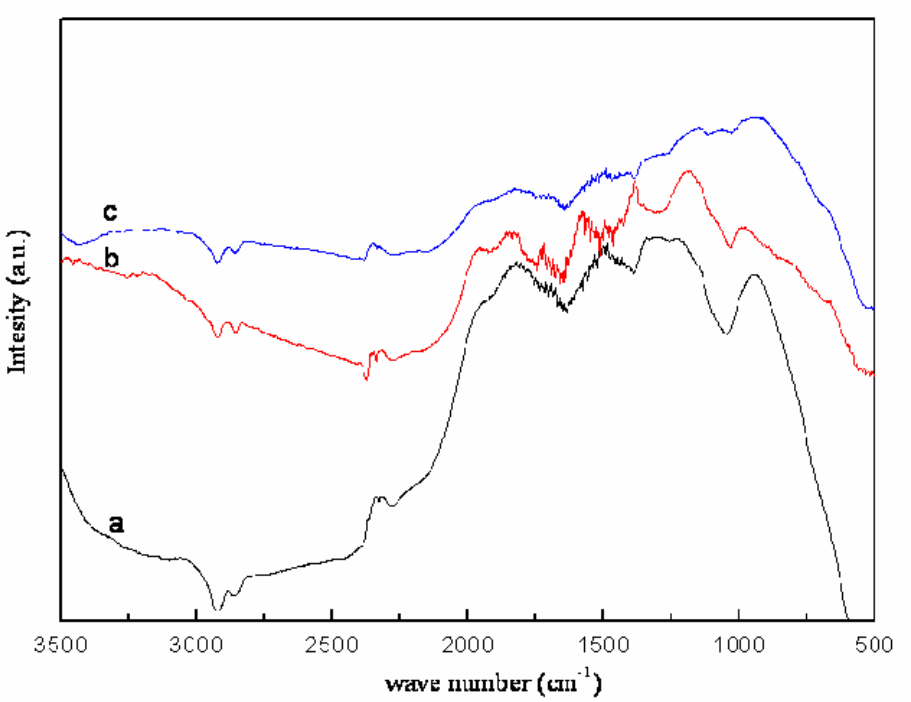

Fig. 5-22 FTIR spectra of (a) pristine, (b) oxidized and (c) thiolated MWCNTs.

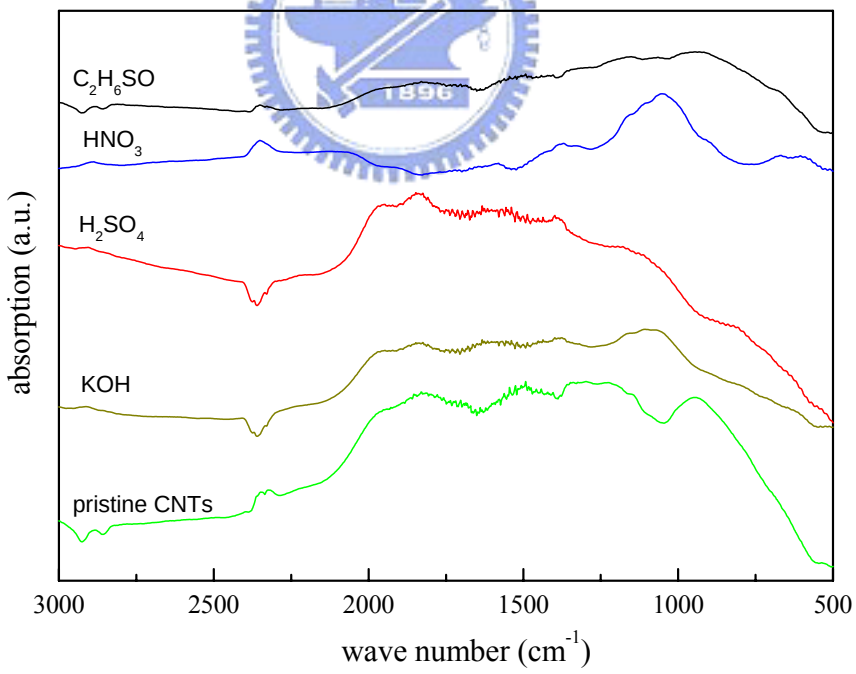

Fig. 5-23 FTIR spectra of MWNTs modified with different solutions.

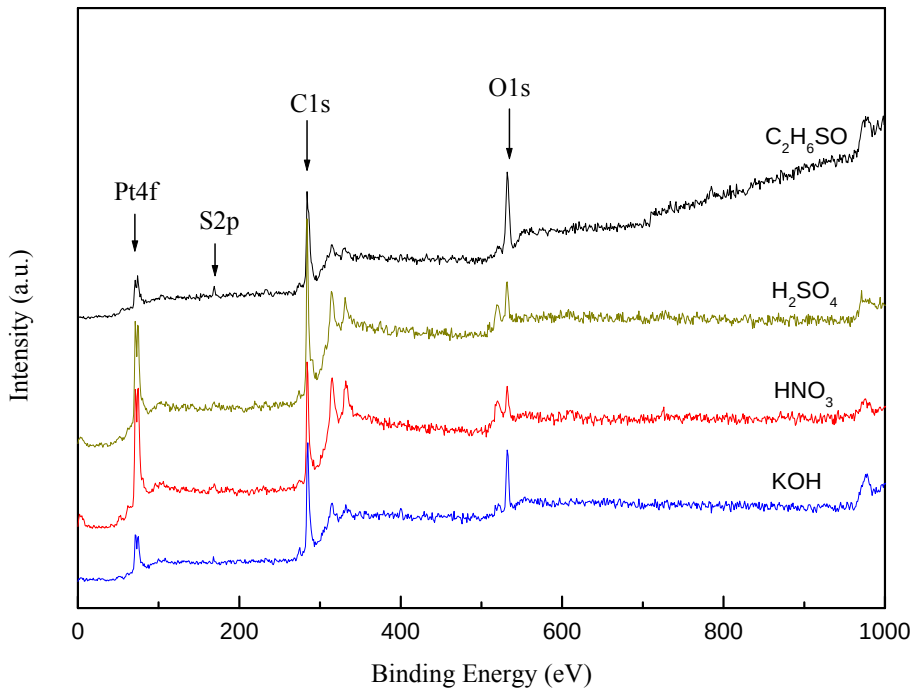

Fig.5-24 XPS surveys of Pt/MWCNTs modified by various solutions.

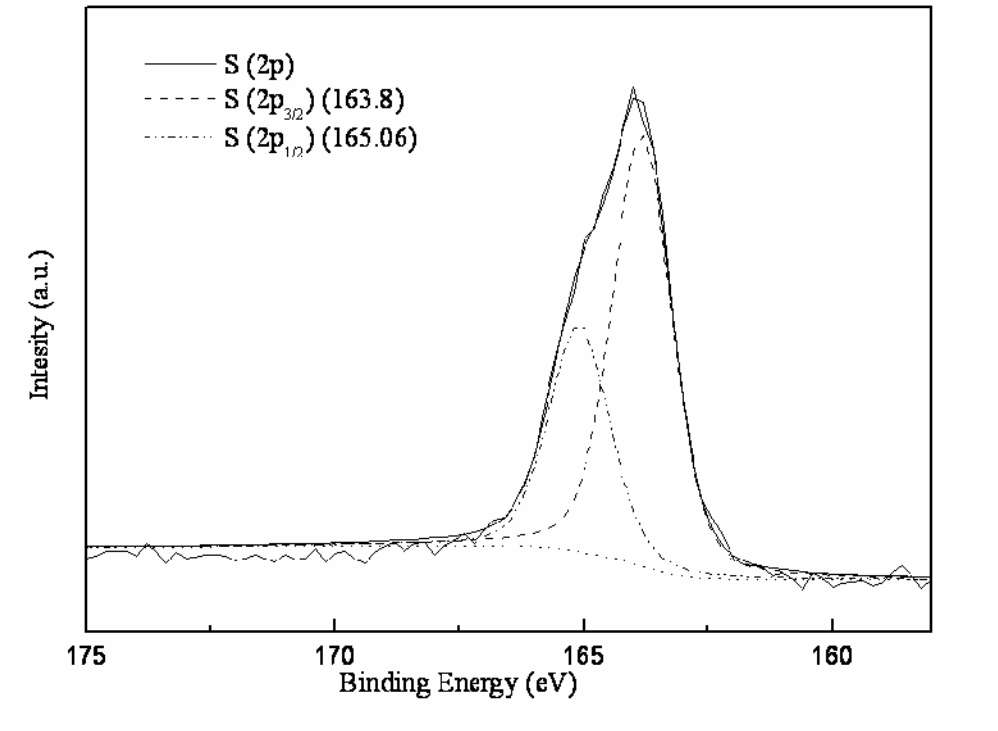

Fig.5-25 The S2p spectra of XPS of MWCNTs modified in C_2H_6SO.

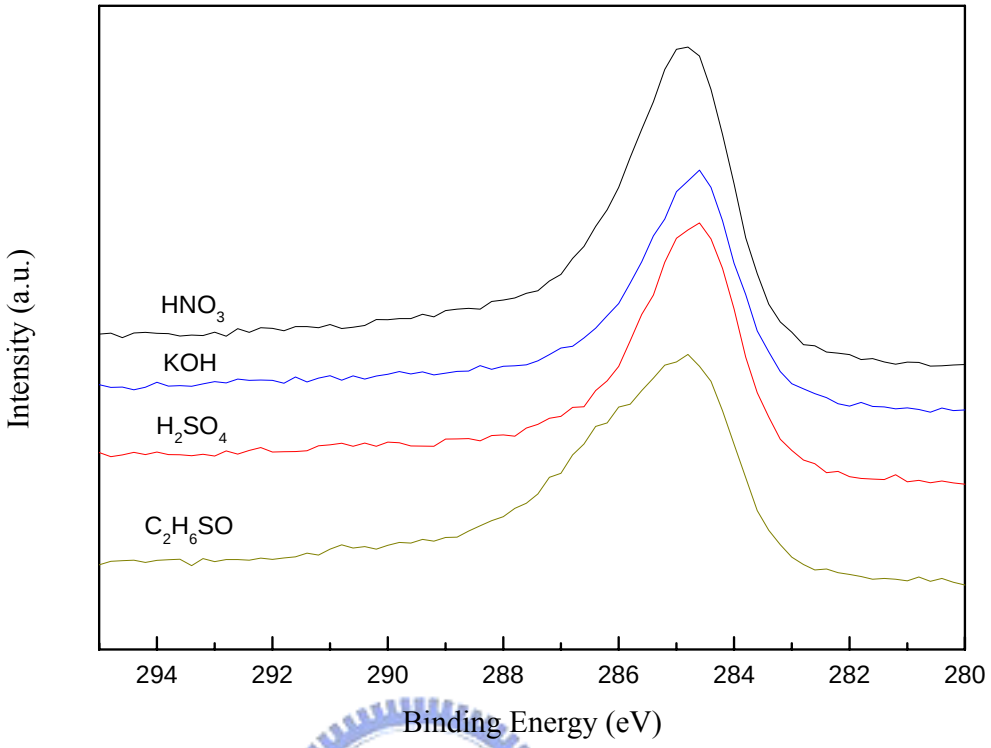

Fig.5-26 The C1s spectra of XPS of MWCNTs modified in different solutions.

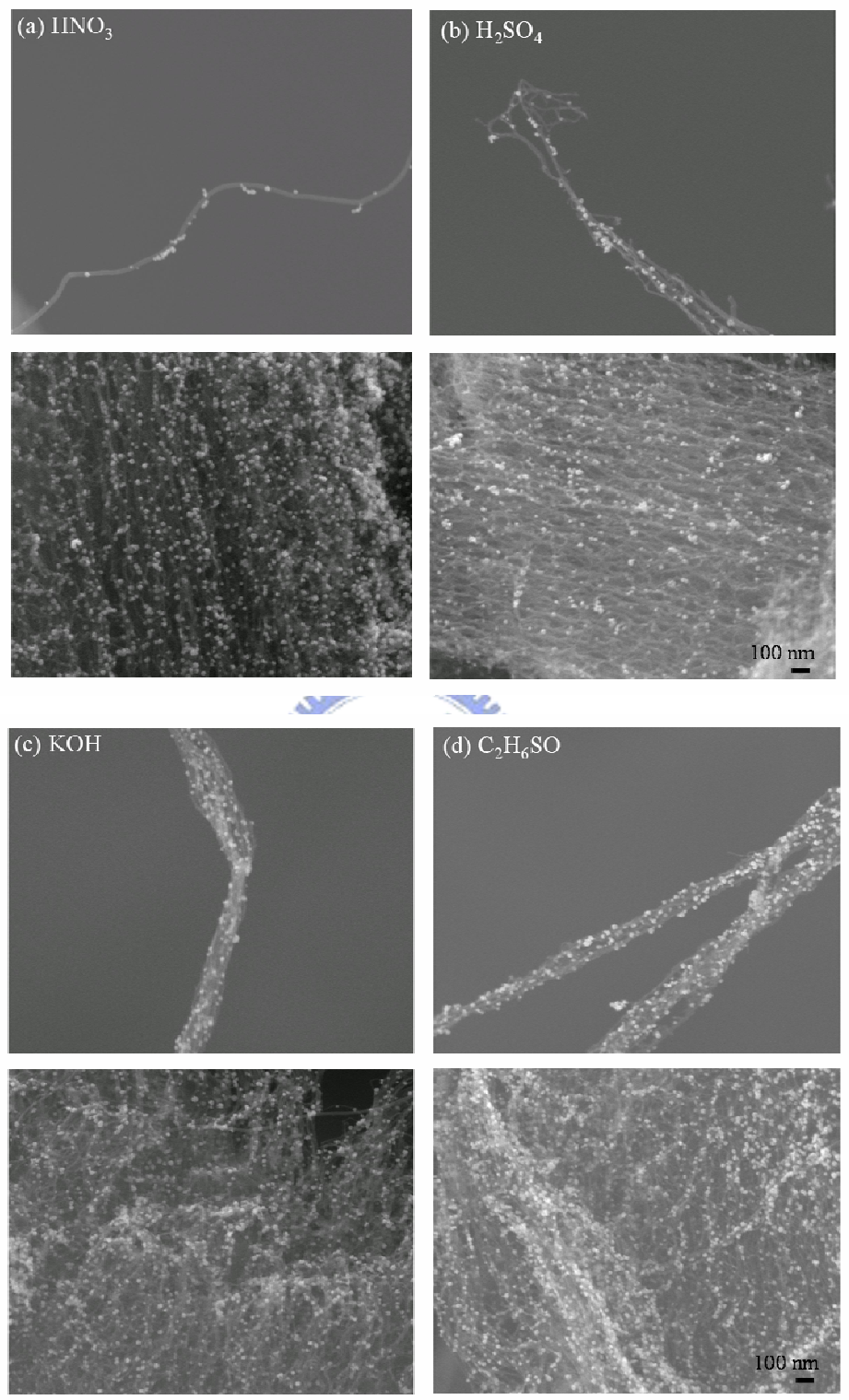

Fig.5-27 SEM images of Pt nanoparticles dispersed on MWCNTs modified by (a)HNO_3 (b)H_2SO_4 (c)KOH and (d)C_2H_6SO.

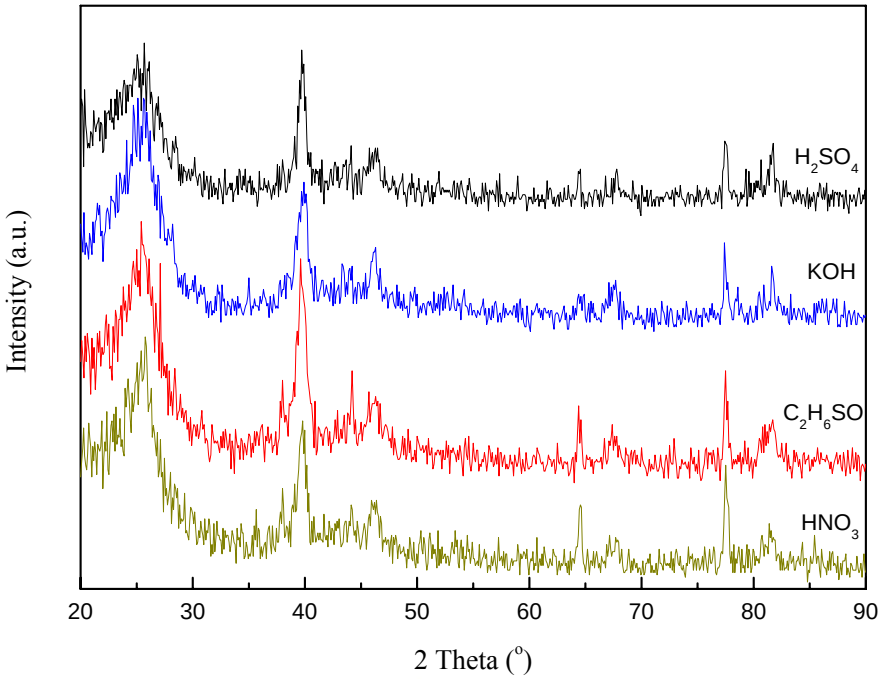

Fig.5-28 The XRD patterns for Pt/MWCNTs with different treatments.

Tab.5-4 Diffraction angle, half-width, and calculated mean particle size

Solution	2θ 0f (220), degree	β (2θ), degree	Mean particle size
HNO_3	67.89	1.48	6.01 nm
H_2SO_4	67.78	1.26	6.91 nm
KOH	67.81	1.34	6.15 nm
C_2H_6SO	67.79	1.59	5.21 nm

The electrochemical properties of Pt deposited on MWCNTs which were modified in various solutions are investigated by cyclic voltammetry in 1M H_2SO_4 solution and 1M H_2SO_4 + 1M CH_3OH solution. Fig.5-29 is the CVs of these samples in 1M H_2SO_4 solution with a scan rate of 50 mV/s. The real surface areas of Pt is determined by integrating the adsorption peak of hydrogen in the cathodic potential sweep according to Eq.4-1. The calculated real surface areas of Pt/MWCNTs modified in HNO_3, KOH, H_2SO_4 and C_2H_6SO are 51.4, 42.1, 42.9 and 54.6 cm^2, respectively. This consists with the result of particle size from XRD. The smaller particles have larger surface area. The electro-oxidation of methanol was analyzed by CVs in 1M H_2SO_4 + 1M CH_3OH solution, which is shown in Fig.5-30. The

Pt/sulfonated-MWCNTs electrode shows great electrocatalytic performance in methanol oxidation. The electrochemical properties of these samples are listed in Tab.5-5. The peak current density of methanol oxidation in the solution of 1M H_2SO_4 + 1M CH_3OH solution can reach 152.1 mA/cm^2 and have a maximum mass efficiency about 304mA/g, which is four times larger than Pt/pristine-MWCNTs electrode. The single cell performance of Pt/thiolated-MWCNTs based DMFC with high Pt loading of 0.5 mg/cm^2 is presented in Fig.5-31. The power density of Pt/thiolated-MWCNTs based DMFC can reach 20.6 mW/cm^2. This result shows the great improvement of the cell performance of DMFC with a Pt/thiolated-MWCNT based electrode.

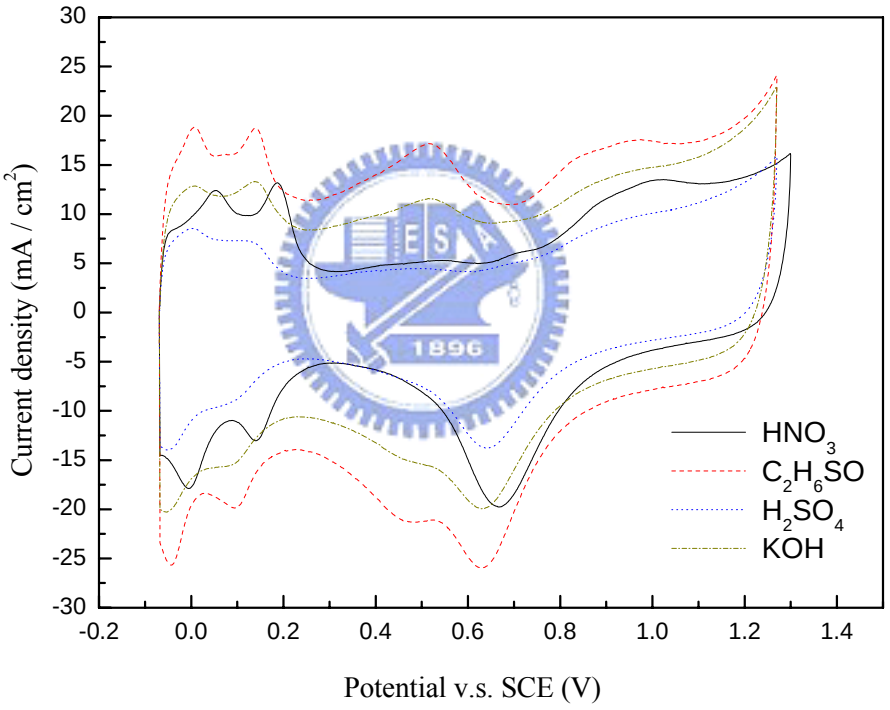

Fig.5-29 Cyclic votammograms of different Pt/CNTs electrodes in 1.0 M H_2SO_4 aqueous solution.

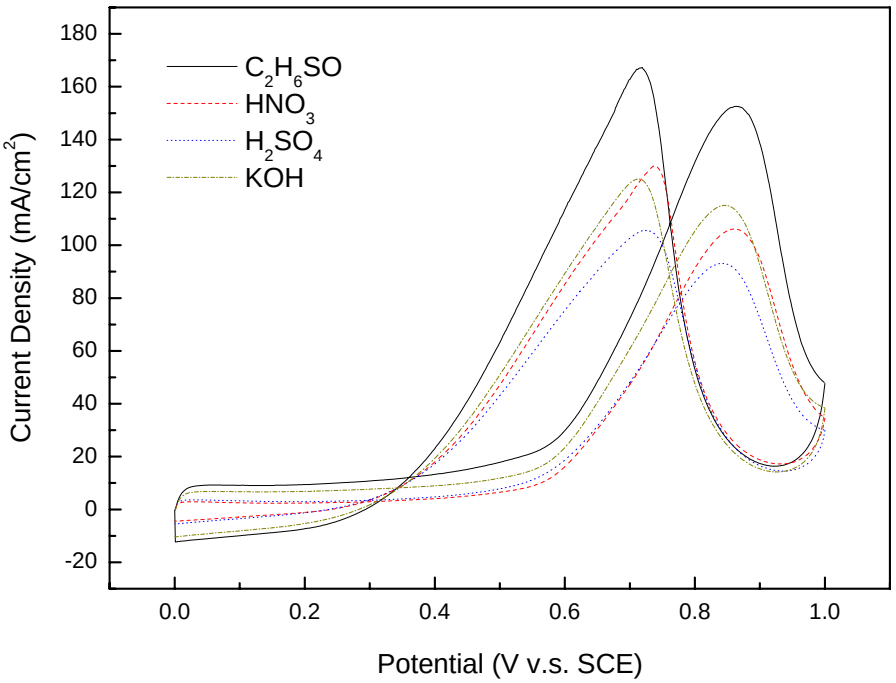

Fig.5-30 Cyclic votammograms of different Pt/CNTs electrodes in 1.0 M H_2SO_4 aqueous solution.

Tab.5-5 Electrochemical properties of Pt nanoparticles dispersed on MWCNTs modified by HNO_3, H_2SO_4, KOH and C_2H_6SO

Solution	Functional group	Loading (mA/mg^2)	$I_{0.8V}$ (mA/cm^2)	S_{Pt} (cm^2)	ME (mA/mg)
HNO_3	-COOH	0.5	115.1	51.4	230.2
H_2SO_4	-OH	0.5	92.6	42.1	185.2
KOH	-OH	0.5	105.5	42.9	210.1
C_2H_6SO	-SH	0.5	152.1	56.6	304.2

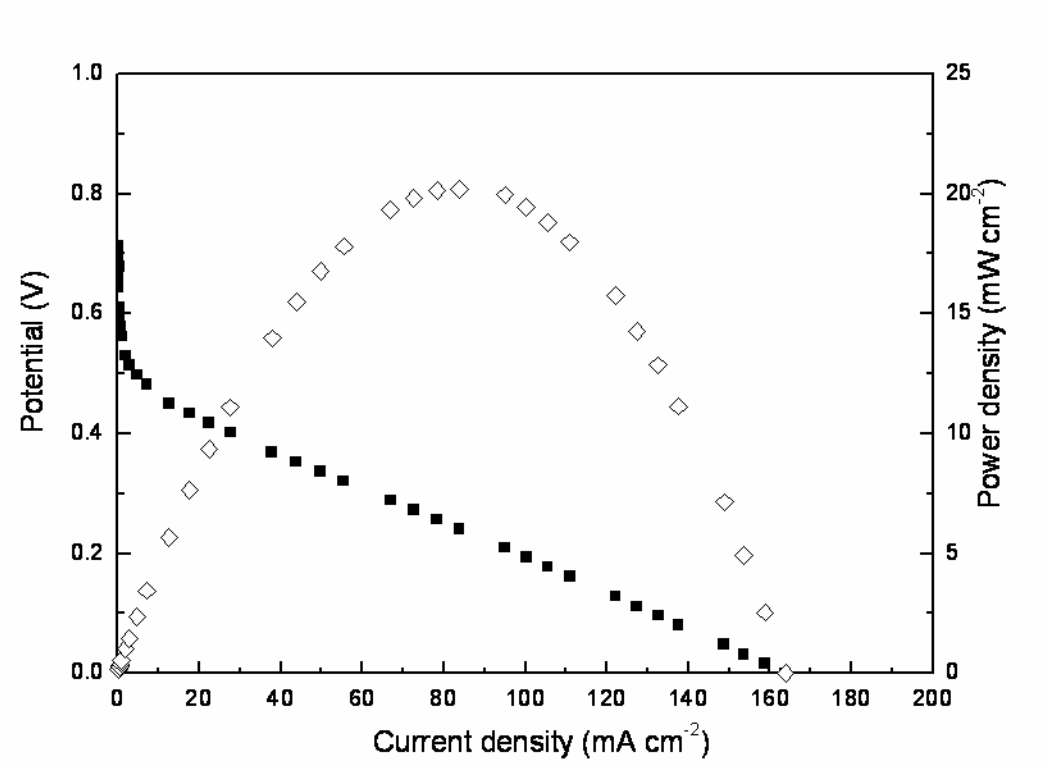

Fig.5-31 Polarization curves of the Pt/ thiolated-CNTs in 1cm^2 single cell with CH_3OH/O_2 at flow rates of 50/500 sccm and 70^{o}C. The Pt loading is 0.5 mg/cm^2.

5.2.4 Conclusions

Functionalized MWCNTs with highly dispersed Pt nanoparticles were obtained by introducing different functional groups like carboxyl, hydroxyl, and thiol groups on MWCNTs surfaces, using HNO_3, KOH, H_2SO_4 and C_2H_6SO solutions. Thiolation of MWCNTs by 2-mercaptoethanol could have smaller Pt particle size due to the lower electrostatic force of thiol group. The Pt/sulfonated-MWCNTs electrode shows great electrocatalytic performance in methanol oxidation from the CV. The peak current density of methanol oxidation in the solution of 1M H_2SO_4 + 1M CH_3OH solution can reach 152.1 mA/cm^2 and have a maximum mass efficiency about 304mA/g, which is four times larger than Pt/pristine-MWCNTs electrode. The power density of Pt dispersed on thiolated MWCNTs is 20.6 mW/cm^2 at 70^{o}C, with 0.4 mg/cm^2 Pt loading.

Chapter 6

Conclusions

In this thesis, high surface area and high conductivity carbon nanotubes were successfully used as the catalyst supports to improve the utility of catalysts in direct methanol fuel cells. Tab.6-1 shows the summaries of the experimental results of our group and other research groups. The sputter deposited and wet impregnation deposited Pt/CNTs are designated as s-Pt/CNTs and w-Pt/CNTs. Pt/o-CNT and Pt/s-CNT represent the Pt deposited on oxidized and thiolated CNTs. Main results of this thesis are summarized as follows.

Part I : Dispersion of Pt nanoparticles on MWCNTs by different routes

1. It is a fast and convenient way for dispersing Pt on CNTs by sputtering.
2. The metal loading of Pt/CNTs catalyst can be easily controlled by varying sputtering time.
3. Dispersion of Pt by sputtering can have a small particle size and a narrow size distribution.
4. The powder density of sputter deposited Pt/CNTs is 8.2 mW/cm^2 with a Pt loading of 0.4 mg/cm^2 at 70^oC.
5. Shield effect of CNTs restrains the further application of sputtering method.
6. Pt nanoparticles were successfully synthesized by polyol process and dispersed on MWCNTs by wet impregnation.
7. The Pt particle size ranges from 5 to 10 nm, which is larger than the sputter deposited Pt nanoparticles.
8. Dispersing Pt catalysts on MWCNTs by wet impregnation can solve the shield effect of sputtering method.
9. Lower methanol oxidation current density and poor single cell performance were found due to the agglomeration of Pt nanoparticles.

Part II : Surface modification of CNTs

1. The agglomeration of Pt nanoparticles can be greatly improved by functionalizing the surface of MWCNTs.
2. The power density of Pt dispersed on HNO_3 treated MWCNTs is 15.8, 12.6 and 8.6 mW/cm^2 at 70^oC, 50^oC and 30^oC with 0.4 mg/cm^2 Pt loading ,respectively.
3. Microwave digestion method was used for effectively modifying CNTs and shorting the

process time

4. The aggregation of Pt nanoparticles can be significantly improved by functionalizing the surface of MWCNTs using the microwave digestion method.
5. The CVs results show that the microwave digestion modified Pt/MWCNTs electrode exhibits the larger electrochemical Pt surface area and higher current density of methanol oxidation than pristine and HNO_3 treated Pt/MWCNTs electrodes.
6. Thiolation of MWCNTs by 2-mercaptoethanol could have smaller Pt particle size due to the lower electrostatic force of sulfur atom.
7. The Pt/sulfonated-MWCNTs has the maximum methanol oxidation current density about 152.1 mA/cm^2 and mass efficiency about 304mA/g, which is much higher than the Pt/HNO_3 treated-MWCNTs.
8. The power density of Pt dispersed on thiolated MWCNTs is 20.6 mW/cm^2 at 70^oC, with 0.5 mg/cm^2 Pt loading**.**

Tab.6-1 Summaries of the experimental results of our research and other research groups.

Group	Material	Pt loading	Current density (mA/cm^2)	Mass efficiency (mA/mg)	Power density (mW/cm^2)
Our research	s-Pt/CNT	0.4 mg/cm^2	18	43.6	8.4 (2M,70°C)
	w-Pt/CNT	0.4 mg/cm^2	28	70	4.6 (2M,70°C)
	Pt/o-CNT	0.24 mg/cm^2	59	246	15.8(2M,70°C,. 0.4 mg Pt/cm^2)
	Pt/s-CNT	0.5 mg/cm^2	151	304	20.6(2M,70°C)
G.. Q. Lu et al. 2004	Pt/C	1.3 mg/cm^2	----	----	50 (2M,70°C)
W. Chen et al. 2005	Pt/CNT	18.1 %	130	4150	----
		9.4 %	65	4850	----
	E-TEK Pt/C	18.8 %	80	3000	----
J. G. Liu et al. 2005	E-TEK Pt/C	2.0 mg/cm^2	----	----	20 (5M,36.5°C)
Z. He et al. 2004	Pt/Graphite	0.4 mg/cm^2	12	30	----
	Pt/CNF	0.37 mg/cm^2	17	46	----
H. Tang et al. 2004	Pt/Graphite	0.2 mg/cm^2	30	150	----
	Pt/CNF	0.188 mg/cm^2	55	292	----
C. L. Lee et al. 2005	Pt/GN	0.146 mg/cm^2	17	116.5	----
	Pt/MWCNT		5	34	----
	Pt/SWCNT		3	20.5	----
T.Maiyalagan et al. 2005	E-TEK Pt/C	20%	1.3	----	----
	Pt/N-CNT	----	13.3	----	----
	Bulk Pt	----	0.17	----	----

Group	Material	Pt loading	Current density (mA/cm^2)	Mass efficiency (mA/mg)	Power density (mW/cm^2)
J.E. Huang et al. 2005	Pt/o-SWCNT	10%	18.0	----	----
Z.Q. Tian et al. 2006	Pt/MWCNT-100s	40%	90.3	384.3	----
	Pt/MWCNT-120s	40%	40.0	170.2	
	Pt/MWCNT-10nm	40%	101	429.8	
	Pt/MWCNT-30nm	40%	90.3	384.3	
	Pt/MWCNT-50nm	40%	74.5	317	
	E-TEK Pt/C	40%	69.1	294.4	
B. Rajesh et al. 2004	Pt/polymeric nanocones	0.08 mg/cm^2	31.3	391	----
G.Wu et al. 2005	Pt/SWCNT	0.1 mg/cm^2	5.0	50	----
	Pt/MWCNT	0.1 mg/cm^2	4.8	48	----
	E-TEK Pt/C	0.1 mg/cm^2	3.5	35	----

Reference

[1] Adapted from http://fuelcellsworks.com/Typesoffuelcells.html

[2] A. Hamnett, "Mechanism and electrocatalysis in the direct methanol fuel cell ", Catal. Today 38, 445, 1997

[3] S. Wasmus, A. Kuver, "Methanol oxidation and direct methanol fuel cells: a selective review", J. Electroanal. Chem. 461, 14, 1999

[4] T. Matsumoto, T. Komatsu, K. Arai, T. Yamazaki, M. Kijima, H. Shimizu, Y. Takasawa, J. Nakamura, "Reduction of Pt usage in fuel cell electrocatalysts with carbon nanotube electrodes", Chem. Commun. 7, 840, 2004

[5] S.D.Thompson, L.R. Jordan, M. Forsyth, "Platinum electrodeposition for polymer electrolyte membrane fuel cells", Eleatrochimica Acta 46, 1657-1663, 2001

[6] K. A. Mauritz, C. J.Hora, A. J. Hopfinger, Advances in Chemistry 187, 124, 1980

[7] H. L. Yeager, A. J. Steck, Electrochem. Soc.128, 1880, 1981

[8] A. Eisenberg, B. Hird, R. B. Moore, "A new multiplet-cluster model for the morphology of random ionomers", Macromolecules 23, 4098, 1990

[9] T. D. Gierke, G. E. Munn, F. C. Wilson, J. Polym. Sci.19, 1687,1981

[10] G. B. Butler, K. F.O'Driscoll, G. L. Wilkes, Chem. Phys. C34, 325, 1994

[11] A. Eisenberg and H. L. Yeager, ACS Symp. Ser. No.180, American Chemical Society: Washington, DC, pp. 1-6, 41-63, 1982

[12] L.A. Utracki and R.A. Weiss, ACS Symp. Ser. No. 395; American Chemical Society: Washington, DC, p.401-417, 1989

[13] A. Eisenberg and M. King, Ion-Containing Polymers: Physical Properties and Structure, Vol. 2, pp. 163-169, 1977

[14] W. Y. Hsu, T. D. Gierke, Macromolecules 15, 101,1982

[15] A. V. Anantaraman, C. L. Gardner, " Studies on ion-exchange membranes. Part 1. Effect of humidity on the conductivity of Nafion®", J. Electroanal. Chem. 414, 115-120, 1996

[16] C. S. Kim, Y. G. Chun, D. H. Peck, D. R. Shin, " A novel process to fabricate membrane electrode assemblies for proton exchange membrane fuel cells " Int. J. Hydrogen Energy 23,1045-1048, 1998

[17] D.Bevers, N. Wagner, M. VonBradke," Innovative production procedure for low cost PEFC electrodes and electrode/membrane structures " Int. J. Hydrogen Energy 24,

57-63, 1998

[18] L. Giorgi, E. Antolini, A. Pozio, E. Passalacqua, "Influence of the PTFE content in the diffusion layer of low-Pt loading electrodes for polymer electrolyte fuel cells ", Electrochim. Acta 43, 3675-3680, 1998

[19] H. S.Wroblowa, Y. C. Pan, G. J. Razumnet, Electroanal. Chem. 69, 195, 1976.

[20] A. J. Appleby, M. J.Savy, Electroanal. Chem., 92,15, 1978.

[21] R. W. Zurilla, R. K. Sen, E. J.Yeager, Electrochem. Soc. 125, 1103, 1978

[22] Gruver, G. A.; Pascoe, R. F.; Kunz, H. R. J. Electrochem. Soc. 127, 1219, 1980

[23] M. C. Lefebvre, Z. Qi, P. G. Pickup," Electronically Conducting Proton Exchange Polymers as Catalyst Supports for Proton Exchange Membrane Fuel Cells. Electrocatalysis of Oxygen Reduction, Hydrogen Oxidation, and Methanol Oxidation", J. Electrochem. Soc. 146, 2054, 1999

[24] J. Shan, P. G. Pickup," Characterization of polymer supported catalysts by cyclic voltammetry and rotating disk voltammetry ", Electrochim. Acta 46, 119-125, 2000

[25] I. D. Raistri, Symposium on Diaphragms, Separators, and Ion-Exchange Membranes, Pennington, NJ, 172, 1986

[26] S. Srinivasan, D. J. Manko, H. Koch, M. A. Enayetullah, A.J. Appleby, "Recent advances in solid polymer electrolyte fuel cell technology with low platinum loading electrodes ", J. Power Sources, 29, 367, 1990

[27] S. Hirano, J.Kim, S. Srinivasan, " High performance proton exchange membrane fuel cells with sputter-deposited Pt layer electrodes", Electrochim. Acta 42, 1587, 1997

[28] S. Y. Cha, W. M. Lee," Performance of Proton Exchange Membrane Fuel Cell Electrodes Prepared by Direct Deposition of Ultrathin Platinum on the Membrane Surface", J. Electrochem. Soc. 146, 4055, 1999

[29] S. Iijima, Nature, "Helical microtubules of graphitic carbon", 354, 56, 1991

[30] Z. W. Pan, S. S. Xie, B. H. Chang, C. Y. Wang; L. Lu; W. Liu, W. Y. Zhou, W. Z. Li, L. X. Qian, "Very long carbon nanotubes ", Nature 394, 6694, 631 – 632, 1998

[31] Jeroen W. G Wilder, Liesbeth C. Venema, Andrew G. Rinzler, Richard E. Smalley, Cees Dekker, Nature 391, "Electronic structure of atomically resolved carbon nanotubes " 6662, 59-62, 1998

[32] T. Spires and R. Malcolm Brown, Jr. Department of Botany, The University of Texas

at Austin, Austin,Tx., 78713 ,1996

[33] P. Avouris, "a nanotube researcher at the IBM labs.", Michigan State University, 2000

[34] T. W. Odom, J. L. Huang, P. Kim, C. M. Lieber, "Atomic structure and electronic properties of single-walled carbon nanotubes", Nature 391, 6662, 62-64,1998

[35] A. Thess, R. Lee, P. Nikolaev, H. Dai, P. Petit, J. Robert, C. Xu, Y. H. Lee, S. G. Kim, A. G. Rinzler, D. T. Colbert, G. Scuseria, D. Tománek, J. E. Fischer, R. E. Smalley," Crystalline Ropes of Metallic Carbon Nanotubes", Science 273, 483, 1996

[36] Adapted from http://www.wag.caltech.edu/foresight/foresight_2.html

[37] Adapted from http://www.pa.msu.edu/~tomanek/tomanek.html

[38] S. Frank, P. Poncharal, Z. L. Wang, and W. A. de Heer, "Carbon Nanotube Quantum Resistors", Science 280, 1744, 1998

[39] S. Sanvito, Y. K. Kwon, D. Tománek, C. J. Lambert, "Carbon Nanotube Quantum Resistors", Phys. Rev. Lett. 84, 1974, 2000

[40] J. Hone, M. Whitney, A. Zettle," Thermal conductivity of single-walled carbon nanotubes ", Synthetic Metals, 103, 2498, 1999

[41] Adapted from http://www.foresight.org/Conferences/MNT7/Papers/Che/index.html

[42] S. Berber, Y. K. Kwon, D. Tománek," Unusually High Thermal Conductivity of Carbon Nanotubes", Phys. Rev. Lett. 84, 4613-4616, 2000

[43] W. Li, C. Liang, J. Qiu, W. Zhou, H. Han, Z. Wei, G. Sun, Q. Xin," Carbon nanotubes as support for cathode catalyst of a direct methanol fuel cell ", Carbon 40,791, 2002

[44] D. B. Buchholz, S. P. Doherty, R. P. H. Chang," Mechanism for the growth of multiwalled carbon-nanotubes from carbon black", Carbon 41, 1625, 2003

[45] H. Tang, J.H. Chen, Z.P. Huang, D.Z.Wang, Z.F.Ren, L. H. Nie, Y. F. Kuang, S.Z. Yao, " High dispersion and electrocatalytic properties of platinum on well-aligned carbon nanotube arrays" Carbon 42,191, 2004

[46] H. Hou and Darrell H. Reneker, "Carbon Nanotubes on Carbon Nanofibers: A Novel Structure Based on Electrospun Polymer Nanofibers", Advanced Materials 16, 1, 69, 2004

[47] C.Wang, M. Waje, X. Wang, J. M. Tang, Robert C. Haddon, Y. Yan, "Proton Exchange Membrane Fuel Cells with Carbon Nanotube Based Electrodes", Nano Letter, 4,2, 345, 2004 .

[48] Z. Zhou, W. Zhou, S. Wang, G.. Wang, L. Jiang, H. Li, G. Sun and Q. Xin, "Preparation of highly active 40 wt.% Pt/C cathode electrocatalysts for DMFC via different routes ", Catalysis Today, 93-95, 523-528, 2004

[49] H. Tang, J. H. Chen, Z. P. Huang, D. Z. Wang, Z. F. Ren, L. H. Nie, Y. F. Kuang and S. Z. Yao, "High dispersion and electrocatalytic properties of platinum on well-aligned carbon nanotube arrays", Carbon, Volume 42, Issue 1, 191-197, 2004

[50] S. Yugo, T. Kanai, T. Kimura, T. Muto," Generation of diamond nuclei by electric field in plasma chemical vapor deposition", Appl. Phys. Lett. 58, 1036, 1991

[51] J. T. Huang, W. Y. Yeh, J. Hwang, H. Chang, "Bias enhanced nucleation and bias textured growth of diamond on silicon(100) in hot filament chemical vapor deposition" Thin Solid Films 315, 35, 1998

[52] R. Sto¨ckel, K. Janischowsky, S. Rohmfeld, J. Ristein, M. Hundhausen, and L. Ley, " Diamond growth during bias pre-treatment in the microwave CVD of diamond", Diamond Relat. Mater. 5, 321, 1996

[53] M. Umeda, M. Kokubo, M. Mohamedi, I. Uchida, "Porous-microelectrode study on Pt/C catalysts for methanol electrooxidation ", Electrochimica Acta 48, 10, 1367, 2003

[54] S.Kerkeni, E. Lamy-Pitara, J.Barbier, "Copper–platinum catalysts prepared and characterized by electrochemical methods for the reduction of nitrate and nitrite ", Catal. Today 75, 35, 2002

[55] H. Wang, T. Loffler, H. Baltruschat, "Formation of intermediates during methanol oxidation: A quantitative DEMS study", J. Appl. Electrochem. 31, 759, 2001

[56] D. Cao, S. H. Bergens," Pt–Ru_{adatom} nanoparticles as anode catalysts for direct methanol fuel cells ", Journal of Power Sources, Volume 134, Issue 2, 12, 170-180, 2004

[57] M. Carmo, V.A. Paganin, J.M. Rosolen and E.R. Gonzalez, " Alternative supports for the preparation of catalysts for low-temperature fuel cells: the use of carbon nanotubes ",Journal of Power Sources, Volume 142, Issues 1-2, 24, 169-176, 2005

[58]G. G. Park, T. H. Yang, Y. G. Yoon, W. Y. Lee, C. S. Kim, "Pore size effect of the DMFC catalyst supported on porous materials ", International Journal of Hydrogen Energy, Volume 28, Issue 6, 645-650, 2003

[59] Y. Takasu, T. Kawaguchi, W. Sugimoto and Y. Murakami, " Effects of the surface area of

carbon support on the characteristics of highly-dispersed Pt---Ru particles as catalysts for methanol oxidation", Electrochimica Acta, Volume 48, Issues 25-26, 15, 3861-3868, 2003

[60] Z. Wei, H. Guo, Z. Tang, " Methanol electro-oxidation on platinum and platinum-tin alloy catalysts dispersed on active carbon ", Journal of Power Sources, Volume 58, Issue 2, 239-242,1996

[61] Z. He , J. Chen , D. Liu , H. Tang , W. Deng, Y. Kuang," Deposition and electrocatalytic properties of platinum nanoparticals on carbon nanotubes for methanol electrooxidation", Materials Chemistry and Physics, Volume 85, Issues 2-3, 396, 2004

[62] Z. He, J. Chen, D. Liu, H. Zhou, Y. Kuang, "Electrodeposition of Pt–Ru nanoparticles on carbon nanotubes and their electrocatalytic properties for methanol electrooxidation", Diamond and Related Materials, Volume 13, Issue 10, 1764, 2004

[63] M. Carmo, V.A. Paganin, J.M. Rosolen and E.R. Gonzalez,"Alternative supports for the preparation of catalysts for low-temperature fuel cells: the use of carbon nanotubes", Journal of Power Sources, Volume 142, Issues 1-2, 24, 169-176, 2005

[64] Y. Sun, Y. Xia," Large-Scale Synthesis of Uniform Silver Nanowires Through a Soft, Self-Seeding, Polyol Process", Adv. Mater., 14, 833, 2002

[65] Y. Sun, Y. Xia," Shape-Controlled Synthesis of Gold and Silver Nanoparticles", Science, 298, 2176, 2002

[70] Y. Liu, Z. Shen, K. Yokogawa, " Investigation of preparation and structures of activated carbon nanotubes ", Materials Research Bulletin, Volume 41, Issue 8, 1503-1512, 2006

[71] E. Frackowiak, S. Delpeux, K. Jurewicz, K. Szostak, D. Cazorla-Amoros, F. Béguin, "Enhanced capacitance of carbon nanotubes through chemical activation ", Chemical Physics Letters, Volume 361, Issues 1-2, 24, 35-41, 2002

[72] Q. Jiang, M. Z. Qu, G. M. Zhou, B. L. Zhang, Z. L. Yu," A study of activated carbon nanotubes as electrochemical super capacitors electrode materials ", Materials Letters, Volume 57, Issue 4, 988-991, 2002

[73] K.I. Han, J.S. Lee, S.O. Park, S.W. Lee, Y.W. Park, Hasuck Kim," Studies on the anode catalysts of carbon nanotube for DMFC ", Electrochimica Acta 50, 791–794, 2004

[74] T. Murakami, T. Sako, H. Harima, K. Kisoda, K. Mitikami and T. Isshiki, " Raman study of SWNTs grown by CCVD method on SiC ", Thin Solid Films, Volumes 464-465,

319-322, 2004

[75] G. W. Lee, J. Jurng, J. Hwang, " Formation of Ni-catalyzed multiwalled carbon nanotubes and nanofibers on a substrate using an ethylene inverse diffusion flame ", Combustion and Flame, Volume 139, Issues 1-2, 167-175, 2004

[76] S. Lefrant, "Raman and SERS studies of carbon nanotube systems ", Current Applied Physics, Volume 2, Issue 6, Pages 479-482, 2002

[77] U. D. Weglikowska, J. M. Benoit, P. W. Chiu, R. Graupner, S. Lebedkin, S. Roth, "Chemical functionalization of single walled carbon nanotubes ", Current Applied Physics, Volume 2, Issue 6, 497-501, 2002

[78] Z. Q. Tian, S. P. Jiang, Y. M. Liang, P. K. Shen, "Synthesis and Characterization of Platinum Catalysts on Multiwalled Carbon Nanotubes by Intermittent Microwave Irradiation for Fuel Cell Applications", J. Phys. Chem.B, Vol.110, No. 11, 5343, 2006

[79] V. Lordi, N. Yao, J. Wei, "Method for Supporting Platinum on Single-Walled Carbon Nanotubes for a Selective Hydrogenation Catalyst", Chem. Mater., 13, 733, 2001

[80] V. Radmilovic, H.A. Gasteiger, P.N. Ross Jr., "Structure and Chemical Composition of a Supported Pt-Ru Electrocatalyst for Methanol Oxidation" J. Catal., , 154, 98, 1995

[81] W. Li, W. Zhou, H. Li, Z. Zhou, B. Zhou, G. Sun, Q. Xin, "Nano-stuctured Pt–Fe/C as cathode catalyst in direct methanol fuel cell ", Electrochimica Acta, 49, 1045–1055, 2004

[82] A.R West, Solid State Chemistry and its Applications, first ed., Wiley, New York, 1984

[83] K. Kinoshita, P. Stonehart, Modern Aspects of Electrochemistry, Plenum, New York, 1977.

[84] V. Lordi, N. Yao, J. Wei, "Method for Supporting Platinum on Single-Walled Carbon Nanotubes for a Selective Hydrogenation Catalyst", Chem. Mater., 13, 733, 2001

[85] Z. Liu, X. Lin, J.Y. Lee, W. Zhang, M. Han, L.M. Gan, "Preparation and Characterization of Platinum-Based Electrocatalysts on Multiwalled Carbon Nanotubes for Proton Exchange Membrane Fuel Cells", Langmuir , 18, 4054, 2002.

[86] K.I. Han, J.S. Lee, S.O. Park, S.W. Lee, Y.W. Park, H. Kim,"Studies on the anode catalysts of carbon nanotube for DMFC", Electrochim. Acta , 50, 791, 2004

[87] D. J. Guo, H. L. Li, " High Dispersion and Electrocatalytic Properties of Platinum on Functional Multi-Walled Carbon Nanotubes" ,Electroanalysis,17, 869, 2005

[88] X. Sun, R. Li, D. Villers, J.P. Dodelet, S. Desilets, “Composite electrodes made of Pt nanoparticles deposited on carbon nanotubes grown on fuel cell backings”, Chem. Phys. Lett. , 379, 99, 2003

[89] J. Hu, J. Shi, S. Li, Y. Qin, Z. X. Guo, Y. Song, D. Zhu, ”Efficient method to functionalize carbon nanotubes with thiol groups and fabricate gold nanocomposites” , Chemical Physics Letters, Volume 401, Issues 4-6, 352, 2005

[90] W. Li, C. Liang, W. Zhou, J. Qui, Z. Zhou, G. Sun, Q. Xin,“Preparation and Characterization of Multiwalled Carbon Nanotube-Supported Platinum for Cathode Catalysts of Direct Methanol Fuel Cells ”, J. Phys. Chem. B, 107, 6292, 2003

[91] M.C. Román-Mart´ınes, D. Cazorla-Amorós, A. Linares-Solvano, C. Salinas-Mart´ınez de Lecea,“Metal-support interaction in pt/c catalysts. Influence of the support surface chemistry and the metal precursor”, Carbon, 33, 3, 1995

[92] M.A. Fraga, E. Jordão, M.J. Medes, M.M. Freitas, J.L. Faria, J.L. Figueiredo, “Properties of Carbon-Supported Platinum Catalysts: Role of Carbon Surface Sites”, J. Catal., 209, 355, 2002

[93] J. Liu, A.G. Rinzler, H. Dai, J.H. Hafner, R.K. Bradley, P.J. Boul, A. Lu, T. Iverson, K. Shelimov, C.B. Huffman, F. Rodriguez-Macias, Y. S. Shon, T.R. Lee, D.T. Colbert, R.E. Smalley,” Fullerene Pipes”, Science 280, 1253, 1998

[94] D.B. Mawhinney, V. Naumenko, A. Kuznetsova, J.T. Yates Jr., J. Liu, R.E. Smalley, “Infrared Spectral Evidence for the Etching of Carbon Nanotubes: Ozone Oxidation at 298 K”, J. Am. Chem. Soc. , 122, 2383, 2000

[95] D.B. Mawhinney, V. Naumenko, A. Kuznetsova, J.T. Yates, J. Liu, R.E. Smalley, “Surface defect site density on single walled carbon nanotubes by titration ”, Chem. Phys. Lett. , 324, 213, 2000

[96] T. Kyotani, S. Nakazaki, W.-H. Xu, A. Tomita, “Chemical modification of the inner walls of carbon nanotubes by HNO_3 oxidation”, Carbon, 39, 782, 2001

[97] J. Zhang, H. Zou, Q. Quan, Y. Yang, Q. Li, Z. Liu, X. Guo, Z. Du, “Effect of Chemical Oxidation on the Structure of Single-Walled Carbon Nanotubes” J. Phys.Chem. B , 107, 3712, 2003

[98] V. Srinivasan, E.I. Stiefel, A. Elsberry, R.A. Walton, J. Am. Chem. Soc., 101, 2611, 1979

Vita

姓名：陳建仲

性別：男

生日：66 年 3 月 23 日，台北人

電子郵件信箱：cjz0323@yahoo.com.tw

永久地址：台北縣中和市中山路二段 463 號 4 樓

學歷：

博士班：國立交通大學材料科學與工程學系暨研究所	2002. 9 ~ 2006. 8
研究所: 國立台灣科技大學化學工程研究所	2000. 9 ~ 2002. 6
大學：中原大學化學工程系	1996. 9 ~ 2000. 6

碩士論文題目：奈米碳管於低溫下合成的結構及場發射特性探討

著作：

1. Chien-Chung Chen, Chia Fu Chen, Cheng-Hang Hsu and I-Hsuan Li
   "Growth and characteristics of carbon nanotubes on carbon cloth as electrodes"
   Diamond and Related Materials, Volume 14, Issues 3-7, March-July 2005, Pages 770-773
2. Chien-Chung Chen, Chia-Fu Chen, I-Hsuan Lee and Chien-Liang Lin
   "Fabrication of high surface area graphitic nanoflakes on carbon nanotubes templates"
   Diamond and Related Materials, Volume 14, Issues 11-12, November-December 2005, Pages 1897-1900
3. Chien-Chung Chen, Chia-Fu Chen, Chieng-Ming Chen, Fang-Tzu Chuang "Modification of multi-walled carbon nanotubes by microwave digestion method as electrocatalyst

supports for direct methanol fuel cell applications”*Electrochemistry Communications*, In Press, Available online 25 July 2006

4. Chien-Chung Chen, Yi-Hui Chen and Chia-Fu Chen

   “The parametric study of carbon nanotips grown by MWPECVD with controllable sharpness using various metallic catalysts” *Microelectronic Engineering*, In Press, Available online 5 July 2006

5. Cheng Hang Hsu, Chia-Fu Chen, Chien-Chung Chen and Shih-Yu Chan

   “Density-controlled carbon nanotubes” *Diamond and Related Materials*, Volume 14, Issues 3-7, March-July 2005, Pages 739-743